Chem Soc Rev

REVIEW ARTICLE

View Article Online
View Journal



Cite this: DOI: 10.1039/d1cs01170g

# Interaction of SARS-CoV-2 with host cells and antibodies: experiment and simulation

Hung Nguyen, †[a] Hoang Linh Nguyen, †[bc] Pham Dang Lan, [de] Nguyen Quoc Thai, [f] Mateusz Sikora [gh] and Mai Suan Li *[a]

Received 3rd April 2023

DOI: 10.1039/d1cs01170g

rsc.li/chem-soc-rev

Severe acute respiratory syndrome coronavirus 2 (SARS-CoV-2) is the causative agent of the devastating global COVID-19 pandemic announced by WHO in March 2020. Through unprecedented scientific effort, several vaccines, drugs and antibodies have been developed, saving millions of lives, but the fight against COVID-19 continues as immune escape variants of concern such as Delta and Omicron emerge. To develop more effective treatments and to elucidate the side effects caused by vaccines and therapeutic agents, a deeper understanding of the molecular interactions of SARS-CoV-2 with them and human cells is required. With special interest in computational approaches, we will focus on the structure of SARS-CoV-2 and the interaction of its spike protein with human angiotensin-converting enzyme-2 (ACE2) as a prime entry point of the virus into host cells. In addition, other possible viral receptors will be considered. The fusion of viral and human membranes and the interaction of the spike protein with antibodies and nanobodies will be discussed, as well as the effect of SARS-CoV-2 on protein synthesis in host cells.

## 1. Introduction

In November 2019 the first case of COVID-19 disease (coronavirus disease 2019) was detected in Wuhan, China.[1–3] The disease has been spreading very quickly around the world, and due to a sharp increase in both the number of cases and deaths, in March 2020 WHO declared COVID-19 a pandemic. Based on its close association with the severe acute respiratory syndrome coronavirus (SARS-CoV-1), which caused the SARS epidemic in 2003, the new virus was named SARS-CoV-2.[4]

The number of cases and death toll from COVID-19 make it one of the worst catastrophic infectious diseases in human history. As of February 2023, more than 671 million cases and more than 6.8 million deaths have been reported globally.[5] Although the pandemic began over three years ago, the origin of SARS-CoV-2 is still ambiguous. One of hypotheses suggests a zoonotic origin for SARS-CoV-2, in which the virus is transmitted to humans from wild animals such as bats.[3,6] A meta-analysis suggests that the likelihood of a natural disaster that results in millions of deaths, like COVID-19, is infinitesimal, while a virus leak from a laboratory accident has a higher probability,[7] supporting the hypothesis that the virus is a product of genetic research. Another possibility is that the virus emerged through an evolutionary and selective process, with a human-transmitted variant of the coronavirus circulating in the population, resulting in a pandemic.[8]

Since the beginning of the pandemic, the research community has made tremendous efforts to find effective treatments for COVID-19. Despite the great success of current vaccines, in particular mRNA vaccines,[9] antibodies[10,11] and drugs such as Remdesivir, Molnupiravir and Paxlovid[12–15] the fight against SARS-CoV-2 continues as more and more variants of concern such as Omicron emerge. The pandemic has gone through several waves,[16,17] with first, second and third waves caused by an ancestral strain from Wuhan, Beta, and Delta variants,[18] respectively. The fourth and fifth waves were triggered by the Omicron variant and its sub-lineages,[17,19] which compete with each other to become the dominant lineage.[20] Even individuals who received the parental mRNA vaccine and bivalent BA.5 booster exhibited weak neutralization against the Omicron

[a] Institute of Physics, Polish Academy of Sciences, al. Lotnikow 32/46, 02-668 Warsaw, Poland. E-mail: masli@ifpan.edu.pl
[b] Institute of Fundamental and Applied Sciences, Duy Tan University, Ho Chi Minh City 700000, Vietnam
[c] Faculty of Environmental and Natural Sciences, Duy Tan University, Da Nang 550000, Vietnam
[d] Life Science Lab, Institute for Computational Science and Technology, Quang Trung Software City, Tan Chanh Hiep Ward, District 12, 729110 Ho Chi Minh City, Vietnam
[e] Faculty of Physics and Engineering Physics, VNUHCM-University of Science, 227, Nguyen Van Cu Street, District 5, 749000 Ho Chi Minh City, Vietnam
[f] Dong Thap University, 783 Pham Huu Lau Street, Ward 6, Cao Lanh City, Dong Thap, Vietnam
[g] Malopolska Centre of Biotechnology, Jagiellonian University, Kraków, Poland
[h] Department of Theoretical Biophysics, Max Planck Institute of Biophysics, Frankfurt am Main, Germany
† These authors contributed equally.

BA.2.75.2, BQ.1.1 and XBB.1 subvariants,[21] which poses new threats to public health.[22,23] Such observations urge researchers to better understand the interaction of novel variants with human cells, including the immune escape mechanism and details of viral replication mechanisms to develop more effective antibodies and vaccines,[24] emphasizing the ongoing interest in COVID-19 research.

The number of results for the keyword "COVID-19" is about 958 000 and "SARS-CoV-2" is about 517 000 from Google Scholar as of February 2023. In the history of scientific research, we have never seen such a huge number of articles appear in such a short period of time as in the last 3 years. Among them are many review articles on various aspects of COVID-19. The reviews of Liu *et al.*[25] and Hu *et al.*[26] described the structure and basic virology of SARS-CoV-2, as well as recent advances in the development of therapeutic agents and vaccines. V'kovski *et al.*[27] summarized the findings that enrich our knowledge of SARS-CoV-2 infection *via* the virus life cycle and discussed its relationship to our understanding of coronavirus biology. The structural features of viral proteins, as well as their interaction with host cell proteins, have been considered, but the mechanism of molecular interaction in many cases remains ambiguous.[28] Minkoff *et al.* reviewed the immune evasion of SARS-CoV-2.[29] The ongoing spread of COVID-19 is fueling the emergence of new variants of SARS-CoV-2 that have significantly different virus characteristics. Review by Harvey *et al.* focuses on variants and the effect of mutations on immune escape.[30] Experimental data on virion structure, and viral replication were summarized,[31] while Jackson *et al.*[32] discussed the molecular mechanisms of SARS-CoV-2 entry into human cells. A recent interesting review covers many aspects of the virus such as structure, variants, pathogenesis and transmission mechanisms, receptors, and vaccines.[33] The ability of the Omicron variant and its lineages to evade the host cell is discussed in detail from an experimental point of view.[34] Similarly, Fan *et al.* reviewed experimental results on

**Hung Nguyen**

*Hung Nguyen studied Theoretical Physics at Ho Chi Minh City University of Science, Vietnam and received his master's degree in Applied Physics from Ho Chi Minh City University of Technology. He works on his doctoral dissertation at the Institute of Physics, Polish Academy of Sciences, under the supervision of Prof. Mai Suan Li. His PhD study focuses on the interaction of antibodies with the SARS-CoV-2 spike protein and how SARS-CoV-2 binds to ribosomes to prevent protein synthesis. The goal is to find solutions to better treat COVID-19.*

**Hoang Linh Nguyen**

*Hoang Linh Nguyen is a researcher at the Institute of Fundamental and Applied Sciences, Duy Tan University, Ho Chi Minh city, Vietnam. Hoang Linh Nguyen obtained his PhD in Engineering Physics in 2023 from Ho Chi Minh City University of Technology (HCMUT), a member of Vietnam National University-Ho Chi Minh City (VNU-HCMC). His research interests lie in the field of computational biophysics and computational medicine.*

**Pham Dang Lan**

*Pham Dang Lan is a researcher of Life science lab at the Institute for Computational Science and Technology, Ho Chi Minh city, Vietnam. He obtained a Master's degree in theoretical physics from the University of Science, Ho Chi Minh, Vietnam. His current research focuses on protein folding, co-translational protein quality control using coarse-grained models, protein–protein interactions related to COVID-19.*

**Nguyen Quoc Thai**

*Nguyen Quoc Thai obtained his BS and MS degree in physics from Can Tho University in 2006 and 2008. Since 2008, he has been lecturing at Dong Thap University, Vietnam. From 2011 to present, he is a Research Fellow at the Life Science Lab of the Institute for Computational Science and Technology, Ho Chi Minh city, Vietnam. He received his PhD in computational physics in 2022 from Ho Chi Minh City University of Technology (HCMUT). He is the author of more than 10 articles and various inventions. His research interests include the computer-aided drug design for the Alzheimer's disease, influenza A virus, and COVID-19.*

infectivity, immune invasion, and antiviral drugs against Omicron.[35]

It should be emphasized that the reviews mentioned above focus mainly on microbiological aspects, ignoring biophysical, in particular, computational studies. The benefits of molecular dynamics simulations in COVID-19 research were highlighted in Padhi *et al.*[36] Computational methods that are useful for studying COVID-19 were discussed.[37] However, some important issues, such as fusion of viral and host cell membranes and the effect of SARS-CoV-2 on protein synthesis, have not been described.

Several antibodies which bind to RBD, NTD, S2 subunit of spike protein are summarized.[38] The experimental features of nanobodies are review in work of Bhattacharya *et al.*[39] The emergence of variants, the structural basis of antibodies and immune escape mutations are discussed in review of Mittal and co-workers.[40] The experimental observations about membrane attachment and fusion of SARS-CoV-2 are discussed in review of Negi *et al.*[41] However, the detailed comparison between experiment and simulations of virus-host cell interaction, the membrane fusion, effect of SARS-CoV-2 on protein synthesis, other receptors of SARS-CoV-2, antibodies and nanobodies have not yet been reviewed systematically. In this review, we summarize literature on these problems focusing on computational aspect to fill this gap.

The membrane fusion mechanism of coronaviruses and their associated drug targets have been described in an excellent review by Tang *et al.*,[42] while experimental observations of membrane attachment and fusion of SARS-CoV-2 have been discussed in Negi *et al.*,[41] but these reviews did not mention important computational research. Thus, one of our goals is not only to fill this gap, but also to present the membrane-bound intermediate as a new intermediate state between the pre- and post-fusion states.[43]

Non-structural proteins (NSPs) formed after the entry of the coronavirus into host cells have been found to interfere with various steps in human protein synthesis,[44] weakening the immune system, but this interesting area has not been systematically summarized. Here, we discuss how SARS-CoV-2 NSPs affect RNA splicing, mRNA translation, and protein transport, focusing on recent experimental and computational studies.

The review is organized as follows. In Section 2 the structure of SARS-CoV-2 is described in detail and compared with SARS-CoV-1, and the life circle of the virus is also presented. The details of binding the spike protein with receptors of human cells are shown in Section 3. Section 4 focuses on molecular interactions of SARS-CoV-2 variants of concern with human ACE2. The possibility of the virus entering human cells by binding to receptors other than ACE2 is discussed in Section 5. The main steps in SARS-CoV-2 triggered membrane fusion are discussed in Section 6. The neutralizing and binding activities of antibodies and nanobodies are presented in Section 7. Section 8 concentrates on the impact of SARS-CoV-2 non-structural proteins on major steps in human protein synthesis, including RNA splicing, mRNA translation, and protein trafficking. Some issues of interest for future work are highlighted in Section 9.

## 2. Structure of SARS-CoV-2

The Coronaviridae family consists of four genera including alpha, beta, gamma, and delta-coronaviruses. There are seven known human coronaviruses of alpha- (HCoV-229E and NL63) and beta- genera (MERS-CoV, SARS-CoV-1, HCoV-OC43 and HcoV-HKU1), now including also the SARS-CoV-2. Although SARS-CoV-2 shares 79% homology with SARS-CoV-1 and 50% with MERS,[45] both causes of pandemic breakouts in 2002 and 2012, it is not their direct descendant, but rather is a result of an animal-human host jump.[46]

All of the coronaviruses encode their genes in a positive sense (5′ → 3′ orientation), single stranded RNA, which

**Mateusz Sikora**

*Mateusz Sikora is a leader of the Max Planck "Dioscuri Centre for Modelling of Posttranslational Modifications" at the Malopolska Centre of Biotechnology in Krakow, Poland. He obtained a PhD in biophysics from the Institute of Physics, Polish Academy of Sciences, Warsaw, Poland. He is interested in the role of posttranslational modifications in the protein–protein interactions, in particular glycan shielding, protein unfolding under external force, cell–cell adhesion, viral adhesion proteins (COVID-19). In his research he combines computer simulations with experimental techniques.*

**Mai Suan Li**

*Mai Suan Li is Professor of Physics at the Institute of Physics, Polish Academy of Sciences and Scientific Advisor to the Institute for Computational Science and Technology, Ho Chi Minh city, Vietnam. He obtained a PhD in theoretical physics from Chisinau State University, Moldova, and a habilitation degree from the Institute of Physics, Polish Academy of Sciences. His research interests are: development of coarse-grained models for studying protein folding and aggregation, factors governing protein aggregation, co-translational folding on ribosomes, protein unfolding under an external mechanical force, and computer-aided drug design for Alzheimer's disease, influenza A virus, breast cancer, and COVID-19.*

corresponds to mRNA, *i.e.* upon successful injection of the genetic material can be directly translated by the host ribosomes to produce viral proteins. Coronaviral genome, with ~26.4–31.7 kbase[47] is the second largest known RNA genome. It contains 14 open reading frames (ORFs)[48] encoding four structural proteins involved in genome packing and virion assembly (M-membrane, E-envelope, N-nucleocapsid, S-spike) and 16 non-structural proteins (NSP), including components of the replication-transcription complex (RTC) required for transcription and replication. The main ORFs encompass ORF1a and overlapping with it ORF1b, which takes advantage of the programmed and tightly controlled[49] ribosomal frame shift, producing either polyprotein 1a (ppa1a) or polyprotein 1ab (ppa1ab), featuring approximately 2700 additional amino acids. Polyproteins contain papain-like protease and main protease, which self-cleave the polyprotein into functional NSPs. NSP 2-16 co-assemble with host factors into RTCs, which are hosted in ER-derived, interconnected double-membrane vesicles (DMVs)[27,50] enriched in double-stranded RNA.[51] RTCs replicate virial positive-sense RNA into the negative-sense strand, which is then used to either produce positive-sense RNA for the next generation of virions, or to transcribe sub-genomic mRNAs, which are translated into structural proteins. New virion assembly occurs in ER-Golgi intermediate compartment (ERGIC),[52] where structural proteins co-cluster with RNA, bud in the vicinity of Golgi.[51] As other enveloped viruses, SARS-CoV-2 hijacks host membranes, which most likely include ERGIC-like lipids,[53] with composition possibly further altered to include unusual amounts of phosphatidylserine and phosphatidylethanolamine and very little cholesterol.[54] Finally, virions egress either *via* secretory pathway[55] or exploiting lysosomal trafficking.[56] The released virions progress the infection by attacking new cells or being secreted with bodily fluids to infect new individuals.

### 2.1. SARS-CoV-2 virion and S-protein

Cryo-electron tomography (CryoET) studies of virions both released[57–60] or captured during maturation,[61] have revealed roughly spherical shapes, with a diameter of approximately 60–100 nm.[57,58,60] As a striking feature and a namesake for the virus family, virions are decorated with 26–40 elongated S (spike) proteins anchored in the viral envelope *via* flexible stalk,[57,58,60] assembled in a resemblance of a crown (latin *corona*) (Fig. 1E). Remaining structural proteins are virtually inaccessible from the outside: E-protein presents a 16-AA C-terminal tail[62] and M-protein 19-AA N-terminal tail, which

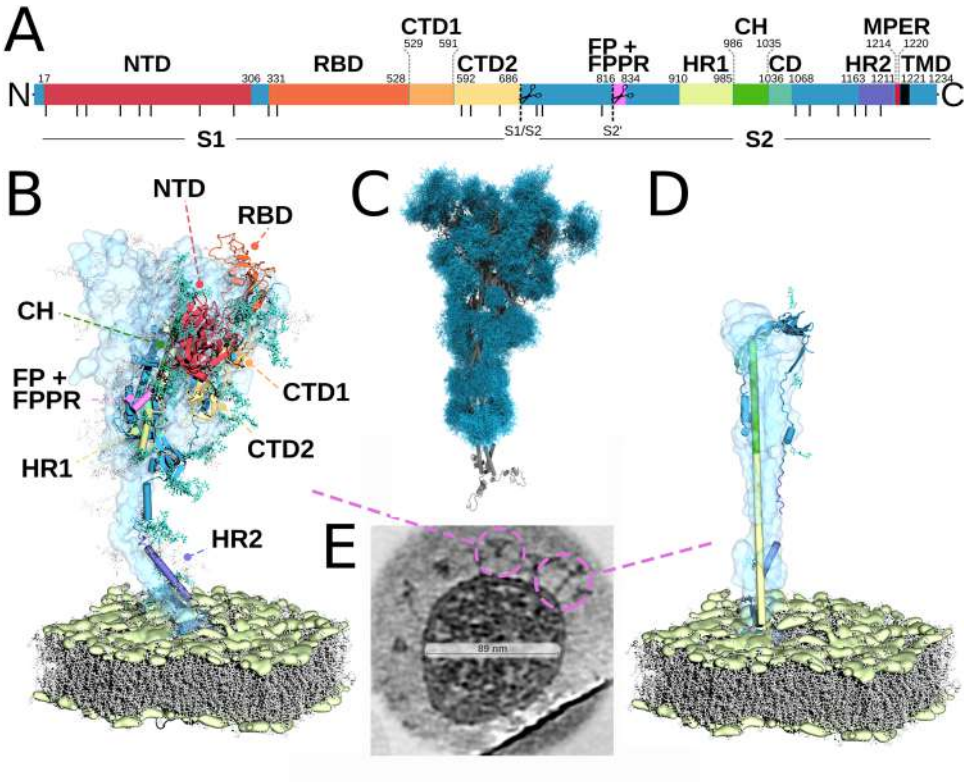


Fig. 1 Structure and glycosylation of the SARS-CoV-2 spike protein. (A) Sequence of the spike protein (blue rectangle) with domains shown with different colors, indicating flanking residues. Glycan positions are shown as vertical lines. Peptidase cleavage sites are indicated by scissors over dashed lines. (B) Spike protein in pre-fusion state embedded in a lipid membrane patch (yellow and gray), modified from.[71] Two chains in down state are shown as semitransparent surface, with glycans shown as gray sticks. The remaining chain captured in up state is shown as cartoon, with colors denoting distinct domains. Glycans are shown as sticks. (C) Visualisation of the surface shielding of the spike protein (gray cartoon) by glycans (blue sticks). For each glycosylation site, 50 conformations of a complex triantennary glycan are shown (generated by GlycoSHIELD using default settings.[72] (D) similar to (B) but for a post-fusion state with only resolved domains and glycans displayed (PDB ID 7E9T). (E) pre-fusion and post-fusion states (marked with dashed circles) captured by cryo-electron tomography *in situ*, from EMPIAR dataset 10453.[60]

 

is further protected by a glycosylation site. Here, due to its therapeutic accessibility and availability for the immune system, we focus primarily on the structure of the spike protein. Detailed review of the current knowledge of other structural and NSPs can be found elsewhere.[63]

Spike protein is a 1273-amino acid long, trimeric type-I transmembrane protein distantly related to its Influenza or HIV counterparts. Spike protein can be further subdivided into a number of structural domains (Fig. 1A). Prior to infection, spike proteins are found primarily in the characteristic lollipop-like prefusion state (see Fig. 1B), with large domain attached to viral membrane through an elongated and partially flexible stalk. During the infection, spike protein binds primarily to ACE2, after which it undergoes massive structural rearrangements into the club-like post-fusion state (Fig. 1D). This drives fusion of the virion with the host cell,[64] leading to the release of the genetic material. Spike protein can be divided into S1 and S2 structural domains separated through a furin cleavage site $Q_{677}$TNSPRRAR ↓ $SV_{687}$. Unlike other SARS-related coronaviruses, cleavage in SARS-CoV-2 occurs already during biogenesis.[65] S2 is further processed by cleavage at the S2′ site K811-PSKR ↓ SFI-818 by TMPRSS2 and catepsin L.[66,67] The cleavage into three distinct polypeptides destabilizes the spike protein and primes it for a transition into post-fusion state, enhancing viral entry and pathogenesis.[68,69] Interestingly, mutation of the furin cleavage site leads to improved fitness of the virus in Vero E6 cells, but attenuated replication in human respiratory cell lines.[70]

The main effort of the host of structural studies has been focused on the spike protein and its variants, which is reflected in 1265 Protein Data Bank entries (as of 2.1.2023) describing its distinct parts and interaction partners. The early studies focused on the recombinant versions of Wuhan-1 strain[65,73] as well as the structures of RBD bound to ACE2.[74,75] These studies used an altered version of spike protein, where furin cleavage site was removed and additional strategies employed to stabilize spike protein in its prefusion trimeric state. The subsequent cryoET studies revealed very similar structures *in situ*,[57,58,60] providing an important validation for mRNA vaccines and therapeutic designs that rely on recombinant proteins.

The majority of structural studies agree on the division of spike protein into domains (Fig. 1A): S1 is further divided into an N-terminal signal peptide, N-terminal domain (NTD), receptor binding domain (RBD) and two minidomains: C-terminal domain 1 and C-terminal domain 2 (CTD1, CTD2). S2 is typically divided into fusion peptide (FP) and fusion peptide proximal region (FPPR), heptad repeat 1 (HR1), central helix (CH), connector domain (CD) heptad repeat 2 (HR2) which is connected to a transmembrane domain (TMD) *via* membrane proximal region, terminating in the C-terminal unstructured domain. Spike protein, similar to other viral fusion proteins, is heavily glycosylated, with 22 *N*-glycosylation and several *O*-glycosylation sites.

### 2.2. S1

Each chain of S1 subunit is beta-strand rich, with a massive N-terminal domain projected away from the central axis of the protein. The three NTDs form characteristic edges of the triangle when viewing from the top.[76] The backbone then continues in the direction of the stalk, turns up in a V-shape turn and continues through two minidomains (CTD1, CTD2) towards the apical RBD domain (Fig. 1). After doubling back through the minidomains, main chain reaches the furin cleavage site, roughly half way through the body of the spike. In an intact trimer, each NTD contacts the RBD of an adjacent monomer. All three RBDs are then packed against the central helical core.

**2.2.1 N-terminal domain.** The NTD consists of a galectin-like antiparallel beta sandwich fold, flanked from the top by two antiparallel beta strands and from the bottom by two beta sheets and a helix. NTD has extensive unstructured regions: first N-terminal residues as well as several loops, termed N1-N5 and encompassing residues 14 to 26, 67 to 79, 141 to 156, 177 to 186, and 246 to 260. N1-N5 can only be resolved when bound to neutralizing antibodies.[77] The overall organization is very similar to that of SARS-CoV-1[78] and MERS.[79] The precise role of the NTD has not been elucidated to date. Similarity to other viruses indicates a possibility of glycan (sialic acid) recognition,[80] which would allow the virus to retain partial attachment to the host cell while searching for ACE2 receptors. NTD is shielded by 8 glycosylation sites, which however allow for partial recognition by antibodies within at least two glycan-free antigenic supersites. Antibody binding involves reorganization and binding of the unstructured loops and potentially also glycans.[77,81,82] Unfortunately, the loops are not well conserved and seem to act as potent decoys of the immune system. Indeed, the variants of concern have multiple mutations in the NTD regions, thus turning this domain into an immune decoy and leading to an immune escape.[83,84]

**2.2.2 Receptor binding domain.** The RBD is a relatively compact structure, consisting of a 5-stranded antiparallel beta sheet. It can adopt either an 'up' or 'down' conformational state.[85] Up state can exist for one, two or three RBDs simultaneously,[86] facilitating binding of up to three ACE2 receptors. In a down state, all three RBDs make extensive contacts with one another and are tucked against CTD1 of 'self' protomers and NTDs of neighboring protomers. Close packing against the central helical core of S2 together with dense glycan coverage make RBD shielded from interactions with the immune system or ACE2. Transition to an up state facilitates binding of a peptidase domain of the human ACE2 receptor, particularly *via* Receptor Binding Motif (RBM) – an extended loop[87] which forms the majority of a binding site. The spike-ACE2 interface exploits a number of hydrogen bonds and salt brides stabilizing it and forming two strong flanks that can resist mechanical pulling.[88] In addition to protein contacts, the interface is flanked by both host and viral glycans. The ACE2 glycosylation at site N322 was suggested to increase the overall binding strength by binding to the RBD surface.[89] The interface itself was a subject to many mutations in the variants of concern, leading to increased affinity for ACE2,[90] which could potentially lead to affinity-driven immune escape[91] where receptor binding out-competes interactions with antibodies.

There are numerous antibody binding sites recognizing multiple epitopes present on the surface of RBD, confirming its dominant role in the immune response. They can either block the ACE2 binding,[92,93] interfere with essential conformations of the RBD domains or induce S1 dissociation.[94] Interestingly, in the recent Omicron variant, the proportion of all-RBD-down conformations is increased,[95] hinting to the increased masking of the RBD epitopes and explaining the immune evasion mechanism. Interestingly, high speed AFM of spike proteins deposited on mica revealed that RBDs can adopt very extended and dynamic conformations in which they can still bind to ACE2 receptors.[88] This dynamic behavior seems to enhance viral infectivity by allowing spike proteins to efficiently scan the cell surface for multiple ACE2 receptors. This behavior was abolished upon the removal of the key glycan, which is responsible for maintaining the RBD in its open conformation (N234Q).

**2.2.3 CTD1 and CTD2.** CTDs are beta-rich domains that form an elongated hinge between S1 and S2. Because of the direct involvement in the up-down transition, CTDs affect the dynamic equilibrium between up and down states, and thus affect balance of infectivity and susceptibility of the virus to the immune system.[96] Indeed, one of the first mutations that occurred and have been propagated with respect to the original Wuhan-1 strain was D614G in CTD2, which increases the rate of processing by furin and promotes the RBD-up state,[97] but can also affect the fusion peptide located in a direct proximity. Furthermore, CTD2 has been suggested as a regulator of S1–S2 dissociation, thus allowing spike protein to enter post-fusion state.[32] This makes the CTDs essential regulators for ACE2 binding, immune evasion and membrane fusion.

**2.2.4 Transition between closed and open states.** Since, as mentioned above, RBD can bind to ACE2 when the spike protein is in the open state, it is worth considering the transition between open (up) and closed (down) states in more detail (Fig. 2). This process is not driven but stochastic. Lu *et al.*[98] carried out smFRET experiments to understand the flexibility inherent in the SARS-CoV-2 RBD region and observed at least four distinct conformational states of the trimeric spike protein, including a ground state with three RBDs down (0.5-FRET), the receptor-activated-state with three RBDs up (0.1-FRET), and the initial receptor-binding conformations with one/two RBDs up (0.3-FRET). The 0.5-FRET ground state is the most abundant with about 38% occupancy compared to 22% for 0.1-FRET and 26% for 0.3-FRET, indicating the down state is more favorable. The occupancy of the 0.1-FRET up-conformation increases to 48% and 58%, respectively, in the presence of monomeric and dimeric ACE2 receptor, which supports the role of ACE2 as a receptor for virus entry. A noticeable shift in the conformational landscape of the spike protein from the ground state to the receptor-bound state was also confirmed by the Cryo-EM study.[99] Spike opening dynamics can be detected indirectly through a decrease in the rate of transition between the 0.1-FRET and 0.3-FRET states in the presence of ACE2.[98] The spike protein tends to dwell in ACE2-accessible RBD-up conformations, reflecting a larger

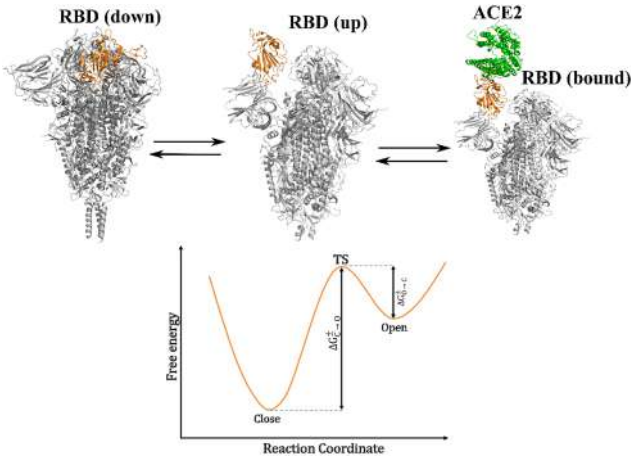


Fig. 2 (Upper) Down (close) state (PDB ID: 6XR8), up (open) state (PDB ID: 6VYB), and bound state (PDB ID: 6VYB and 6M0J), in which RBD is bound to ACE2. RBD can only bind to ACE2 when it is in the open state. The arrows indicate a reversible transition between different states. (Bottom) Free energy landscape of the close–open transition, TS refers to the transition state. The transition from the close state to the open state requires crossing the free energy barrier $\Delta G^{\ddagger}_{C\rightarrow O}$ which is higher than the reverse open–close barrier $\Delta G^{\ddagger}_{O\rightarrow C}$.

population of the up state in the presence of ACE2 as measured by smFRET. This observation has been employed to explain the increased binding affinity and increased kinetic stability of the spike protein interacting with the ACE2 receptor of various SARS-CoV-2 variants.[100]

Computationally, the molecular mechanism of RBD opening has been extensively studied using molecular dynamics (MD) simulations with enhanced sampling.[101–104] In a 0.1 second simulation, the one-up RBD states was found to be more favorable than the other open states.[102] The pathway from the one-up RBD to two-up RBD conformations was explored using generalized replica exchange MD,[105] which provides an atomistic picture of the conformational flexibility of the spike protein interacting with ACE2. Steered MD (SMD) in combination with umbrella sampling simulations was employed to show that RBD opening can be modulated though interactions in an allosteric pocket.[103] This allosteric pocket is adjacent to a double-stranded hinge region that links CTD1 and RBD and allows RBD to move between closed and open geometries.[106]

Using replica-exchange and umbrella sampling simulations, the minimum energy path connecting the down and up states was derived from the potential of mean force (PMF),[104] and in agreement with experiment,[98] the time of the down-up transition time is longer than the reverse transition. This means that the close–open free energy barrier $\Delta G^{\ddagger}_{C\rightarrow O}$ is higher than the open–close barrier $\Delta G^{\ddagger}_{O\rightarrow C}$ (Fig. 2). Combining normal mode analysis and umbrella sampling MD, the free energy barrier from ACE2-inaccessible to fully accessible states of SARS-CoV-2 with one RBD up, $\Delta G^{\ddagger}_{C\rightarrow O}$ was estimated to be $\approx$4.4 kcal mol$^{-1}$, which is greater than that of SARS-CoV-1 ($\approx$1.7 kcal mol$^{-1}$), demonstrating that SARS-CoV-2 is more difficult to be opened.[107] This conclusion was also confirmed by SMD and parallel cascade selection molecular dynamics studies.[108,109]

Moreover, free energy landscape analysis showed that in the active state SARS-CoV-2 is less stable than SARS-CoV-1[109] due to fewer interdomain salt bridges and hydrogen bonds of RBD in the up state,[101] suggesting the transient nature of the active state before binding to the host cell. This result partially supports the hypothesis that RBD hidden in the spike protein is likely to assist SARS-CoV-2 in maintaining efficient cell invasion while evading immune surveillance.[110] Together with the spike protein preactivation by furin, this property may contribute to the rapid spread of the virus.

In the closed state, RBD is extensively shielded by glycans, and it's only in the open state that the RBD emerges from this shielding.[111] Therefore, glycans play an essential role in the open–closed transition. Their contributions to the stability of the spike protein in closed and open conformations and to the modulation of the opening transition have been thoughtfully studied both in experiments and in MD simulations. Casalino *et al.*[111] disclosed the important role of glycans at positions N165 and N234 of the RBD in its conformational transitions and ACE2 recognition using all-atom MD simulations. Their result is supported by the biolayer interferometry experiment demonstrating that the N165A and N234A mutations that remove these *N*-glycans, substantially impaired binding to the host cell due to the RBD conformational shift towards the closed state. Contact analysis based on MD modeling showed that, in the open state, RBD maximizes interaction with neighboring NTD *via* hydrogen bonding to N165 and N122 glycans, resulting in increased stability of this state. In the presence of glycans, the opening barrier will increase by $\sim 7$ kcal mol$^{-1}$.[104] There is evidence of a gated role of the N343 glycan, which enhances RBD opening.[112,113] The influence of glycans on the closed-open conformational transition has been examined experimentally by glycan removing or mutation.[111,113]

### 2.3. S2

While S1 subunits are primarily responsible for host cell binding and protection of the fusion machinery, the alpha-helical core of the S2 subunits is essential for triggering the fusion of the viral envelope with the host cell, leading to the release of the genetic material. In the prefusion state, the FP directly adjacent to FPPR is perched below the neighbouring CTD2 and next to 'self' CTD1, forming a short helix (Fig. 1B). The stable core of the spike is formed by the central coiled–coil region packed together with HR1 region and forming a 9-helix bundle. The elongated beta-strand section of the CD is tucked between the helices, subsequently turns into a bulky beta-strand rich, heavily glycosylated region at the bottom of Spike. After that, it acquires a unique[114] right-handed coiled–coil structure[60] (typically the only part of the stalk visible in cryoEM reconstructions) which continues to the HR2 region. The HR2 portion of the stalk has not been resolved from averaged cryoEM reconstructions due to the flexibility of the stalk, however it remains visible at single tomogram level,[60] occasionally in a frayed form, suggesting low stability of HR2 which can be essential for the refolding into the post-fusion state. HR2 is connected to the TMD *via* a short and very conserved among coronaviruses[115] linker region, which resembles membrane proximal extended region (MPER) in HIV.[116] Indeed, recent NMR model[117] yield a suggestive tripod-like structure with an amphipatic helix that could interact with the membrane. MPER region of HIV is a target of broadly neutralizing HIV antibodies,[118] making this region of spike protein particularly interesting from the pan-coronaviral vaccine development perspective.[116] Recent preprint reports an extremely potent antibody targeting a quaternary epitope between the N1194 glycan and the membrane.[119] The TMD seems to be important during the initialization of the fusion process.[120,121] The TMD features a number of conserved cysteines grouped in four clusters. The post-translational modification of these sites with palmitylic acid was found to be essential for the Spike mediated cell fusion.[122] The C-terminal domain remains disordered[123] and seems to be important for the regulation of infectivity.[124]

Binding of ACE2 exposes the S2' site, allowing for cleavage and leaving FP as the new N-terminus of the S2[125] and complete shedding of S1.[76] Subsequently, FP is expected, like in the case of influenza fusion protein, to protrude axially towards host membrane,[126,127] where insertion *via* two amphipatic helices and strategically positioned disulfide bridge ensures stable anchoring.[128] Transition to a post-fusion state converts the S2 into an elongated (180 Angstrom long) club-like structure composed of a HR1 and CH forming one continuous alpha-helix[76] (Fig. 1D). HR2 forms a supplementary helix, which binds to a groove between monomers within the CH-HR1 junction. Next, S2 refolds into a six-helix bundle *via* a proposed 'jack-knife' mechanism and pulls host membrane towards viral envelope to initialize fusion.[129]

### 2.4. Glycosylation

Glycosylation is a post-translational or co-translational covalent addition of a polysaccharide chain to the protein, and mainly occurs as *N*-glycosylation (attached to the nitrogen of an Asparagine in a Asn-X-Ser/Thr consensus sequence) or *O*-glycosylation (attached to an oxygen atom of Serine/Threonine). Glycosylation occurs mainly in Golgi apparatus and is template-free, with the final composition of a glycan depending on the accessibility of a given glycosylation site on protein surface and availability of glycosyl transferases, leading to macroheterogeneity (presence/absence of a glycan) and microheterogeneity (the variability of a composition of a glycan). Beyond specialized glycan-binding proteins, glycans do not interact strongly with proteins, which increases the solubility of glycoproteins and makes glycans commonly used as folding aid and protein synthesis quality control, which is also true for spike protein.[130] Glycans decorate the majority of membrane and secreted proteins, which makes them poor epitopes, generally recognized by the immune system as ''self''. Enveloped viruses exploit this fact and heavily glycosylate their fusion proteins to evade the immune system, delaying the host immune response and hampering the development of successful vaccines, like *e.g.* in the case of HIV.[131] Dense glycosylation restricts the access of the glycotransferases in the ER and Golgi,

resulting in incomplete glycan processing and oligomannose-type glycosylation. The presence of such glycans is a strong indicator of dense glycan shield and thus efficient masking of the underlying epitopes.[132] SARS-CoV-2 spike features 22 conserved *N*-glycosylation sites and 17 *O*-glycosylation sites,[133–135] providing nearly uniform coverage of the spike protein with the exception of RBD and furin cleavage sites (Fig. 1A–C). The furin cleavage itself seems to be downregulated by the presence of an *O*-glycan (T676 and 678).[136] Mutations of neighbouring P681 in the transmissive alpha and delta variants abrogate these *O*-glycosylations and thus increase cleavage by furin.

In solution, glycans remain very flexible, exploring multiple conformations at a nanosecond time scale. This means, that despite discrete localization of the glycosylation sites, their effect on protein–protein interaction (and antibody) shielding is much broader. Conformational freedom of the glycans can be limited by the shape of the protein. For example, only glycans heavily restrained in their motion can be traced in experimental electron density maps, like in the case of N234, whose conformational freedom is strongly reduced by its location in a narrow cleft.[73] On the contrary, if extensive branched glycan structures can move freely, they are averaged out in the structural studies. The best example here is the typically large, 4-antennary, sialylated glycan at the position N1194, which remains poorly visible in cryoET reconstructions.[60] The dynamics of this particular glycan seems to be important in the context of shielding of epitopes on HR2 and membrane-proximal regions affect the dynamics of the stalk. Interestingly, the HR2 glycans retain their shielding role in the post-fusion state[76] and (Fig. 1D). Protein shape and glycan density influence the accessibility for transferases, influencing the type of the glycan that can be synthesized at given site and leading to heterogeneity. This can have critical implications for vaccine constructs, as they are typically produced in expression systems, which differ from human tissues, typically present truncated variants, where glycosylation site accessibility can be much higher, resulting in more finely processed glycans.[132,137]

Atomistic MD simulations[60,111,113,138] as well as simplified approaches[72] have been used to bridge this gap, revealing that large swathes of S-protein surface are partially or fully covered by glycans. This dynamic shield seems to focus the action of the immune response to a number of unshielded sites[71] (Fig. 1C).

The range of expression systems used in the vaccine construct generation as well as computational predictions suggest that the precise type of the glycan is much less important than its presence/absence on a site.[139,140] Glycans also affect the conformational state of the spike: N165, N234 and N343 glycans were shown to modulate the fraction of RBD-up conformation,[112,113] with clear dependence on the glycan size. The recently lost and otherwise highly conserved N370[141] seems to be a novel adaptation of the SARS-CoV-2, leading to higher fraction of the RBD-up state and therefore increased infectivity. Despite constantly emerging new variants, glycosylation sites in SARS-CoV-2 have been preserved, with a notable exception of the delta variant, which lost N17 glycosylation site, and the gamma variant, which includes two new glycosylation sites: N20 and N188, potentially contributing to the increased infectivity. Interestingly, these two sites are not completely novel as they have been observed in other sarbecoviruses.[142] Additional *O*-glycosylation site was also observed in Omicron at T376. How these additional or altered sites contribute to the epitope masking and immune escape remains poorly understood.

Beyond spike protein glycosylation, interaction of the spike protein with glycocalyx, a dense mesh of extracellular proteoglycans remains an area of intense studies. Spike protein binding to the host cell has been shown to depend on the formation of a ternary complex with ACE2 and heparan sulfate, main component of the glycocalyx, a property used by commercially available diagnostic tools. The binding could potentially occur in many positively charged clefts on the spike protein surface, on RBD, NTD or furin cleavage site, with binding affinity increasing in the new variants.

### 2.5. Comparison with the SARS-CoV-1

Structurally, SARS-CoV-2 is very similar to its predecessor and cause of the 2002–2004 pandemic–SARS.[73,143] The S2 and related fusion machinery seems to retain a high degree of similarity, compared to S1 ($\sim$90% *vs.* $\sim$60%),[144] with SARS-CoV-2 using the same receptor to enter the host cells as SARS-CoV-1,[66] although exploiting a set of different amino acid contacts at the interface.[145,146] This change results in an order of magnitude higher binding affinity for SARS-CoV-2.[75] The RRAR furin cleavage site at the junction of S1/S2 is absent in SARS-CoV-1, likely reducing its transmissibility.[147]

The glycosylation pattern of SARS-CoV-2 retains key specifics of its predecessor. As a general trend in sarbecoviruses,[142] glycans located on S1 are much more variable. This is reflected in identical glycosylation pattern within S2, and three glycosylation S1 sites that differ between these two viruses: N30 and N370 were removed in SARS-CoV-2 and N74 is a novel glycosylation site only present in SARS-CoV-2. The character of the glycans at corresponding sites is mainly preserved, with a notable exception of N61 and N165, which shifted from oligomannose type in SARS-CoV-1 to mainly complex in SARS-CoV-2, indicating local change in protein structure that resulted in an increased accessibility to transferases in SARS-CoV-2.[142]

### 2.6. Two distinct SARS-CoV-2 entry pathways and life circle of the virus

Entry pathways and triggering factors of various enveloped viruses were summarized in White and Whittaker.[148] Generally, viral entry proteins must undergo structural modification that generates sufficient energy to overcome the natural repulsion between the virus and cell membranes. In the case of SARS-CoV-2, the spike protein converts to a metastable state, which tends to transformation to a lower energy state, before membrane fusion. As with other coronaviruses, this transition undergoes two crucial cleavage steps after binding to ACE2. These two cleavage steps have been demonstrated to be necessary for membrane fusion.[149] The first of them is enabled at the S1–S2 boundary, and the second is enabled in the S2′ site in

 

subunit S2. For SARS-CoV-1, both sites are cleaved by proteases of the target cell. However, for SARS-CoV-2, although target cell proteases are still needed to cleave S2, furin cleaves the S1–S2 junction. More precisely, the Arg–Arg–Ala–Arg motif available at this junction is cleaved by furin. A similar motif has not been observed in SARS-CoV-1,[150] which partially explains why a furin-like cleavage site is absent in this virus. After furin cleavage the S1 subunit can be easily shed from the S2 subunit as they are linked by non-covalent bonds. This is in contrast to other viruses such as avian influenza and HIV-1, whose entry glycoproteins are cleaved by furin but not destabilized.

For both SARS-CoV-1 and SARS-CoV-2, the second step of proteolytic cleavage, which occurs at S2′ in the S2 subunit, follows two different pathways depending on the target cell proteases involved. In the first pathway, the process takes place in the endosome and is triggered by cathepsin L of the host cell (Fig. 3). In the second pathway, the TMPRSS2-mediated cleavage directly occurs at the plasma membrane, because TMPRSS2 is present on the cell surface. Thus, after binding to host cells, coronavirus can enter them either through the plasma membrane or through endosomes depending on cell type and protease availability.[32,66,151,152]

After membrane fusion, the viral genome enters the host cell, triggering viral replication, which includes several processes such as RNA translation, RNA replication, and protein production (Fig. 3). As a result, a new virion is formed and released from the cell, completing the life cycle of the virus.

# 3. Interaction of SARS-CoV-2 spike protein with human ACE2

## 3.1. ACE2 structure and its binding interface with RBD

**ACE2: structure and function.** ACE2 is a receptor for many corona viruses.[154–156] ACE2 was originally identified in 2003 as the receptor for SARS-CoV-1.[157] In particular, the SARS-CoV-2 virus also uses ACE2 as a receptor for binding to the host cell membrane, which is the first step in host cell invasion.[65,87,158–160] The renin–angiotensin system play an important role in cardiovascular, renal function and stability of pulmonary epithelial membranes.[161] ACE2 can convert angiotensin I and angiotensin II to angiotensin 1–9 and angiotensin 1–7, respectively.[162,163] The binding of the virus to the host cell reduces concentration of free ACE2,[164] leading to an increase in the concentration of angiotensin I and angiotensin II. These elevations have effects on aggravation of respiratory distress and hypokalemia in COVID-19 patients.[165,166]

ACE2 comprises of 805 residues, including a signal peptide of 17 residues at the N-terminus, a peptidase domain (PD) (residues 19–615) involving a zinc-binding metalloprotease motif, a C-terminal collectrin like domain (residues 616–768), a transmembrane domain of 22 residues and intracellular C-terminus.[167] The RBD of SARS-CoV-1 and SARS-CoV-2 binds to ACE2 PD and the structure of the RBD-ACE2 PD (hereinafter RBD-ACE2) was resolved experimentally[74,87,168] (Fig. 4) and has been widely used in computational studies. The ACE2-RBD binding surfaces of SARS-CoV-1 and SARS-CoV-2 are concave

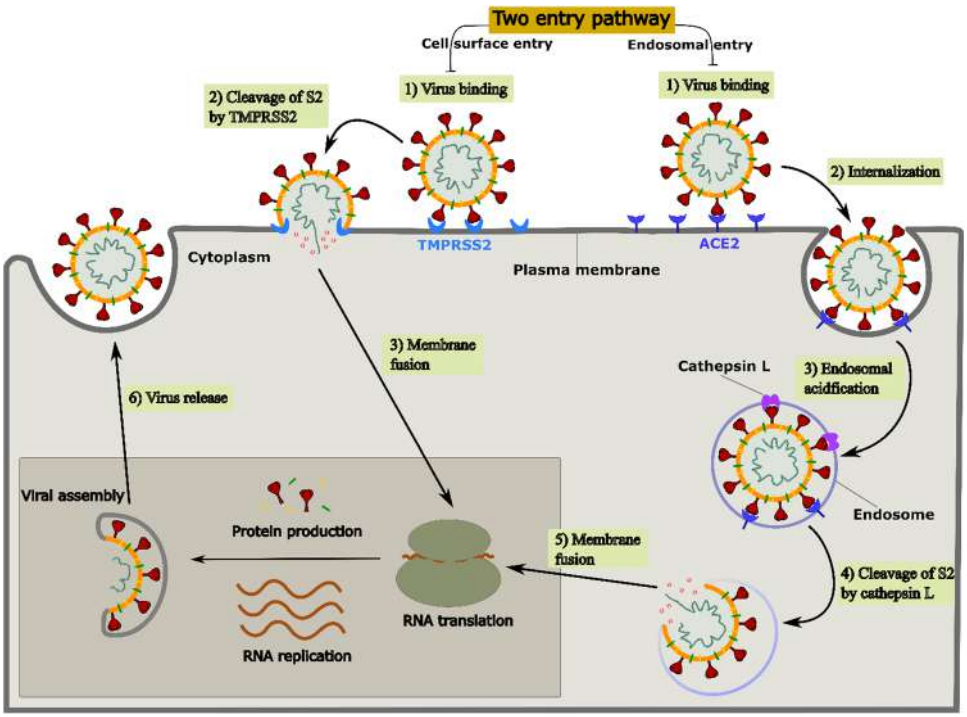


Fig. 3 Two routes of entry for SARS-CoV-2 and viral life circle. After virus binding to the host cell, in the endosomal pathway, S2 is cleaved by cathepsin L, while in the cell surface pathway, TMPRSS2 is called to cleave S2. Some parts of this plot were made following ref. 32 and 153.

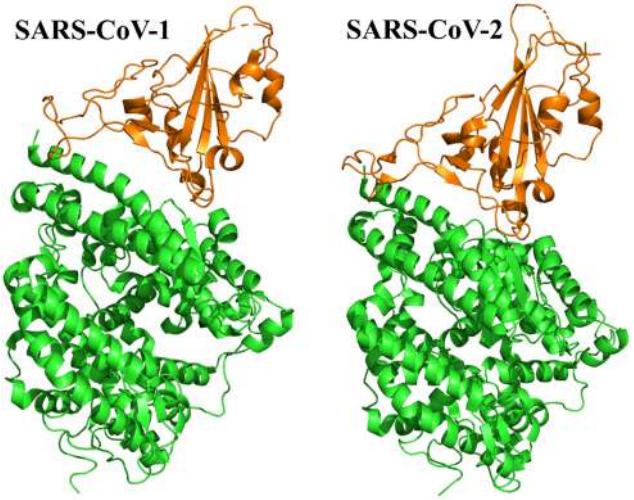


Fig. 4 Structures of the complex of ACE2 with SARS-CoV-1 RBD (PDB ID: 2AJF) and SARS-CoV-2 RBD (PDBID: 6VW1). Orange and green colors refer to RBD and ACE2, respectively.

and highly similar.[87] More information about ACE2 can be found in a recent review.[169]

### 3.2. Experiments on the ACE2-RBD association

**3.2.1. AFM experiment and binding free energy landscape.** Nowadays, single molecule force spectroscopy experiments are widely used to understand the structure and function of biomolecules and their interactions through their response to an external force.[170] Among them, the atomic force microscopy (AFM) is effective for probing the binding properties of protein–ligand and protein–protein complexes, because the mechanical force required for their dissociation is $\sim$100 pN.

The typical AFM setup to study the unbinding of the spike protein from ACE2 is shown in Fig. 5A. A external force is applied to the spike protein through the cantilever and the force experienced by the pulled protein is $k\delta x$, where $k$ is the cantilever stiffness and $\delta x$ is a cantilever bending detected by the laser. The stability of the complex can be characterized by the rupture force, which is the maximum force $F_{max}$ on the force-extension/time profile, obtained by AFM with a constant pulling speed (Fig. 5B).[171] The higher the $F_{max}$, the higher the binding affinity. Based on this hypothesis and the results obtained for SARS-CoV-2 RBD-ACE2 and SARS-CoV-1 RBD-ACE2 Cao *et al.*[172] predicted that SARS-CoV-2 binds to host cells more strongly than SARS-CoV-1, which is consistent with surface plasmon resonance data.[73] In addition, their AFM experiment showed that glycans enhance the binding affinity of coronaviruses.

In AFM experiments[88,173,174] with constant pulling speed $v$ or constant loading rate, $F_{max} \sim \ln(v)$[175] (Fig. 5C). Yang *et al.*[173] applied constant force-distance based AFM to monitor unbinding events of the RBD-ACE2 complex and observed single interactions from the distribution of the rupture force. This allows describing the binding of RBD-ACE2 complex as a two-state process and constructing the free energy landscape where the bound state is separated from the unbound state by a single energy barrier located at a distance $x_u$ (Fig. 5D).

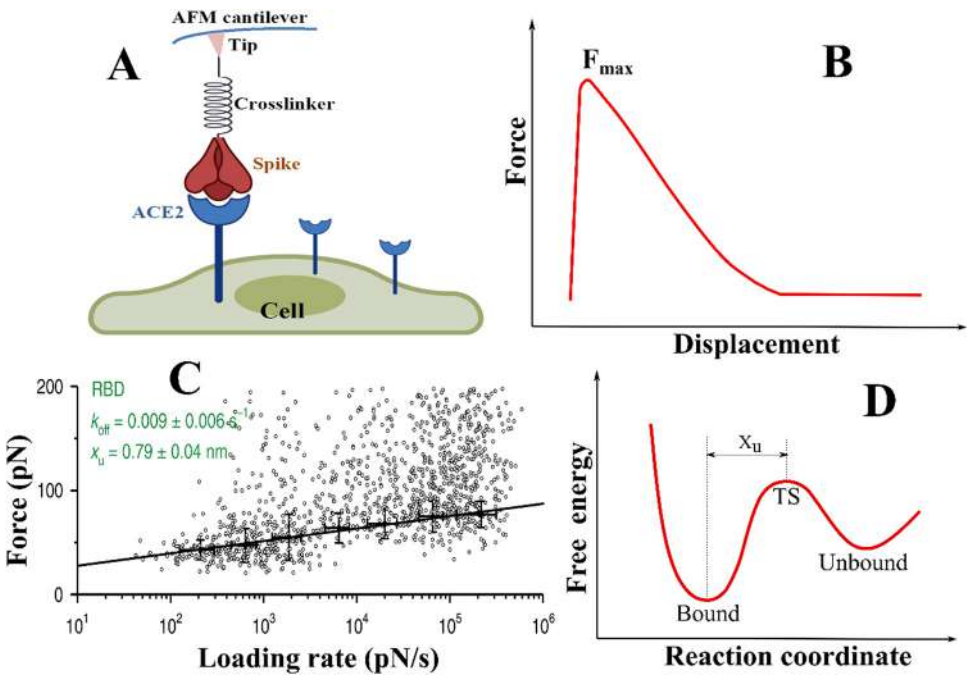


Fig. 5 (A) AFM setup to detach the spike protein from an immobilized ACE2 of the human cell. (B) Typical dependence of the force experienced by a pulled molecule on its displacement from the initial position. (C) The dependence of force on loading rate or pulling speed, which was obtained by Yang *et al.*[173] (D) Free energy landscape, where the bound state is separated from the unbound state by a transition state (TS) and $X_u$ is the distance between the bound state and TS.

 

Using Bell–Evans equation $\tau^{-1} = k_{off}$. $e^{x_u f/k_B T}$[175,176] to fit data representing the dependence of unbinding time $\tau$ on the applied force $f$, Yang *et al.*[173] obtained the distance between the bound and transition states $x_u = 0.79 \pm 0.04$ nm. The fit also yields a kinetic off-rate $k_{off}$ of $0.009 \pm 0.006$ $s^{-1}$, which is in good agreement with the value obtained using the surface plasmon resonance technique ($0.008$ $s^{-1}$). A high value of $x_u$ ($\approx$ 1.7 nm) was reported by Zhu *et al.*,[88] suggesting that the difference in this distance may be due to different experimental conditions of different groups. It seems that $x_u$ is not sensitive to different variants.[177] The single molecule method has also been used to investigate the binding of SARS-CoV-2 to C-type lectin receptors, revealing a mechanism different from ACE2.[178]

**3.2.2. Other experiments: determination of the dissociation constant $K_D$.** For experimental study of the stability of protein–protein complexes, such as ACE2-RBD, surface plasmon resonance (SPR), biolayer interferometry (BLI), and fluorescence flow cytometry (FFC) are used (Table 1). Among them, SPR and BLI are more common than FFC. These methods allow for determining the dissociation constant $K_D$, which can be used as a measure of binding affinity: the lower the $K_D$, the higher the binding affinity or stability of the complex. Dynamic force spectroscopy (DFS) has also been used to estimate $K_D$.[174]

Experimental data from various groups show that the spike protein of both SARS-CoV-1 and SARS-CoV-2 binds strongly to human ACE2 with nanomolar (nM) dissociation constant (Table 1). This strong binding may be responsible for the high infectivity and rapid spread of these viruses. Using the relation $\Delta G_{bind} = -k_B T \ln(K_D)$, where $K_D$ is measured in $M$, we obtain the binding free energy of the SARS-CoV-2 RBD-ACE2 complex $\Delta G_{bind} \sim -9 \div -12$ kcal $mol^{-1}$ at room temperature (Table 1). For the SARS-CoV-1 $\Delta G_{bind} \sim -9 \div -11$ kcal $mol^{-1}$, suggesting that the old variant binds to human cells weaker than the new one. However, since different groups used different experimental methods and conditions to compare their binding affinity, results obtained by the same group should be compared. Using SPR Wrapp *et al.*,[158] Kirchdoerfer *et al.*[179] and Lei *et al.*[180] demonstrated that SARS-CoV-2 binds to the host cell more strongly than SARS-CoV-1 (Table 1). The same trend was observed by Walls *et al.*[65] and Shang *et al.*[74] but the difference in the dissociation constants of the two variants is less pronounced. The higher binding affinity of SARS-CoV-2 is associated with more contacts between ACE2 and RBD compared to the case of SARS-CoV-1.[181] One of the consequences of this biophysical effect is that SARS-CoV-2 infects and spreads faster than SARS-CoV-1.

### 3.3. Computational methods for estimating binding affinity of SARS-CoV-2 – ACE2 complex

**3.3.1. Steered MD simulations.** Computationally, steered molecular dynamics (SMD) simulation was first designed to understand AFM experiment on dissociation of the streptavidin–biotin complex under the external mechanical force.[204] In the case of RBD-ACE2, a spring with stiffness $k$ is attached to a dummy atom on one side and to RBD on the other side[181] (Fig. 6A). Then the dummy atom is pulled with a speed $v$, along the direction which maximizes the number of hydrogen bonds between RBD and ACE2. The force acting on the system at time t is calculated as $F = k(\Delta z - vt)$, where $\Delta z$ and $vt$ are the displacements of the pulled atom and dummy atom along the pulling direction, respectively. This equation provides an easy way to obtain the force profile along the unbinding reaction pathway and characterize major steps in the rupture process by measuring $\Delta z$ alone.

In principle, by combining SMD with Jarzynski's equality,[181] the absolute binding free energy can be estimated if the pulling is slow enough and the number of SMD trajectories is sufficiently large to have good sampling. However, for relatively large complexes, such as RBD-ACE2, this approach is not computationally feasible due to the limited current computational facilities. Hence, the rupture force $F_{max}$, or the work done by a pulled chain, is used to characterize the relative binding affinity, *i.e.* these quantities are useful in discerning strong binders from weak ones.[181]

Using the AMBER-f99SB-ILDN force field, TIP3P water model and a pulling speed $v = 0.5$ nm $ns^{-1}$, Nguyen *et al.*[181] obtained $F_{max} \approx 751$ and 588 pN for SARS-CoV-2 RBD-ACE2 and SARS-CoV-1-RBD-ACE2, respectively (Fig. 6B). This result agrees with surface plasmon resonance[73] and AFM[172,173] experiments, as well as with other SMD simulations,[172] according to which the new virus interacts with host cells more strongly than the old one.

SMD is useful in predicting the relative binding affinity of different variants that are relevant to the evolution of the SARS-CoV-2[205] and in providing mechanistic insights into the interactions between antibodies with the virus.[206–208]

**3.3.2. End-point approaches.** MM-PBSA/GBSA, linear interaction energy (LIE), called end-point methods, are widely used to study protein–protein interactions because they are reasonable in terms of trade-off between computational overhead and efficient prediction of binding affinity. In the LIE method, a scoring function for calculating the protein–ligand binding free energy was developed by combining MD simulations and experimental data.[209] Binding affinity is approximated linearly as the sum of the Val der Waals (VdW) and electrostatic energy differences between the intermolecular interactions of ligand and its environment in the bound state (interact with the solvated receptor) and in the free state (interact only with the solvent). Namely, the binding free energy $\Delta G$ bind = $\alpha(\langle E_{vdW}^{bound}\rangle - \langle E_{vdW}^{free}\rangle) + \beta(\langle E_{elec}^{bound}\rangle - \langle E_{elec}^{free}\rangle) + \gamma$, where $E_{vdW}$ and $E_{elec}$ refer to the van der Waals and electrostatic interaction. Empirical coefficients $\alpha$, $\beta$, $\gamma$ have been trained based on experimental data depending on different target systems.[210]

To predict the binding affinity between ACE2 and SARS-CoV-2 variants,[211] empirical parameters were trained using a set of $K_D$ values obtained from yeast surface display titration for 43 spike RBD variants.[212] The relative binding energies $\Delta\Delta G$ predicted by LIE correlated reasonably with $K_D$ measured by surface plasmon resonance for WT, Alpha, Beta, and Gamma, since the corresponding correlation coefficient $R^2$ is 0.88.[213]

Table 1 Experimental data for the dissociation constant $K_D$ of the complex of human ACE2 with RBD of SARS-CoV-1 and SARS-CoV-2. The results were obtained by various methods shown in the last column. The experimental binding free energy $\Delta G_{bind}$ was extracted from $K_D$ using the relation $\Delta G_{bind} = k_B T \ln(K_D)$, where $K_D$ is measured in M and $T$ = 300 K

| Ref. | Part of spike protein | $K_D$ (nM) | $\Delta G_{bind}$ (kcal mol$^{-1}$) | Method |
|---|---|---|---|---|
| SARS-CoV-1 Wildtype | | | | |
| Wrapp *et al.*[158] | RBD-SD1 | 325.8 | −8.90 | SPR |
| Kirchdoerfer *et al.*[179] | Ectodomain | 185.1 | −9.24 | SPR |
| Walls *et al.*[65] | Ectodomain | 5.0 ± 0.1 | −11.39 ± 0.01 | BLI |
| Lei *et al.*[180] | Whole spike | 177.1 | −9.27 | SPR |
| Shang *et al.*[74] | RBD | 185 | −9.24 | SPR |
| SARS-CoV-2 Wild type | | | | |
| Wrapp *et al.*[158] | Ectodomain | 14.7 | −10.75 | SPR |
| | RBD-SD1 | 34.6 | −10.24 | SPR |
| Walls *et al.*[65] | Ectodomain | 1.2 ± 0.1 | −12.25 ± 0.05 | BLI |
| Lei *et al.*[180] | Whole spike | 11.2 | −10.91 | SPR |
| Liu *et al.*[182] | RBD | 5.77 | −11.31 | SPR |
| Shang *et al.*[74] | RBD | 44.2 | −10.09 | SPR |
| Supasa *et al.*[183] | RBD | 75.1 | −9.78 | BLI |
| Cameroni *et al.*[184] | RBD | 60.0 ± 1.4 | −9.91 ± 0.01 | SPR |
| Zhang *et al.*[185] | RBD | 13.2 | −10.81 | SPR |
| Chan *et al.*[186] | RBD | 22 (ACE2 dimer) | −10.51 | BLI |
| Dejnirattisai *et al.*[187] | RBD | 7.3 | −11.17 | SPR |
| Tian *et al.*[188] | RBD | 8.3 ± 0.25 | −11.09 ± 0.02 | SPR |
| | RBD | 56.9 ± 16.0 | −9.95 ± 0.17 | BLI |
| Yin *et al.*[189] | RBD | 75.5 ± 2.1 | −9.78 ± 0.02 | SPR |
| | Ectodomain | 14.7 ± 4.9 (ACE2 monomer)<br>2.7 ± 1.4 (ACE2 dimer) | −10.75 ± 0.20<br>−11.76 ± 0.31 | |
| Wang *et al.*[190] | Whole spike | 5.20 | −11.37 | SPR |
| Han *et al.*[191] | RBD | 26.34 ± 1.10 | −10.4 ± 0.02 | SPR |
| Zhang *et al.*[192] | Whole spike | 40.1 ± 3.9 | −10.15 ± 0.06 | BLI |
| Barton *et al.*[193] | RBD | 62.6 ± 7.7<br>74.4 ± 4.0 | −9.89 ± 0.07<br>−9.79 ± 0.03 | SPR |
| Yang *et al.*[194] | Whole spike | 3.1 | −11.68 | BLI |
| Collier *et al.*[195] | RBD | 133 | −9.44 | BLI |
| Laffeber *et al.*[196] | RBD | 17 ± 0.6 | −10.67 ± 0.02 | SPR |
| Zhang *et al.*[197] | Whole spike | 19.6 ± 2.5 (ACE2 dimer)<br>288.0 ± 5.1 (ACE2 monomer) | −10.58 ± 0.08<br>−8.98 ± 0.01 | BLI |
| | RBD | 15.5 ± 1.3 (ACE2 dimer)<br>256.0 ± 6.4 (ACE2 monomer) | −10.72 ± 0.05<br>−9.05 ± 0.01 | BLI |
| McCallum *et al.*[198] | RBD | 78 ± 8<br>147 ± 3 | −9.76 ± 0.06<br>−9.38 ± 0.01 | SPR<br>BLI |
| Wang *et al.*[199] | Ectodomain | 87 | −9.64 | BLI |
| Mannar *et al.*[200] | Ectodomain | 7.36 | −11.11 | BLI |
| Bayarri-Olmos *et al.*[201] | RBD | 17 | −10.66 | BLI |
| Koehler *et al.*[174] | RBD | 134 ± 81 | −9.43 ± 0.36 | Dynamic force spectroscopy |
| Cui *et al.*[202] | RBD | 68.3 | −9.83 | SPR |
| SARS-CoV-2 Alpha variant | | | | |
| Dejnirattisai *et al.*[187] | RBD | 1.5 | −12.11 | SPR |
| Tian *et al.*[188] | RBD | 0.5 ± 0.01 | −12.76 ± 0.01 | SPR |
| | RBD | 13.1 ± 3.8 | −10.82 ± 0.17 | FFC, ACE2 on cell surface |
| Cao *et al.*[203] | RBD | 4.8 | −11.42 | SPR |
| Han *et al.*[191] | RBD | 3.64 ± 0.13 | −11.58 ± 0.02 | SPR |
| Yang *et al.*[194] | Whole spike | 1.36 | −12.17 | BLI |
| Collier *et al.*[195] | RBD | 22 | −10.51 | BLI |
| Laffeber *et al.*[196] | RBD | 2.4 ± 0.4 | −11.77 ± 0.10 | SPR |
| McCallum *et al.*[198] | RBD | 15.0 ± 0.4<br>26 ± 4 | −10.74 ± 0.02<br>−10.41 ± 0.09 | SPR<br>BLI |
| Mannar *et al.*[200] | Ectodomain | 5.01 | −11.39 | BLI |
| Bayarri-Olmos *et al.*[201] | RBD | 2.23 | −11.87 | BLI |
| Koehler *et al.*[174] | RBD | 129 ± 81 | −9.45 ± 0.37 | Dynamic force spectroscopy |
| SARS-CoV-2 Beta variant | | | | |
| Dejnirattisai *et al.*[187] | RBD | 3.2 | −11.66 | SPR |
| Tian *et al.*[188] | RBD | 0.5 ± 0.01 | −12.76 ± 0.01 | SPR |
| | RBD | 45.2 ± 13.9 | −10.08 ± 0.18 | FFC, ACE2 on cell surface |
| Cao *et al.*[203] | RBD | 13.5 | −10.80 | SPR |

 

Table 1 (*continued*)

| Ref. | Part of spike protein | $K_D$ (nM) | $\Delta G_{bind}$ (kcal mol$^{-1}$) | Method |
|---|---|---|---|---|
| Han *et al.*[191] | RBD | 8.10 ± 0.06 | −11.10 ± 0.01 | SPR |
| Barton *et al.*[193] | RBD | 17.4 ± 3.1 | −10.65 ± 0.11– | SPR |
| | | 20.0 ± 0.7 | −10.57 ± 0.02 | |
| Laffeber *et al.*[196] | RBD | 5.8 ± 0.8 | −11.30 ± 0.08 | SPR |
| Mannar *et al.*[200] | Ectodomain | 3.9 | −11.54 | BLI |
| Koehler *et al.*[174] | RBD | 80 ± 49 | −9.74 ± 0.36 | Dynamic force spectroscopy |
| SARS-CoV-2 Gamma variant | | | | |
| Dejnirattisai *et al.*[187] | RBD | 2.4 | −11.83 | SPR |
| Cao *et al.*[203] | RBD | 16.7 | −10.67 | SPR |
| Han *et al.*[191] | RBD | 5.16 ± 0.04 | −11.37 ± 0.01 | SPR |
| Barton *et al.*[193] | RBD | 12.2 ± 3.4 | −10.86 ± 0.17 | SPR |
| | | 13.5 ± 0.45 | −10.80 ± 0.02 | |
| Zhang *et al.*[197] | Whole spike | 2.4 ± 0.3 (ACE2 dimer) | −11.83 ± 0.07 | BLI |
| | | 14.8 ± 0.2 (ACE2 monomer) | −10.75 ± 0.01 | |
| | RBD | 8.8 ± 0.6 (ACE2 dimer) | −11.05 ± 0.04 | |
| | | 124 ± 2 (ACE2 monomer) | −9.48 ± 0.01 | |
| Mannar *et al.*[200] | Ectodomain | 3.58 | −11.59 | BLI |
| Koehler *et al.*[174] | RBD | 21 ± 16 | −10.54 ± 0.45 | Dynamic force spectroscopy |
| SARS-CoV-2 Delta variant | | | | |
| Dejnirattisai *et al.*[187] | RBD | 4.9 | −11.40 | SPR |
| Cao *et al.*[203] | RBD | 10.9 | −10.93 | SPR |
| Zhang *et al.*[197] | Whole spike | 176 ± 56 (ACE2 dimer) | −9.27 ± 0.19 | BLI |
| | | 208 ± 6 (ACE2 monomer) | −9.17 ± 0.02 | |
| | RBD | 7.7 ± 0.6 (ACE2 dimer) | −11.13 ± 0.05 | BLI |
| | | 199 ± 4.5 (ACE2 monomer) | −9.20 ± 0.01 | |
| McCallum *et al.*[198] | RBD | 63 ± 3 | −9.88 ± 0.03 | SPR |
| | | 180 ± 30 | −9.26 ± 0.10 | BLI |
| Wang *et al.*[199] | Ectodomain | 41 | −10.14 | BLI |
| SARS-CoV-2 Omicron variant | | | | |
| Dejnirattisai *et al.*[187] | RBD | 7.8 | −11.13 | SPR |
| Yin *et al.*[189] | RBD | 38.9 ± 10.5 | −10.17 ± 0.16 | BLI |
| | Ectodomain | 2.5 ± 0.6 (ACE2 monomer) | −11.80 ± 0.14 | BLI |
| | | 0.3 ± 0.2 (ACE2 dimer) | −13.07 ± 0.40 | |
| Wang *et al.*[190] | Whole spike | 2.10 (BA.1) | −11.91 | SPR |
| | | 2.21 (BA.2) | −11.88 | |
| | | 2.36 (BA.2.12.1) | −11.84 | |
| | | 2.79 (BA.1.1) | −11.74 | |
| | | 1.66 (BA.4, BA.5) | −12.05 | |
| Zhang *et al.*[192] | Whole spike | 8.3 ± 0.3 (BA.1) | −11.09 ± 0.02 | BLI |
| Cui *et al.*[202] | RBD | 24.4 (BA.1) | −10.45 | SPR |

Like LIE, the solvated interaction energy (SIE) method also uses a parameter fitting procedure for energy terms.[214,215] The disadvantage of this method is the use of MD simulation with the AMBER force field to test the performance of optimal parameters without extending to other force fields.[214] SIE has been used to study the transmission of SARS-CoV-2 and SARS-CoV-1 at different ambient temperatures. Consistent with MM-PBSA results, SIE confirmed a stronger binding of SARS-CoV-2 to ACE2 in a temperature range of 200–350 K compared to SARS-CoV-1.[216] This result is also consistent with experiment at room temperature[73] (see also Table 1). SIE predicted the binding affinity of WT SARS-CoV-2 RBD to ACE2 (−13.75 ± 0.02 kcal mol$^{-1}$),[217] in good agreement with experiments (Table 1) and a reasonably increased binding affinity of ∼1.3 kcal mol$^{-1}$ due to N501Y mutation. However, it overestimated the impact of other important mutations, such as E484K, L452R, T478K, and failed to describe the impact of mutations at residue K417 on the binding affinity.[193,196]

MM-PBSA and MM-GBSA[218,219] are often used to access docking pose, structural stability, and predict binding affinities and hotspots. In addition to deriving the binding energy, the advantage of MM-PBSA and MM-GBSA is that they allow the analysis of the contributions of individual residues or energy terms using free energy decomposition analysis, which gives detailed residue-specific energy contributions to the binding of the system and identifies dominant interactions during the binding process and thereby facilitates the design of systems with the desired binding affinity. In MM-PB/GBSA, the binding free energy of a receptor–ligand or protein–protein complex is estimated as the difference between the free energy of the bound complex and the free energy of the unbound components.

In practice, MD simulation is carried out only for a bound complex, and the free binding energy is calculated as follows:

$$\Delta G_{bind} = \Delta E_{elec} + \Delta E_{vdW} + \Delta G_{polar} + \Delta G_{nonpolar} - T\Delta S \quad (1)$$

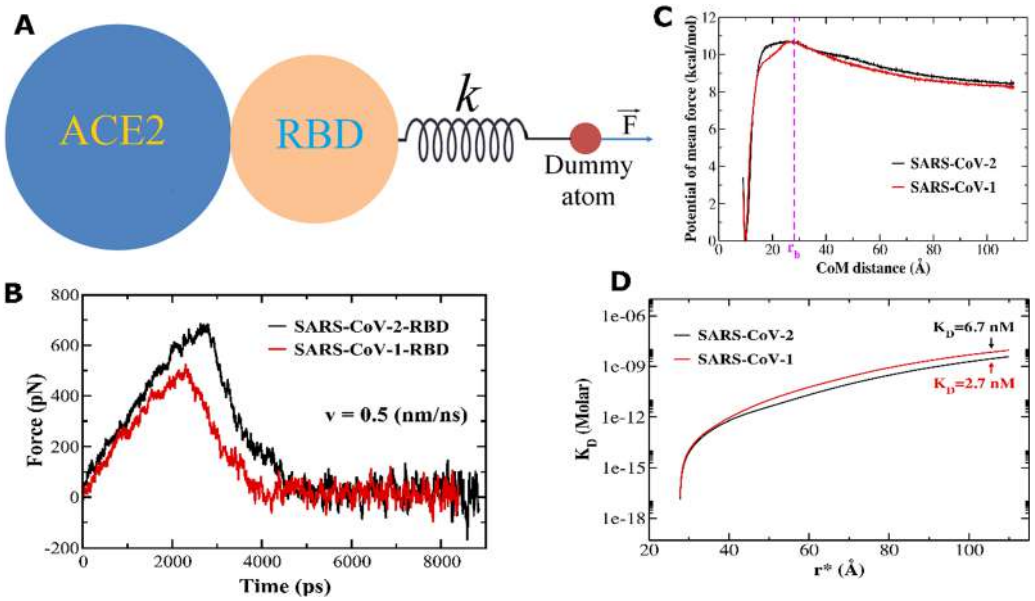


Fig. 6 (A) A typical setup for SMD simulation to mimic an AFM experiment: an external force is applied to a dummy atom connected to RBD through a spring with a spring constant of $k$, while ACE2 is fixed. (B) Force-time profiles derived from all-atom SMD simulations for SARS-CoV-2 and SARS-CoV-1. (C) One-dimensional potential of mean force of SARS-CoV-1 (black) and SARS-CoV-2 (red). The distance $r_b$ that separates the bound and unbound regions is used for calculating $K_D$ (eqn (3)–(5)). (D) Dependence of $K_D$ on the maximum radius $r^*$ corresponding to the volume $V(r^*)$ where free monomers can exist. $K_D$ was obtained at $r^*$ = 105 Å using eqn (3).[181]

which is the sum of the electrostatic ($\Delta E_{elec}$) and van der Waals ($\Delta E_{vdW}$) interaction energies, the solvation energy of the polar ($\Delta G_{polar}$) and nonpolar ($\Delta G_{nonpolar}$) components, and the change in conformational entropy ($-T\Delta S$). The non-polar energy is estimated by using the formula $\Delta G_{nonpolar} = \gamma\Delta SASA$, where $\gamma$ = 0.0072 kcal mol$^{-1}$ nm$^{-2}$, and the solvent-accessible surface area (SASA) is calculated at a solvent probe radius of 1.4 Å.[220] For polar solvation energy, the Poisson–Boltzmann (PB) and the generalized Born (GB) implicit solvent models are widely used. While PB is the more accurate, GB is less computationally expensive, but both have been used to study large systems such as SARS-CoV-2-ACE2.

The accuracy of the MM-PB/GBSA method is mainly determined by the reliability of the determination of the polar solvation energy. Since the error is proportional to the polarity of the molecules under consideration,[221] this limits the accuracy of estimating the binding free energy of highly polar or charged molecules, such as SARS-CoV-2 RBD and ACE2. However, MM-PB/GBSA is still the most widely used in studying SARS-CoV-2 RBD interaction with ACE2 (Table 2) because more precise methods such as umbrella sampling and free energy perturbation are impractical when using all-atom models.

Due to the high charge of the SARS-CoV-2 RBD-ACE2 complex, the electrostatic and polar solvation energies are inconsistent between different groups, which might depend on methods use to analyze them. The polar term depends on the dielectric constant $\varepsilon_{in}$ and in order to obtain agreement with experimental data, its high value has been recommended to reduce the strong electrostatic energy.[214] However, this seems unclear for the SARS-CoV-2-ACE2 complex, because the application of a large $\varepsilon_{in}$ reduces the large negative electrostatic energy, but at the same time reduces the polar energy.[222] For most of the studies with the details provided, $\varepsilon_{in}$ = 1, or 2 was used (Table 2), The free binding energy obtained with $\varepsilon_{in}$ = 4 is still largely negative.[223] In general, the predicted binding free energies are much lower than the experimental results (Table 1). To solve this problem, Ding *et al.* suggested to take into account the screening effect to the electrostatic interaction between charged biomolecules.[222]

Normal mode (NM) analysis has been used to calculate the entropy term in eqn (1). However, this method requires large computational resources and poor convergence for large systems, such as the RBD-ACE2 complex, where a truncated structure was used to speed up the calculation.[224] One alternative approach to NM replacement is the interaction entropy (IE) method,[225] in which the entropy change is estimated through the protein–protein interaction energy sampled during MD simulation without extra computational effort. Although IE does not provide the absolute entropy, it can predict reasonable relative entropy changes when MM-PBSA is used to analyze the SARS-CoV-2 RBD-ACE2 complex.[222,226] The quasi-harmonic approximation or more recent model based on weighted solvent accessible surface area is another approach that directly computes conformational entropy from MD simulations for SARS-CoV-2 RBD and ACE2.[227,228] Anharmonicity and high-order correlations should be considered for flexible or multiple energy well binding sites[229,230] if they represent SAR-CoV-2 variants. The predicted binding affinity is in reasonable agreement with experiment data when the entropy term is included[217,222,224,226,227,231] (Table 2).

 

Table 2 Theoretical binding free energy $\Delta G_{bind}$ obtained by end-point methods for the complex of WT SARS-CoV-2 RBD and ACE2. $\Delta G_{bind}$ is sorted in descending order

| Ref. | $\Delta G_{bind}$ (kcal mol$^{-1}$) | Method | Notes |
|---|---|---|---|
| Negin[224] | −9.84 ± 1.52 (full struct.)<br>−14.65 ± 1.52 (truncated struct.) | MM-GBSA | FF: ff14SB<br>No glycan<br>Analysis: MMPBSA.py<br>GBNSR6 model, radii mbondi. ($\varepsilon_{in}$ = 1)<br>Entropy: normal mode method |
| Jawad[231] | −12.86 ± 0.1 ($\varepsilon_{in}$ = 1) | MM-GBSA | FF: ff14SB<br>No glycan<br>Analysis: MMPBSA.py<br>GB$^{OBC}$ model, GB = 2, radii mbondi2. ($\varepsilon_{in}$ = 1, 5, 10)<br>Entropy: quasi-harmonic approximation method |
| Ding[222] | −13.3 | MM-PBSA | FF: ff14SB<br>No glycan<br>Analysis: g_mmpbsa<br>Screening effect.<br>($\varepsilon_{in}$ = 2)<br>Entropy: interaction entropy (IE) method |
| Naresh[217] | −13.75 ± 0.02 | SIE | FF: ff14SB<br>No glycan<br>($\varepsilon_{in}$ = 2.25) |
| Zhang[227] | −16.04 ± 0.05 | MM-GPSA | FF: ff14SB, glycan: GAFF2<br>Delphi, ($\varepsilon_{in}$ = 1)<br>Entropy: WSASA method |
| Nguyen[226] | −18.32 ± 1.62 (homoglycan model)<br>−17.57 ± 3.12 (heteroglycan model)<br>−19.88 ± 3.27 (no glycan) | MM-PBSA | FF: ff19SB<br>Glycan: GLYCAM06j<br>Delphi, ($\varepsilon_{in}$ = 1)<br>Entropy: interaction entropy (IE) method |
| Jafary[232] | −31.58 ± 2.44 | MM-PBSA | FF: ff14SB<br>No glycan |
| Wu[233] | −33.13 ± 3.26 | MM-GBSA | FF: ff14SB<br>No glycan |
| Nguyen[228] | −41 (No glycan)<br>−35 (Man9)<br>−45 (FA2) | MM-PBSA | FF: CHARMM36m for protein, CHARMM36 for glycans |
| de Andrade[234] | −48.97 ± 7.79<br>−25.22 ± 18.77 | MM-GBSA<br>LIE | FF: AMBER03<br>No glycan |
| Ma[235] | −54.03 ± 7.50 | MM-GBSA | FF: ff14SB<br>No glycan, $\varepsilon_{in}$ = 1 |
| Piplani[236] | −57.6 ± 0.25 | MM-PBSA | FF: ff99SB-ILDN<br>No glycan |
| Khan[237] | −62.43 | MM-GBSA | FF: ff18SB<br>No glycan |
| Wang[238] | −62.49 ± 7.65 | MM-GBSA | FF: ff14SB<br>No glycan |
| Ali[146] | −126.25 | MM-GBSA | FF: OPLS<br>No glycan |
| Lupala[239] | −143.83 | MM-PBSA | FF: CHARMM36<br>No glycan |
| Mandal[240] | −244.37 ± 36.02 | MM-PBSA | FF: CHARMM36<br>No glycan |
| Zhou[241] | −259.00 | MM-PBSA | FF: CHARMM36<br>No glycan, $\varepsilon_{in}$ = 2 |
| Istifli[242] | −287.25 ± 2.10 | MM-PBSA | FF: AMBER03<br>No Glycan, $\varepsilon_{in}$ = 2 |
| Guo[243] | −309.7 ± 5.63 | MM-PBSA | FF: OPLS-AA<br>No glycan |
| Shah[223] | −590.73 ± 42.84 | MM-PBSA | FF: CHARMM36<br>No glycan, $\varepsilon_{in}$ = 4 |

*Role of glycans in RBD-ACE2 stability.* The role of glycans in the RBD-ACE2 stability remains unclear. Using ff19SB for proteins, GLYCAM06j for glycans, and MM-PBSA, Nguyen *et al.*[226] obtained $\Delta G_{bind}$ = −19.88 ± 3.27 kcal mol$^{-1}$ for the WT without glycans, which is close to −18.32 ± 1.62 to −17.57 ± 3.12 kcal mol$^{-1}$ in the presence of homogeneous and heterogeneous glycans, respectively. The same conclusion was reached by Nguyen *et al.*[228] Therefore, glycans have little effect on the stability of RBD-ACE2 complex, which is consistent with experimental data reported by Allen *et al.* showing that glycans play a minor role in SARS-CoV-2 recognition by ACE2.[244] However, computational studies of Zhao *et al.*,[133] Mehdipour and Hummer,[89] Barros *et al.*[245] and Rahnama *et al.*[246] showed that glycans surrounding ACE2 are important for RBD binding.

The difference between different groups may be due to different force fields used and system settings. Barros *et al.*[245] and Nguyen *et al.*[226] investigated the same RBD-ACE2 complex without membranes. However, Mehdipour and Hummer[89] studied B0AT1-ACE2–RBD in the presence of a viral membrane, whereas Zhao *et al.*[133] examined the interaction between the RBD dimer and the membrane-embedded ACE2 homodimer. Thus, further computational and experimental work is needed to fully understand the effect of glycans on the stability of the RBD-ACE2 complex.

**3.3.3. Coarse-grained umbrella sampling simulation.** While all-atom models are used to estimate binding affinity, the coarse-grained (CG) models are often used to investigate the structures and dynamics of macromolecular complexes on large time scales. Multi-microsecond simulations were carried out to study the mechanism of SARS-CoV-2 RBD binding to full-length ACE2 in the presence of the B0AT1 transporter and the POPC membrane, indicating an important role of B0AT1 in preventing viral invasion.[247] The CG model developed by the Warshel group[248,249] successfully predicted the effect of single mutations on the change in free binding energy.[250,251]

Combining the CG model[252] and replica-exchange umbrella simulations, the dissociation constant $K_D$ of the RBD-ACE2 complex was extracted from the potential of mean force (PMF).[181] In this Cα CG model the interaction energy between amino acids is given by the following equation:

$$\begin{aligned} E = &\sum_i k_b (r_i - r_0)^2 + \sum_i \sum_j k_{\varphi,ij}\left(1 + \cos\left[\varphi_{ij} - \delta_{ij}\right]\right) \\ &+ \sum_i \exp\left[-\gamma k_\alpha (\theta_i - \theta_\alpha)^2\right] + \exp\left[-\gamma k_\beta (\theta_i - \theta_\beta)^2\right] \\ &+ \sum_{ij} \frac{q_i q_j e^2}{4\pi\varepsilon_0 \varepsilon_r r_{ij}} \exp\left[-\frac{r_{ij}}{l_D}\right] + \sum_{ij\in\{NC\}} \varepsilon_{ij}^{NC}\left[13\left(\frac{\sigma_{ij}}{r_{ij}}\right)^{12} - 18\left(\frac{\sigma_{ij}}{r_{ij}}\right)^{10}\right. \\ &\left. + 4\left(\frac{\sigma_{ij}}{r_{ij}}\right)^{6}\right] + \sum_{ij\notin\{NC\}} \varepsilon_{ij}^{NN}\left(\frac{\sigma_{ij}}{r_{ij}}\right)^{12}. \end{aligned} \quad (2)$$

The energy in eqn (2) is the sum, respectively, of $C_\alpha$–$C_\alpha$ virtual bonds, dihedral angles, bond angles, electrostatic interactions, Lennard-Jones-like native interactions, and repulsive non-native interactions. Charges $q = +1e$ and $-1e$ respectively are assigned to the positively charged and negatively charged residues, and the remaining residues have $q = 0$. The electrostatics interaction is described by the Debye–Hückel theory with a Debye screening length, $l_D$, of 10 Å and a dielectric constant of 78.5. The Lennard-Jones-like interactions are described by the 12-10-6 potential.[253]

The dissociation constant $K_D$ of the RBD-ACE2 complex can be expressed as a function of the probability of bound ($P_b$) and unbound ($P_u$) states and the free monomer concentration of protein [Protein]:[181]

$$K_D = \frac{P_u}{P_b}[\text{Protein}]. \quad (3)$$

Here $P_u = 1 - P_b$, and [Protein] which represents either free monomer concentration of ACE2 or RBD is given by

$$[\text{Protein}] = \frac{P_u}{V(r^*)} C_0. \quad (4)$$

Coefficient $C_0 = 1660$ is constant of proportionality. $V(r^*)$ is the simulation volume in which free monomers can be found. $P_b$ is calculated by numerical integrating PMF as:

$$P_b = \frac{\int_0^{r_b} 4\pi r^2 e^{-\beta G_{1D}(r)} dr}{\int_0^{r^*} 4\pi r^2 e^{-\beta G_{1D}(r)} dr}, \quad (5)$$

where $G_{1D}(r)$ is the 1-dimensional PMF, calculated using the histogram-free formulation of the WHAM equations. $r_b$ which separates bound and unbound states is defined as corresponding to the peak of the 1D-PMF (Fig. 6C).

Using eqn (3)–(5), Nguyen *et al.*[181] obtained $K_D$ = 6.7 and 2.7 nM for SARS-CoV-1 and SARS-CoV-2, respectively (Fig. 6D). Since the higher the $K_D$ the stronger the binding, this result is consistent with experiments[65,73] and other computational studies showing that SARS-CoV-2 binds more strongly to ACE2 than SARS-CoV-1. In addition, CG models in combination with enhanced sampling methods are likely to provide a reasonable estimate of the dissociation constant of protein–protein complexes, and research in this direction is encouraging, since the corresponding simulations are less time consuming compared to the all-atom simulations. Another advantage of CG umbrella sampling is that it calculates $K_D$ that can be directly compared with experiment, while other methods such as end-point methods provide $\Delta G_{bind}$ that cannot be directly measured experimentally.

# 4. Interaction of SARS-CoV-2 variants of concern with ACE2

Since the outbreak of SARS-CoV-2, the virus has accumulated mutations in its gene. A number of mutations are determined to change the fitness of virulence and transmissibility of virus. In consequence, multiple variants have emerged that have different characteristics compared to wild type. According to WHO, there were five COVID-19 variants of concern (VOC) including Alpha (B.1.1.7), Beta (B.1.35), Gamma (P.1), Delta (B.1.617.2) and Omicron (B.1.1.529),[254,255] as well as two variants of interest (VOI), Lambda and Mu.[90] VOCs appear to exhibit enhanced transmissibility and resistance to therapeutic agents, leading to high rates of hospitalization and mortality.[256,257] Each variant can be classified into several sublineages. For example, Omicron has at least 5 sublineages BA.1, BA.2, BA.3, BA.4 and BA.5.[258] In this review, we will focus on the variants of concern and their sublineages and mutations are shown in Fig. 7.

## 4.1. Alpha variant

The alpha variant has a higher transmissibility, viral load and longer time in the respiratory tract than WT.[259–263] Mutations in this variant are shown in Fig. 7. An *in vitro* study indicated

 

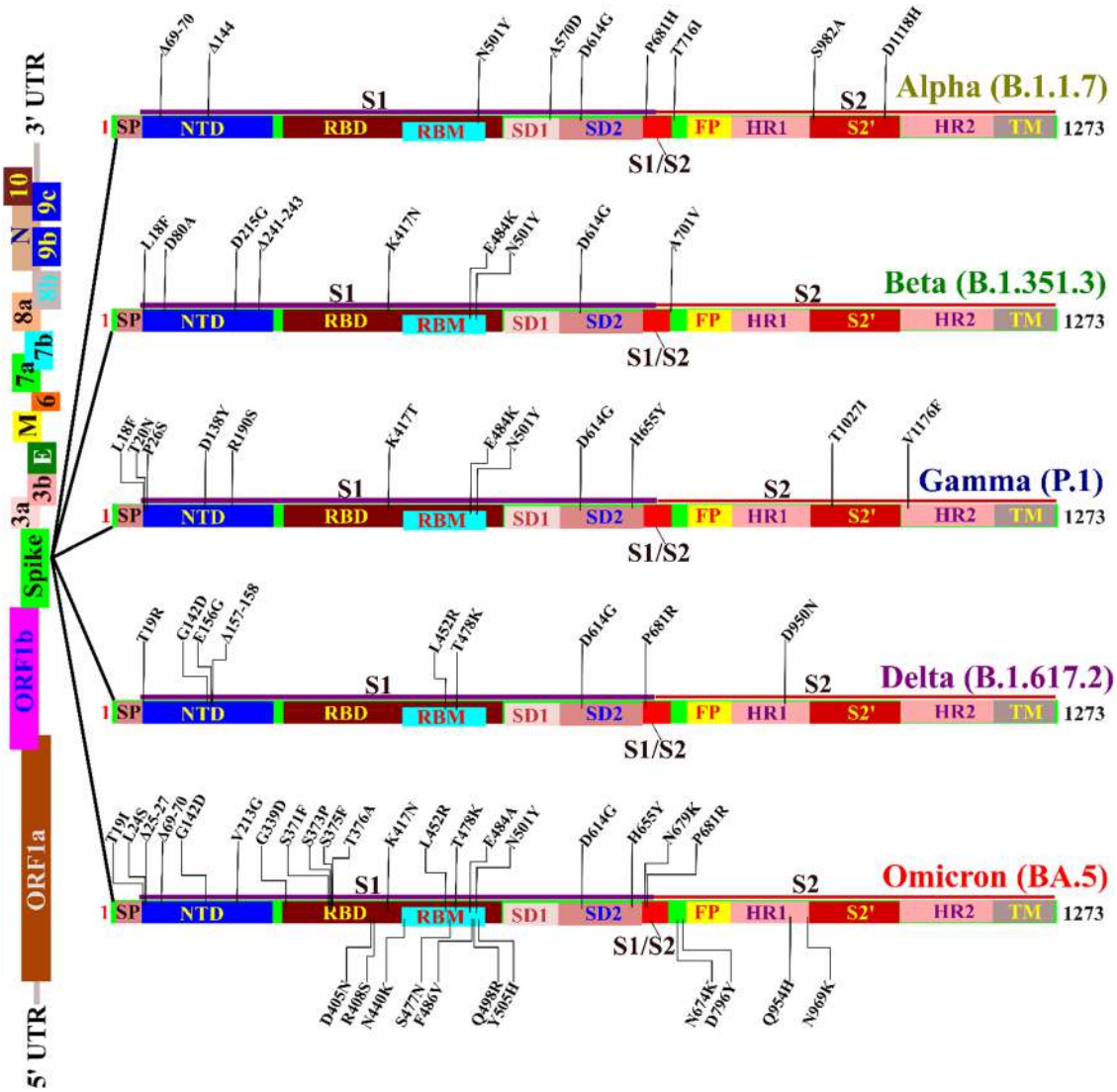


Fig. 7 Mutations in the spike protein of variants of concern (Alpha, Beta, Gamma, Delta and Omicron) designated by WHO. The corresponding lineage is shown in parentheses.

that the Δ69–70 mutation does not contribute to antibody resistance.[264] However, this mutation enhances the fusion of host cell and virion membranes. The presence of the P681H mutation improves furin-mediated spike cleavage by approximately 2-fold compared to WT.[265] However, the work of Lubinski *et al.* indicates little effect of P681H on furin cleavage and membrane fusion.[266]

The effective transmissibility of the Alpha variant may be due to tighter binding to ACE2 than WT[198,200] (Table 1). Measurement of the binding affinity of Alpha RBD to ACE2 on the cell surface using fluorescence flow cytometry indicates that the N501Y mutation in the RBD region enhances the interaction of these two proteins, since $K_D$ for WT and Alpha is 47.2 ± 7.4 nM and 13.1 ± 3.8 nM,[188] respectively, which is consistent with other studies[194,196,201] (Table 1). The π–π stacking interaction between the Alpha Y501 residue and ACE2 Y41 is responsible for the enhanced stability of the complex. In line with the studies above, using bio-layer interferometry Collier *et al.*[195] obtained $K_D \approx 133$ and 22 nM for WT and Alpha, respectively. This result is consistent with the surface plasmon resonance data reported by Barton *et al.*[193] (Table 1) that N501Y mutation in the Alpha variant increases the RBD binding to ACE2 by reducing $K_D$ from 62.6 ± 7.7 (WT) to 5.5 ± 2.4 nM (Alpha).

The atomic force microscopy experiment showed that the unbinding force of Alpha RBD (57 ± 18 pN) is slightly higher than WT (49 ± 11 pN).[188] Steered molecular dynamics (SMD) simulation suggests that the Alpha Y501 residue has a π–π interaction with ACE2 Y41 and a π-cation interaction with ACE2 K353, while WT N501 does not have such an interaction, which agrees with experiment.[188] Using MM/PBSA method, the AMBER14SB force field and TIP3P water, it was shown that the binding energies are equivalent for the WT and Alpha variant.[267]

Using the Binding Free Energy Estimator 2 [100] with CHARMM36, ZAFF and water TIP3P force fields, Coderc *et al.*[268] obtained very good agreement with the experimental data on the binding free energy for RBD of Alpha, Beta, Delta and Omicron BA.2 to ACE2. A simulation using umbrella sampling shows that the N501Y mutation increases the binding free energy by about 4 kcal $mol^{-1}$ compared to the WT,[269] which is due to the fact that compared to WT, the Alpha Y501 residue has two contacts more, including one hydrogen bond with K353 and one π–π contact with Y42 of ACE2. Increased binding affinity due to N501Y was also observed using the MM/GBSA method.[270]

### 4.2. Beta variant

The Beta variant contains mutations K417N, E484K, and N501Y in the RBD region (Fig. 7), which increases the ACE2 affinity ($K_D$ = 5.01 nM) in compared to the WT ($K_D$ = 7.36 nM), as shown in the bio-layer interferometry experiment[200] (Table 1). An experiment by Tian *et al.* indicates that the N501Y mutation dramatically changes the binding affinity of RBD and human ACE2.[188] K417N weakens the RBD-ACE2 stability while E484K boosts it a bit. The combination of these three mutations leads to increased stability of this complex.[188] Barton *et al.* showed that the Beta variant binds to ACE2 weaker than Alpha, although these two variants have the same N501Y mutation,[193] consistent with Laffeber *et al.*[196] (Table 1). The K417N mutation reduces the binding affinity of RBD to ACE2 to a greater extent than the increasement effect by E484K.[193,196]

In the absence of ACE2, the RBD of the Beta variant is more flexible than the WT and Alpha in the area that will form an interface with ACE2.[271] In complex with ACE2 the Beta RBD becomes less flexible because it has more contacts with ACE2 than WT and Alpha variant. The K484 residue forms a salt bridge with ACE2, but the salt bridge between the mutation K417N and ACE2, which is responsible for the impact of these mutations on the binding with the host cell, is broken.[271]

### 4.3. Gamma variant

The Gamma variant has the mutations K417T, E484K, and N501Y in the RBD region (Fig. 7). These mutations have little effect on the RBD structure,[197] but they increase the RBD binding to ACE2 compared to WT.[193,197,200] For example, using surface plasmon resonance, Barton *et al.*[193] obtained $K_D$ = 62.6 and 12.2 nM for WT and Gamma, respectively. Like other variants in which K417 is replaced by a neutral residue, the K417T mutation reduces the affinity of RBD binding to ACE2, while E484K, N501Y increase it.[193]

### 4.4. Delta variant

The Delta variant caused a devastating pandemic wave in many countries. This variant has a higher replication rate and intercellular fusion than WT, Alpha, Beta, and Gamma variants.[197,272,273] Compared to WT, the Delta spike protein has a higher propensity for an open RBD configuration, which facilitates interaction with host cells.[199] Delta RBD has only two mutations L452R and T478K (Fig. 7) which do not cause the RBD structural rearrangement,[197] but lead to its stronger binding to ACE2 compared to WT.[95,199,274] Liu *et al.*[274] reported $K_D$ = 75 nM and 57 nM for WT and Delta, respectively and these values are close to Wang *et al.*,[199] who showed that the T478K mutation significantly stabilizes the RBD-ACE2 complex. Using biolayer interferometry, Zhang *et al.* demonstrated that both the entire Delta spike protein and the Delta RBD bind to the ACE2 dimer more strongly to the ACE2 monomer[197] (Table 1).

McCallum *et al.* showed that the Delta variant has no improvement in the binding affinity of RBD to ACE2[198] (Table 1). The discrepancy between different groups may be due to different experimental conditions. High levels of Delta infection may be associated with mild dissociation of S1, but not with tighter ACE2 binding.[197] In addition, the P681R mutation in Delta makes furin cleavage and cell fusion more efficient than WT and Alpha,[265,273] making Delta more infectious.

Modeling using the MM/GBSA method with the AMBER14SB force field and TIP3P water model reveals that the Delta variant ($\Delta G_{bind}$ = −42.76 ± 2.38 kcal $mol^{-1}$) has a lower binding free energy than Omicron (−29.43 ± 3.01 kcal $mol^{-1}$) and WT (−33.13 ± 3.26 kcal $mol^{-1}$).[275] Although residue 452 is outside the binding surface with ACE2, the replacement of the neutral amino acid (Leu) with a positive charge Arg increases the interaction between RBD and ACE2.[269,276] A simulation study using the pyDockEneRes tool[277] showed that the mutations L452R and T478K in the Delta variant increase the strength of ACE2 binding.[278]

### 4.5. Omicron variant

Omicron is a prevalent variant with a faster spread than Delta.[279] The number of mutations in the Omicron RBD region is higher than in other variants (Fig. 7). New sub-lineages of Omicron have emerged and have replaced over its original BA.1 lineage.[280] Various $K_D$ values of Omicron binding to human ACE2 are shown in Table 1. Dejnirattisai *et al.* showed that Omicron RBD binds to ACE2 with a $K_D$ equivalent to WT and higher than other variants,[187] but another study provided a similar value of $K_D$ for Omicron and Delta.[281] Gobeil *et al.* reported that Omicron binds to ACE2 more strongly than WT but weaker than Delta.[95] The trend that the Omicron variant has a lower $K_D$ than WT is supported by other studies (Table 1).

RBD-RBD interface in the down state of 3 RBDs is densely packed in sub-lineages BA.1 and BA.2.[95,282] Stabilization of the closed state of spike protein can occlude the binding with antibodies and receptors such as ACE2. However, this is compensated by rearrangement of the linker connecting NTD and RBD, which increases the propensity of BA.1 RBD to open state.[95] Moreover, the fusion peptide of Omicron is more easily exposed than the WT and Delta variant. The K417N mutation attenuates the interaction between the viral spike and ACE2, while Q493R, G496S, and Q498R stabilize this complex. The N501Y mutation promotes the π-stacking interaction with Y41 of ACE2.[281] The BA.1 Omicron variant needs a higher level of ACE2 expression for efficient membrane fusion compared to WT, Alpha, Beta, and Delta variants.[192]

 

Furin cleavage in the Omicron variant is inefficient, which may be due to the presence of two mutations N679K and P681H.[192] Since these two mutations also occur in the Omicron BA.2, BA.3, BA.4 and BA.5 sub-lineages, the molecular mechanism of this effect is intriguing to shed light on the viral infectivity of this variant. The development of pandemic is accompanied by combinations and mutations of Omicron sub-lineages. The sub-lineage BA.2.75 emerges from BA.2, which enhances infection ability and binding affinity to ACE2 compared to sub-lineages BA.2 and BA.5.[283] In particular, mutations N460K and D339H of BA.2.75 increase the binding energy with ACE2. Since the end of 2022 the Omicron sub-lineages XBB, XBB.1, XBB.1.5, CH.1.1, BQ.1.1 have become the prevalent lineages (https://www.nature.com/articles/s41467-023-38435-3). According to yeast surface display assay, the RBD binding affinity of the XBB variant to human ACE2 is higher than that of the BA.2 variant, as $K_D$ = 1.00 ± 0.07 and 1.49 ± 0.05 nM for XBB and BA.2, respectively.[284] The increase in binding affinity is likely due to substitutions R346T, L368I and N460K. The SPR experiment indicates that the full spike proteins of XBB and XBB.1 have a weaker binding affinity to human ACE2 than BA.2.[22] XBB.1.5, one of newest sub-lineage, exhibits a stronger association with ACE2 ($K_D$ = 3.4 nM) than XBB.1 ($K_D$ = 19.0 nM) and BQ.1.1 ($K_D$ = 8.1 nM).[285] Derived from variant BA.5, RBD of BQ.1.1 has lower dissociation constant with ACE2 ($K_D$ = 0.66 ± 0.11 nM) than BA.5 ($K_D$ = 108 ± 0.16 nM) using yeast surface display assay.[286] However, the full spike proteins of BA.5 (0.61 nM), BQ.1 (0.62 nM), and BQ.1.1 (0.56 nM) have equivalent binding affinities.[22] Subvariant BQ.1.1 has mutations R346T and N460K that improve binding to human ACE2 compared to BA.5. An experiment by Cao *et al.*[287] showed that BQ.1.1, XBB, and BA.2 have the same $IC_{50}$, while BA.5 $IC_{50}$ is lower than BA.2, but $IC_{50}$ of CH.1.1 is higher than BA.2.

The change in charge caused by mutations in Omicron enhances the binding energy with host cells.[288–290] A deep learning approach predicted that variants Alpha, Beta, Gamma, Delta, Kappa, Lambda, Omicron BA.1, BA.2, BA.3 bind to ACE2 more strongly than WT[291] and mutations N440K, T478K, and N501Y play a key role. Using MD simulation with the CHARMM36m force field and TIP3P water model, Lupala *et al.* determined that the Omicron variant RBD increases interaction with ACE2 by changing the electrostatic potential and stabilizing hydrogen bonds at the binding surface due to mutations.[290] Nguyen *et al.*[288] also found that the electrostatic interaction between Omicron RBD and ACE2 PD is stronger than WT RBD and ACE2 PD, due to an increase in RBD charge from +3*e* in WT to +6*e* in Omicron. Using MM/PBSA with AMBER19SB, GLYCAM06j force fields and OPC water model, they obtained the free energy of WT and BA.1 Omicron RBD binding to ACE2 PD of ≈−18 and −29 kcal mol$^{-1}$, respectively.[288] The contribution of glycan molecules to the binding free energy of is insignificant, which is consistent with Khan *et al.*[292] who obtained $\Delta G_{bind}$ = −18.72 and −27.27 kcal mol$^{-1}$ for WT and Omicron BA.1, respectively, using the same model as Nguyen *et al.*, but without glycans.

The MM/GBSA method combined with AMBER14SB force field and TIP3P water gave a binding free energy of −12.86 ± 0.1 kcal mol$^{-1}$ and –14.53 ± 0.1 kcal mol$^{-1}$ for WT and BA.1 Omicron, respectively, which is closer to the experimental data compared to MM/PBSA.[289] A joint study of experimental and simulation methods showed that BA.1 Omicron binds to ACE2 more strongly than WT, since $K_D$ = 6.342 ± 2.190 for WT and 2.418 ± 1.166 nM for Omicron.[293] The binding energies obtained from MM/GBSA without entropy contribution using the AMBER19SB force field and TIP3P water for WT and Omicron with ACE2 are −26.66 ± 9.78 and −42.19 ± 6.61 kcal mol$^{-1}$, respectively. In addition, mutations Q493R, G496S, Q498R, N501Y and Y505H in the Omicron RBD interact stronger with ACE2 than WT.

A computational study using the CHARM36 forcefield for complexes of ACE2 PD and RBD of Omicron BA.1 and BA.2 lineages shows that both lineages have a stronger binding affinity than WT.[294] The increase in the number of salt bridges is responsible for their tighter binding. Using MM/PBSA method and neglecting the entropy contribution different groups[295,296] obtained the large negative binding energies, but the main trend remains the same: Omicron binds to host cells more strongly than WT.

Pitsillou *et al.*[278] showed that Omicron BA.1 displays higher binding affinity for ACE2 than Delta and WT when using pyDockEneRes with CHARM36 force field and TIP3P water. The fragment molecular orbital method revealed mutations S371L, S375F, N440K, T478K, E484A, Q493K, and Q498R significantly enhance interaction with ACE2.[297] DFT simulations gave $\Delta G_{bind}$ = −109.77, −154.04, and −271.42 kcal mol$^{-1}$ for WT, Delta, and Omicron BA.1, respectively.[298] Although this result qualitatively agrees with other *in silico* and *in vitro* studies, the absolute binding free energy is are far from experimental data. In general, different Omicron sub-lineages have a slight difference in binding affinity to ACE2[299] indicating their similar ability to enter host cells.

### 4.6. Machine learning and alchemical free energy method for predicting binding affinity of SARS-CoV-2 variants

As can be seen from the discussions above, when using methods based on MD modeling, the binding affinity of SARS-CoV-2 variants to ACE2 reported by various groups is inconsistent and often lower than experimental results. In this case, machine learning can play an important role as it has advantages in choosing features for efficient training of neural networks. The predictive power of this approach depends on the available experimental data, and it is expected that the generated neural network models will be applied to effectively predict not only the absolute binding affinity, but also the change in binding affinity caused by specific mutations. Chen *et al.*[300] run MD simulations for selected 108 single RBD mutations in complex with ACE2 and used 18 decomposed MM-GBSA energy terms as input features and experimental dissociation constant ratios between variants and wild-type[301] to train a neural network regression model. Compared to MD-based methods, their model improved ACE2 binding affinity for most circulating

SAR-CoV-2 strains, although the predicted values do not show significant differences between the different variants, as experimentally demonstrated. More precise methods such as free energy perturbation have been employed to quantify the effect of specific mutants during neural network model training.[302] Topology-based network tree (TopNetTree), a method based on a deep learning algorithm, has been applied to predict the change in binding free energy of thousands of possible RBD mutations and predicted several potential residues in the RBM region that have high mutation probability for the emergence of more contagious trains.[303]

Williams and Zhan[304,305] have also developed a machine learning approach, but based on very limited simulation and experimental data on binding affinity. They proposed a simple semi-empirical formula that makes it possible to reasonably predict $K_D$ of various variants using the binding free energy calculated by the MM-PB/GBSA method.

Machine learning based models are useful for studying the binding of RBD variants not only to ACE2, but also to a wide range of antibodies and nanobodies.[306,307] They can speed up and reduce the cost of finding candidates with high neutralizing ability.

Alchemical free energy methods such as free energy perturbation (FEP) and thermodynamic integration (TI) are the most accurate because they are exact. However, they require efficient sampling and are therefore often impractical for evaluating the absolute binding free energy of large systems such as protein–protein complexes,[221] mainly due to low convergence.[308] However, the alchemical methods are successfully predict the change in the binding free energy caused by mutations of various variants of SARS-CoV-2 with ACE2.[237] Note that alchemical free energy calculations can be combined with advanced sampling methods[309] or QM/MM calculations[310] to efficiently investigate the interaction of small ligand compounds with SARS-CoV-2 drug targets.[311]

Finally, it is worth emphasizing that mutations in ACE2 can change the affinity for the viral RBD. However, this problem is beyond the scope of our review, and the reader can find relevant information in the recent review[312] and original papers.[186,193,313–315]

## 5. Virus entry into human cells by binding to neuropilin-1 and other receptors

ACE2 is widely recognized as the host cell receptor for SARS-CoV-2.[66] Although the transmission of SARS-CoV-2 *via* respiratory tract,[316] several studies suggest that the expression of human ACE2 is significant in heart, kidney, and testis,[167] but low in respiratory and olfactory epithelial cells,[317] which suggests that other proteins may support viral entry into cells with low ACE2 levels.

### 5.1. Neuropilin-1

Recent experiments have found that neuropilin-1 (NRP1) is one of the proteins that facilitates the entry of the SARS-CoV-2, as co-expression of NRP1 with ACE2 and TMPRSS2 greatly enhances viral infection.[318] NRP1 is a transmembrane glycoprotein that is expressed in all vertebrates and plays an important role in a wide range of physiological processes such as axonal guidance, angiogenesis, regulation of vascular permeability, and immunity.[319,320] NRP1 comprises of approximately 900 amino acids, including 850 extracellular, 24 transmembrane, and 40 cytoplasmic residues. The NRP1 ectodomain is divided into five modules a1, a2, b1, b2 and c (Fig. 8). Domains

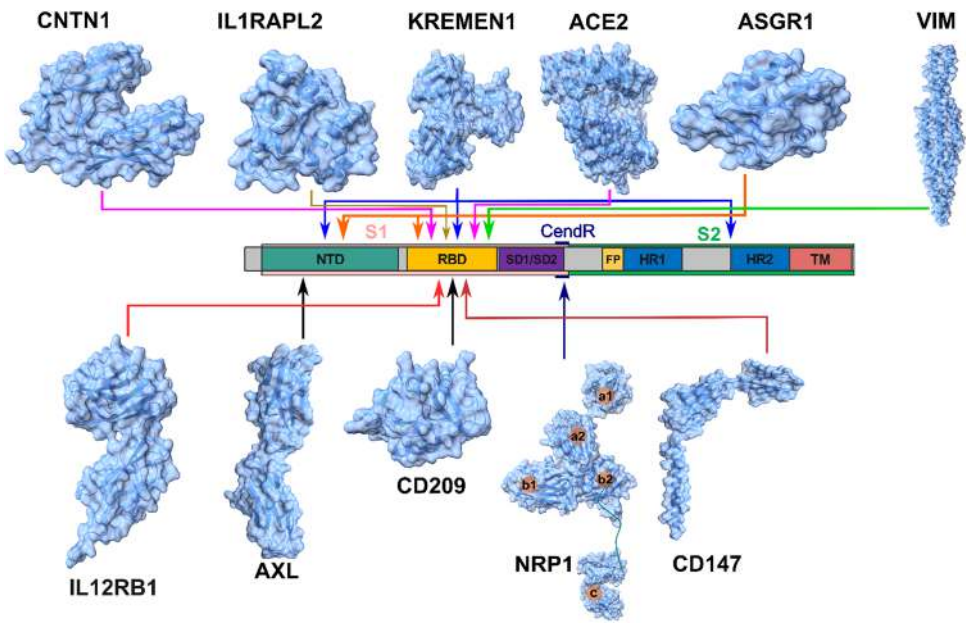


Fig. 8 Schematic of SARS-CoV-2 receptors and their binding region in Spike protein of SARS-CoV-2. The PDB id for AXL is 2C5D, CD209 is 2XR5, extracellular domains of NRP1 are 4GZ9 for a1, a2, b1 and b2 while c is 5L73, CD147 is 6LYY, KREMEN1 is 5FWS, ACE2 is 1R42, ASGR1 is 1DV8, VIM is 3KLT. COVID-19. NRP1 binds to CendR motif (682-RRAR-685).

 

a1, a2, b1 and b2 can serve as binding sites for ligands and proteins while c is responsible for NRP-1 oligomerization.[321]

A structure called CendR (C-end rule) binds and activates NRP1 and NRP2 at the cell surface.[322] This CendR structure is formed by the C-terminal sequence RXXR (R is arginine, X is any amino acid; R can be substituted by lysine (K)). Interestingly, the SARS-CoV-2 spike protein has a furin-cleavage site at the junction of the S1 and S2 subunits, while this site is absent in SARS-CoV-1.[150] This process cleaves the SARS-CoV-2 spike protein into S1 and S2 polypeptides, which are linked to each other by non-bonded interactions. The cleavage by furin at residue 685 of SARS-CoV-2 spike protein generates the short fragment 679-NSPRRAR-685 at the C-terminus of S1 which contains the CendR motif (682-RRAR-685).

The crystal structure of the SARS-CoV-2 spike protein has the S1–S2 junction exposed to solvent, making this region accessible for binding to receptor proteins.[73] It was experimentally found that after furin cleavage the b1 domain of human NRP1 directly binds to the spike protein at CendR of S1 next to S2[318,323] (Fig. 8). When NRP1 is depleted, the SARS-CoV-2 infection is lower than normal cells,[323] suggesting that NRP1 increases SARS-CoV-2 infection. Blocking the interaction of the C-terminal fragment of S1 with NRP1 by small molecules or monoclonal antibodies reduces the effectiveness of viral infection. Also, isothermal titration calorimetry (ITC) showed[323] that the binding affinity of CendR with NRP1 depends on pH with $K_D$ = 20.3 μM and 13.0 μM at pH 7.5 and 5.5, respectively. However, the mechanism of CendR binding to NRP1 remains unclear, which requires further computational studies.

At present, it is not entirely clear whether SARS-CoV-2 virions are internalized *via* NRP1 by endocytosis or direct fusion with the host cell membrane. NRP1 can mediate endocytosis of CendR peptides, but this mechanism differs from known endocytic pathway.[324] This experimental result supports the NRP1 mediated endocytosis pathway of virions. A computational study showed that NRP1 stimulates the separation of the S1 and S2 subunits of the SARS-CoV-2 spike protein,[325] followed by TMPRSS2 cleavage at the S2′ position to expose a fusion peptide. Since dissociation of S1 and S2 induces conformational change in S2 that initiates membrane fusion, NRP1 may play an important role in two pathways for SARS-CoV-2 entry into the host cell: fusion with the host cell plasma membrane or internalization into the endosome.

One of possible strategies to combat COVID-19 is to block NRP1 activity by different inhibitors. Valproic acid was shown to reduce ACE2 and NRP1 expression in cells leading to inhibit SARS-CoV-2 infection.[326] Peptides that are similar to C-end rule peptides,[322,327–329] bicyclic peptides[330] and small compounds[331,332] are potent inhibitors of NRP1. Out of more than 0.5 million compounds, two compounds have been identified that are able to target NRP1 and prevent SARS-CoV-2 from entering the host cell.[333] Blocking NRP1 can affect other normal processes,[334–336] and in some cases it results in embryonic lethality and multiple cardiovascular defects,[337] warning that this strategy should be used with caution in the treatment of COVID-19.

### 5.2. Other possible receptors

In addition to ACE2 and NRP1, it is suggested that CD147 may be a receptor for the SARS-CoV-2 spike protein. CD147 is a cell surface protein of the IgG super family, the transmembrane and extracellular domains of Ig1–Ig2 are shown in Fig. 8. The experiment found that CD147 binds to the RBD of the spike protein with an affinity constant of 0.19 μM,[338,339] which facilitates entry of the virus into the host cell *via* endocytosis. Meplazeumab which is an antibody against CD147 blocks the entry of the SARS-CoV-2 virus.[339] Furthermore, it was hypothesized that severe cases of cytokine storm-associated COVID-19 are induced by an interaction between the spike protein and CD147. Viral infection through CD147 can trigger the mitogen-activated protein kinase pathway and promote the development of a cytokine storm, suggesting an important role of CD147 in COVID-19.[339] However, other experiments show that the SARS-CoV-2 spike protein does not interact with CD147,[340,341] casting doubt on the role of the CD147 as a cofactor for virus entry into the host cell.

Kringle containing transmembrane protein 1 (KREMEN1) and asialoglycoprotein receptor 1 (ASGR1) have been identified as co-receptors for SARS-CoV-2.[342] KREMEN1 is a type I transmembrane protein with an ectodomain and a cytoplasmic tail, the ectodomain is shown in Fig. 8. ASGR1 is also a transmembrane protein consisting of a cytosolic domain, a transmembrane domain, a stalk and a carbohydrate recognition domain (CRD) (Fig. 8). SARS-CoV-2 can infect cells without ACE2 expression, but have KREMEN1 or ASGR1. The combination of ACE2, KREMEN1 and ASGR1 expression levels correlates better with SARS-CoV-2 susceptibility than their individual expression level.[342]

While ACE2 binds to RBD of the spike protein, KREMEN1 binds to the NTD, RBD and S2, and ASGR1 binds to the NTD and RBD. Both KREMEN1 and ASGR1 bind to RBD with higher affinity than other regions with $K_D$ of 19.3 nM and 94.8 nM, respectively. Since $K_D$ of the ACE2-RBD complex is 12.4 nM,[342] the binding affinity of these three proteins to RBD is comparable, implying the complexity of the molecular mechanism of SARS-CoV-2 entry into host cells.

ACE2 expression is low in the lung and trachea,[343] motivating the search for other receptor candidates. Using tandem affinity purification (TAP)-mass spectrometry (MS), Wang *et al.* found that the extracellular Ig-like domains of the tyrosine-protein kinase receptor UFO (AXL) binds to the NTD of SARS-CoV-2 Spike protein (Fig. 8) with a $K_D$ of 882 nM.[343] AXL is expresses at a higher level in human lung tissue than ACE2 and promotes SARS-CoV-2 infection in human cells, which explains why potent antibodies predominantly bind to the NTD of the spike protein.[77,82,344]

SARS-CoV-2 is expected to enter the central nervous system as it has been found in the brain of patients with COVID-19.[345] A similar situation was observed for SARS-CoV-1 and MERS-CoV.[153,346,347] Since the ACE2 concentration in the brain is very low, with the exception of the thalamus and choroid plexuses,[348] these observations suggest that there is another receptor for SARS-CoV-2 to bind before invading the central

nervous system. Using confocal microscopy and cell-based cryo-CLEM and cryo-ET, Pepe *et al.* showed that neuronal cells can be infected when co-cultured with infected epithelial cells.[349] They also found that SARS-CoV-2 uses tunneling nanotubes, which are membrane channels, to infect cells lacking receptors, since the nanotubes allow direct transport of cargo between distant cells.

Tunneling nanotubes facilitate the SARS-CoV-2 transmission between cells containing the ACE2 protein. Virions are observed inside the tunneling nanotube, but the mechanism of their binding and the virion release from the tunneling nanotube into uninfected cells remains unclear. However, these results suggest that tunneling nanotubes are a new cofactor for virus propagation in cells with very low ACE2 concentrations. Further research is required to shed light on the mechanism of SARS-CoV-2 propagation due to tunneling nanotubes.

Using microscale thermophoresis, Wei *et al.*[350] found that the S1 subunit of the SARS-CoV-2 spike protein binds to cholesterol molecules with an $IC_{50}$ of 195.7 $\pm$ 49.1 nM. There are four putative cholesterol binding regions in S1, three in NTD and one in RBD. NTD possibly interacts with high-density lipoprotein (HDL) *via* the binding or transfer of material from HDL to S1, which contribute to the virus infectivity. This increase in infection is mediated by the scavenger receptor B type 1 (SR-B1) protein, which is a cell membrane receptor involved in HDL and cholesterol endocytosis. Interestingly, the effect of HDL on SARS-CoV-2 engagement with host cells is strongest when SR-B1 is co-expressed with ACE2, suggesting that SR-B1 attracts the virion to ACE2 when it interacts with HDL. These observations suggest that SR-B1 may be a host factor for SARS-CoV-2 entry.

Cluster of differentiation 209 (CD209) and related protein CD209L which are also known as dendritic cell-specific intercellular adhesion molecule-3-grabbing non-integrin (DC-SIGN) and liver/lymph node-specific intracellular adhesion molecules-3 grabbing non-integrin (L-SIGN) are transmembrane proteins from the C-lectin superfamily. Lectins are receptors for cell surface oligosaccharides and biological fluid glycoproteins. CD209 and CD209L have a transmembrane and a carbohydrate-recognition domains,[351] the latter is shown in Fig. 8. CD209L is expressed in alveolar and pulmonary endothelial cells[352] while CD209 is expressed in dendritic cells.[353] The CD209L/L-SIGN and CD209/DC-SIGN proteins facilitate SARS-CoV-2 infection through interaction with the RBD region.[354,355] $K_D$ characterizing binding affinity of the spike protein to CD209L/CD209 is 1.18 $\pm$ 0.12, 1.66 $\pm$ 0.12 μM and 11.90 $\pm$ 4.6, 4.33 $\pm$ 0.7 μM for CD209L and CD209, respectively.[355] Removal of the high mannose glycan surrounded by CD209L N92 increases the binding propensity of RBD and CD209L. CD209L and ACE2 can form a heterodimer, suggesting that CD209L mediates infection in both an ACE2-dependent and an ACE2-independent manner.

The interleukin-12 receptor subunit beta-1 (IL12RB1), the interleukin-1 receptor accessory protein-like 1 (IL1RAPL2), as well as the nerve cell surface adhesion protein contactin-1 (CNTN1) have been experimentally found to bind RBD of the SARS-CoV-2 spike protein.[356] In particular, in the presence of ACE2 and TMPRSS2, CNTN1 expression enhances infection, suggesting a role for CNTN1 in low ACE2 levels.

Heparan sulfate (linear polysaccharide) on the surface of the host cell plays the role of a co-receptor for SARS-CoV-2 infection. RBD binds to heparan sulfate with $K_D$ of $\approx$150 nM.[357] The spike protein trimer associates with heparan sulfate more strongly than with RBD because the corresponding $K_D$ is lower ($\approx$3.8 nM). Although both heparan sulfate and ACE2 bind to RBD, their binding regions are different. In addition, heparan sulfate increases the likelihood of an open configuration of RBD, leading to enhancement of the RBD binding to ACE2.

Experimental studies have shown that vimentin (VIM), which is a type III intermediate filament protein, is a co-receptor of SARS-CoV-2.[358,359] VIM occurs at the extracellular surface and binds to RBD of the spike protein. However, the VIM binding region in RBD is different from that of ACE2,[358] as evidenced by the fact that the CR3022 antibody attenuates VIM binding to RBD, but not ACE2 to RBD. This also suggests that VIM and CR3022 clash each other in order to associate with RBD. Interestingly, association of VIM with RBD enhances the binding of ACE2 to RBD,[358] and inhibition of VIM activity reduces infection without abolishing replication.[359] All of these results point to a co-receptor role of VIM for SARS-CoV-2.

Thus, ACE2 is known as the main receptor for SARS-CoV-2 infection, but other receptors have been also reported by several groups. The presence of multiple receptors may be responsible not only for the rapid infectivity of the new virus, but also for the complexity of its invasion mechanism. Since the cell types used in the experiment are limited and there are only few computational studies, further studies are needed to fully understand the molecular mechanism of the interaction of SARS-CoV-2 with host receptors.

## 6. Fusion of virus and human membranes

Fusion of virus and human membranes initiates with the separation of the S1 subunit followed by the virus anchoring to the host cell through binding of the fusion peptide (FP), which is located at the N-terminus of the S2 subunit (Fig. 9A), to the host membrane. The reorganization of S2 between the virus and the host would then cause the two membranes to fuse together, allowing the virus to deliver its genome into the cell for eventual production of new virions.[360] Since merging the membranes together requires crossing sufficiently high energy barriers,[361] membrane fusion is not a diffusive or spontaneous process. In this case, the viral fusion protein plays the role of a catalyst for this reaction, satisfying the energy requirement.

### 6.1. Fusion proteins

Enveloped viruses differ in the number of different types of glycoproteins protruding from their membranes. For example, coronaviruses have a single transmembrane glycoprotein (spike protein), while influenza viruses have two: neuraminidase and hemagglutinin (HA). Other viruses have more than two surface

 

proteins. However, for all known enveloped viruses only one glycoprotein is the fusion protein that actually merges the cellular and viral membranes.

Fusion proteins are divided into three classes, I, II and III. Class I fusion proteins are largely made up of helices, while proteins from class II are composed of beta strands and beta sheets. Both helical and beta structures occur in class III fusion proteins. Fusion proteins of class II and III possess fusion loops at the tip of a β-sheet domain.[362,363] In the case of class II, fusion proteins are dimers in the pre-fusion state, but they transform into trimers once their fusion loops are anchored in the target membrane.[362,364] It is worth noting that despite their different structures before and after fusion, all viral fusion proteins share a common trimer-of-hairpins structure in their post-fusion forms.[148]

For coronaviruses, including SARS-CoV-2, the spike protein is a fusion protein belonging to class I with the trimeric structure.[73] Its subunit S2, which directly involved in membrane fusion, contains fusion peptide (FP), heptad repeat 1 (HR1), heptad repeat 2 (HR2); TM: transmembrane (TM) domain and cytoplasmic (CP) tail region (Fig. 9A). Their role in the membrane fusion pathways will be discussed in detail.

### 6.2. Fusion peptides and fusion loops

Fusion protein segments that directly engage the target membrane are called ''fusion peptides'' if they are at the N-terminus of the fusion subunit, and ''fusion loops'' if they are inside the polypeptide chain. Class II and III fusion proteins have fusion loops at the tips of β-sheet domains. Most class I fusion proteins contain fusion peptides, but filovirus and avian sarcoma leukemia virus proteins contain a fusion loop. Renavirus glycoproteins (GPs) may contain both a fusion loop and a fusion peptide.[366] For coronaviruses the situation is not entirely clear, although it is widely accepted that a peptide fusion is involved in membrane fusion[367–369] and not a fusion loop.

The fusion domain of the spike proteins is strongly persists between β-coronaviruses.[42] The exact ''FP'' has not yet been definitively identified and is the subject of debate,[370–372] but there is consensus that potential FPs typically compose of 15–40 residues.[66,149,367,373–376] Sequence alignment analysis revealed that the SARS-CoV-1 FP sequence spanning residues 798–815 is highly conserved within the Coronavirus family.[365,367] This region, located at the N-terminus of S2 following the S2′ cleavage site (Fig. 9A), is prone to penetrating the cell membrane.[377] Fragment 798–823 was considered a

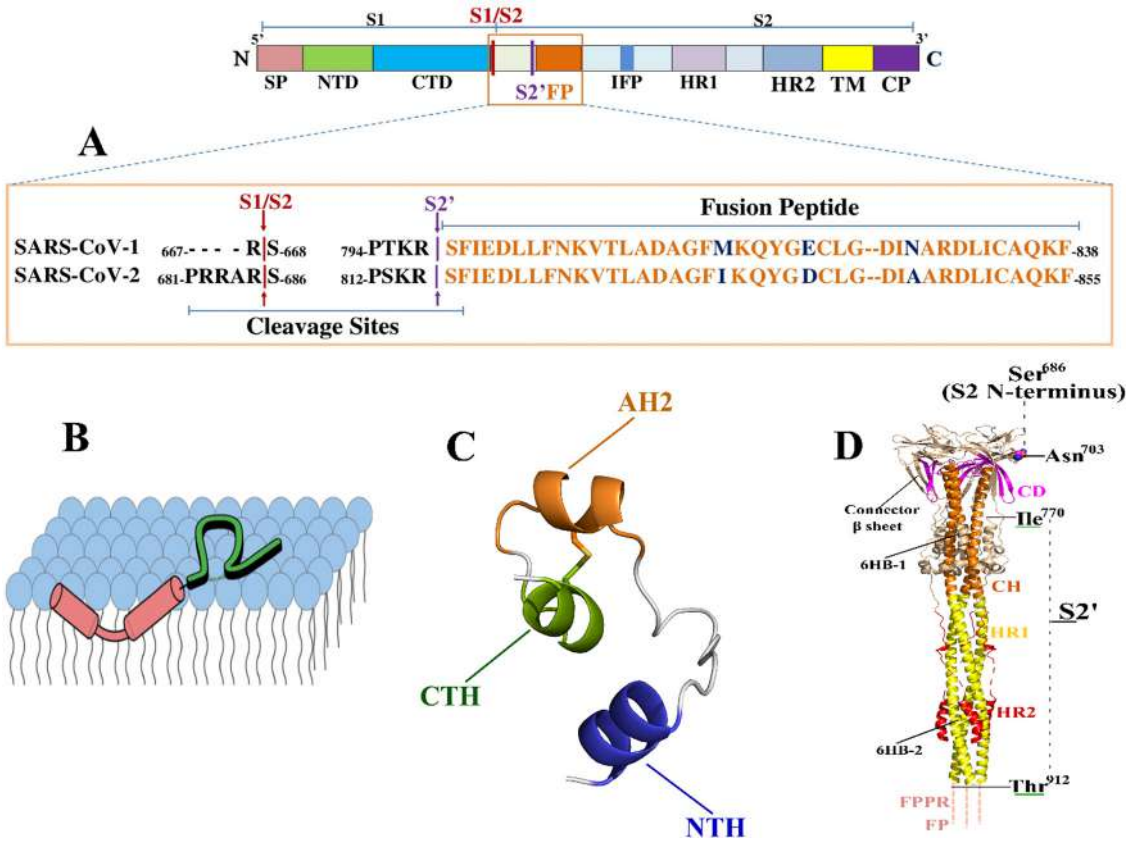


Fig. 9 (A) FP is adjacent to S2′ followed by an internal FP (IFP). SARS-CoV-1 FP has 41 residues between S798 and F838, while SARS-CoV-2 FP has 40 residues between S816 and F855. (B) Experimental structure of SARS-CoV-2 FP on a dodecylphosphocholine membrane that has a helix-turn-helix motif (S816-G838) and a loop (D839-F855)[365] (Reproduced from ref. 365 with permission from American Chemical Society, copyright 2021). (C) FP structure obtained by MD simulation in solution without membrane.[128] It contains an N-terminal amphipathic helix (NTH), a second amphipathic helix (AH2), and a C-terminal helix (CTH). (D) Postfusion structure of SARS-CoV-2 trimeric S2 (PDB ID: 6XRA) including HR1, the central helix (CH), the connector domain (CD) and HR2.

good FP candidate.[378] Bosch *et al.* showed that region 858–886 in the S2 subunit of SARS-CoV-1 can effectively promote membrane fusion.[373] Two segments 770–788 and 864–886 have been identified as potential FPs of SARS-CoV-1,[374] while Guillén *et al.* disclosed that segment 873–888 shows a high binding affinity to negatively charged phospholipids.[375]

As with SARS-CoV-1, several potential FPs have been proposed for SARS-CoV-2. Among them, the most popular is FP containing 40 amino acids in the region 816–855 (Fig. 9A).[42,66] Fragment 816–841 was computationally identified as a possible FP.[378] Since a FP is expected to be short (about 20 residues), hydrophobic, with a possible canonical fusion tripeptide (FXG or YFG) together with the central proline residue,[374] several putative FPs at or near the S2′ N-terminus have been suggested: FP1 (816-SFIEDLLFNKVT-LADAGFIKQY-837), FP2 (835-KQYGDCLGDIAARDLICAQKFN-856), and FP3 (854-KFNGLTVLPPLLTDEMIAQYT-874). In addition to FPs located at the N-terminal of S2, internal FPs (IFPs) that are located between FP and HR1 (Fig. 9A) has been considered.[371,372,379] One example of IFPs is fragment 885-GWTFGAGAALQIPFAMQ-MAYRFNGI-909.[379]

### 6.3. Main steps in fusion process

The main steps in the fusion of virus and host cell membranes are shown in Fig. 10.

**6.3.1. Prefusion state and viral attachment.** The prefusion state is characterized by binding of the virus to host cells (Fig. 10A). In this state, SARS-CoV-2 RBD samples either a ''three down'' or a ''one up'' conformation, followed by a viral attachment (Fig. 10B) step where only RBD in the ''up'' conformation can bind human ACE2 SARS-CoV-2 binding to the host cell has been intensively studied experimentally and theoretically and the main results are reviewed in chapter 3.

**6.3.2. Prehairpin intermediate.** In the pre-fusion state after ACE2 recognition, protease cleavage at the S1/S2 and S2′ sites results in the dissociation of S1 from S2, leading to a conformational change in S2 to form the prehairpin intermediate (PHI).[66,380,381] In this state, the heptad repeat-1 (HR1) domain adopts a three-helix bundle (3HB) structure that facilitate the FP attachment to the host cell membrane, and the distal transmembrane (TM) segment inserts into the viral membrane (Fig. 10C).

Two major events including the dissociation of the S1 subunit and the entry of FP into the host cell membrane have been extensively investigated for the SARS-CoV-2 case. SARS-CoV-2 S1 dissociation was found to occur due to proteolytic cleavage at one or both of the S1/S2 (S704–V705) and S2′ (R815–S816) sites. This conclusion is based on the mechanisms of the related viruses SARS-CoV-1[149] and MERS-CoV,[382] as well

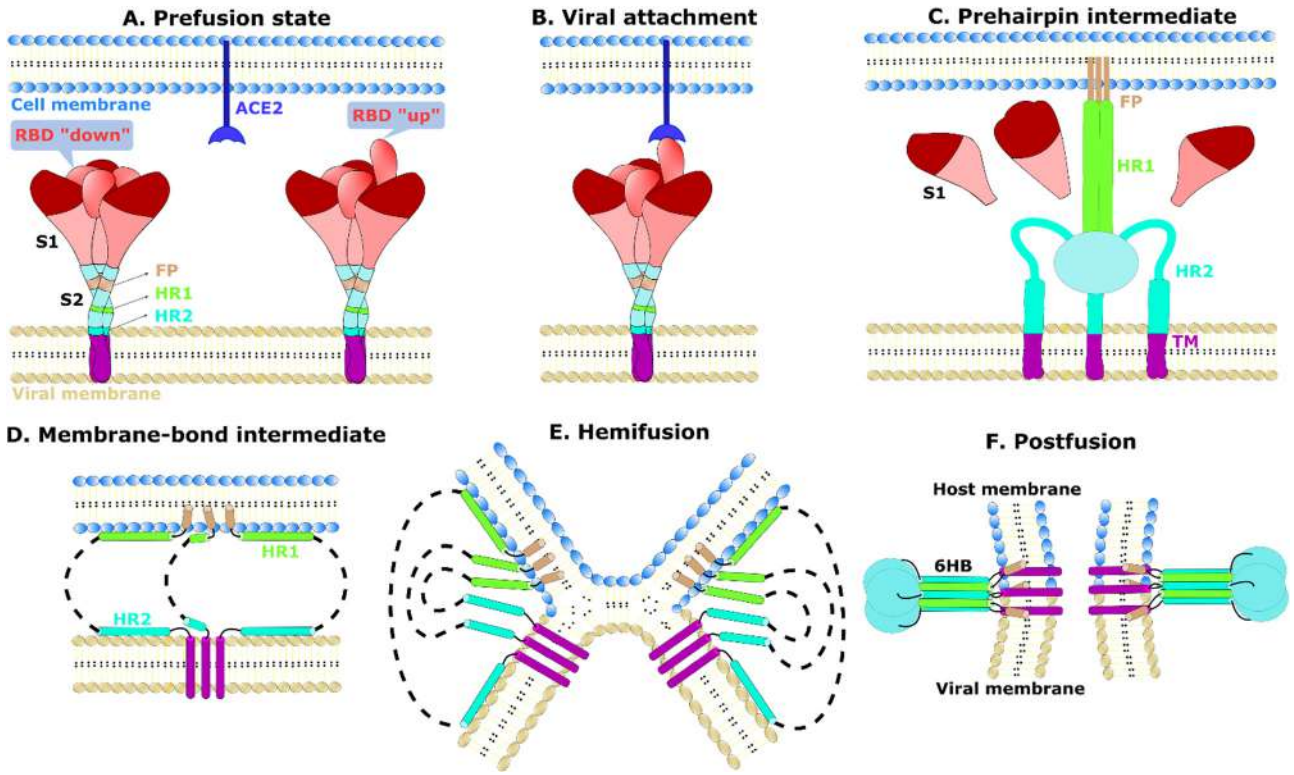


Fig. 10 Main steps in the fusion process. (A) Prefusion state in which the spike protein stochastically switches between RBD down and RBD up conformations. The structure of protein S in this state has been resolved experimentally. (B) Attachment of the virus to host cells *via* binding of open RBD to ACE2. (C) Prehairpin (or fusion) intermediate state: S1 detaches from S2 and FP penetrates into the host cell membrane. (D) Membrane-bound intermediate: HR1 lies on the host cell membrane, while HR2 is found on the viral membrane, (E) Hemifusion: Apposed outer leaflets of the viral and host cell membranes merge, but the inner leaflets remain intact. (F) Postfusion: Both the outer and inner leaflets fuse to form a pore that allows the viral gene to enter the host cell. In the postfusion state, the structure of the S2 trimer was determined experimentally.

 

as recent experimental findings for SARS-CoV-2,[66,383] which showed that the cellular protease furin cleaves the spike protein. Furin binding poses in the S1/S2 region were identified by using docking and molecular dynamics simulation.[384]

To shed mechanistic insights into S1 dissociation upon S1/S2 cleavage, based on cryo-electron tomography data Pak *et al.*[385] developed a coarse-grained model to study the interaction between membrane-bound spike trimers and membrane-bound ACE2 dimers. They found that ACE2-induced S2 core exposure is more sensitive to the extent of S1/S2 cleavage and conformational state populations than the ACE2 binding affinity. These interesting simulations have demonstrated the importance of a concerted interaction between spike trimers and ACE2 dimers that primes the virus entry and membrane fusion, but a coarse-grained model cannot fully reveal the molecular mechanism of S1 dissociation. This problem can be solved with QM-MM simulation, which is probably forbidden by current computing resources.

*Penetration of PF into the membrane.* The thrust of HR1 unfolding triggers insertion of FP into the host-cell membrane[127,386] (Fig. 9B). Given the important role of this step in membrane fusion, various experimental[66] and computational[36,128,375,378,387–389] studies have been performed to shed light on the mechanism of membrane–FP interaction.

Combining various experimental techniques including NMR, paramagnetic relaxation enhancement (PRE) and circular dichroism (CD) the interaction of 40 amino acid FP(816–855)[66] with a membrane was studied.[365] Upon association with the membrane, FP was found to form a helix–turn–helix motif (Fig. 9B) and the entropy gained during the transition from a random coil to this conformation is likely the driving force for membrane insertion below the phospholipid head groups. The loop region (D839–F855) weakly interacts with the membrane and lies on the lipid surface of the membrane.[365]

Using an enhanced sampling scheme and a Markov state model Remington *et al.*[387] considered the FP opening of the SARS-CoV-2 spike protein and disclosed that that the proteolytic cleavage state of the spike protein is associated with the structural flexibility observed in the upper dynamic region of FP in the S2 subunit. This result suggests that after cleavage of the S2' site, FP opening occurs on a sub-μs time scale. Using all-atom MD simulation the Hummer group[128] studied the FP structure in aqueous solution and found two short amphipathic helices, important for membrane fusion, formed at the N-terminus and in the middle, and the third helix was observed at the N-terminus (Fig. 9C). By placing FP in close proximity to the host endosome and plasma membrane and running eight conventional MD simulations of 10 μs, they demonstrated that FP can spontaneously associate with both membranes, and such binding occurs primarily by incorporation of two short helices into the membrane interface. The importance of the LLF hydrophobic motif (L821/L822/F823) from the N-terminal region for fusion activity, which was observed from mutagenesis studies,[367,377,390] has been confirmed by MD simulations.[128] A loop observed experimentally on the membrane surface[365] has not been recognized in simulations[128] and this may be due to the fact that in the experiment the FP interacts with one membrane, while the simulation is carried out in the region near two membranes. Stability of the membrane-FP complex was probed by pulling FP from the membrane using SMD.[128] With the pulling speed of 0.03 m $s^{-1}$ the bound FP can withstand a force of about 250 pN before being separated from the membrane. This force is about 10 times greater than the force required to pull the host cell membrane and the viral membrane together to fuse. Although this high pulling force is due to fast stretching and the presence of a disulfide bond between C840 and C851 in FP, it clearly shows the high mechanical stability of FP embedded in the membrane.

The highly mobile membrane mimetic model was used to study the insertion of a truncated FP of 26 residues (816–841).[389] As in the case of full length,[128] residues L821, L822, and F823 penetrate deeper into the membrane than other residues in all MD runs. However, the truncated FP adopted a binding mode that was not observed for the 40 residue FP.[128] In this mode, the entire peptide acquires helix structure and incorporates on the top of the membrane.[389] It remains unclear whether the absence of such a mode is a real effect or a consequence of a short MD simulation.

Various oligomeric units of SARS-CoV-2 have been investigated as putative FP candidates using MD modeling, where the peptides are located between two membranes.[388] Of all the tested systems, a trimer of 816–855 fragments has the best ability to trigger the initial stage of membrane fusion. Association of this trimer with double membranes lead to lipid migration from the lower leaflet of the upper bilayer to the upper leaflet of the lower bilayer, creating a structure resembling a fusion bridge.[388] This result suggests that spike residues 816–855 represent a true SARS-CoV-2 FP and that computational methods are an efficient way for identification of FPs in viral glycoproteins.

Shen *et al.*[378] performed all-atom MD simulations to compare the binding affinity of the SARS-CoV-1 FP (798–823) and SARS-CoV-2 FP (816–841) to a POPC/POPE/cholesterol bilayer membrane. These FPs are of the same length and are highly conserved with only two mutant residues M816/I834 and E821/D839, but cryoEM analysis revealed a significant difference in their structures.[76,85,391] Namely, the SARS-CoV-2 FP helix ($\approx$1.1 nm) is shorter than that of SARS-CoV-1 FP ($\approx$1.9 nm). The difference in helix length resulted in a higher binding affinity of SARS-CoV-2 FP compared to SARS-CoV-1 FP,[378] which agrees with the experimental result of Lai *et al.*[370] The membrane-entering residues Phe, Ile, and Leu have been found to interact strongly with membrane cholesterol, implying that these hydrophobic residues are critical for membrane binding of FP.

**6.3.3. Membrane-bound intermediate.** The existence of a membrane-bound intermediate (Fig. 10D) is debated because high-solution structures are not yet available.[43] Most fusion models show FP and TM domains of fusion proteins as the membrane-embedded regions, with HR1 and HR2 (residues

1171 to 1207) generally considered as linear extended trimers in this intermediate states.[392] However, a growing body of evidence indicates that the HR1 and HR2 regions of influenza hemagglutinin[393] and HIV-1 gp41[394,395] can interact with membranes and play an essential role in the fusion process. In the micelle-bound state they adopt monomeric α-helices and NMR (nuclear magnetic resonance) measurements demonstrated the absence of HR1-HR2 interactions and that these helices reside at the water–lipid interface.[396] Using POPC and POPC/POPG bilayers and solid-state NMR, Aisenbrey *et al.* also found that HR1 and HR2 are parallel to the membrane surface.[397] Thus, for HIV, both solid-state and solution NMR experiments confirm the existence of a membrane-bound intermediate state with HR1 and HR2 helices embedded at the lipid-water interface of the host cell and virus membranes, respectively.

To test whether a similar membrane-bound intermediate scenario applies to class I fusion proteins, Chiliveri *et al.* performed biophysical measurements to characterize the membrane-binding properties of HR1 and HR2 of the SARS-COV-2 spike protein.[43] In aqueous environment, isolated HR1 and HR2 fragments can adopt either monomeric or tetrameric structures in equilibrium. This observation is consistent with tetramer formation of HR1 and HR2 derived from SARS-CoV-1, HIV and HIV-1.[398,399] Circular dichroism (CD), NMR spectroscopy, and analytical ultracentrifugation (AUC) measurements showed that in the presence of small unilamellar vesicles (SUVs) or phospholipid isotropic bicelles, HR fragments have a monomeric α-helical structure.[43] 15N backbone relaxation and hydrogen exchange (HX) measurements revealed that large internal motions of the dynamic HR1 α-helix occur on a sub-ns time scale. Using residual the dipolar couplings (RDCs) method, a solution structure can be obtained, which shows that the HR1 helical structure has a dynamic kink, while residues exposed to the phospholipid bilayer and to solvent can be identified by paramagnetic relaxation.

As in the HIV case,[397] in the membrane-bound intermediate of SARS-CoV-2, HR1 lies on the host cell membrane, adopting a helix structure, while HR2 lies on the virus membrane.[43] HR2 binds with low affinity with lipid bilayers as a dissociation constant, $K_D \sim 100$ mM.[43] Despite this low binding affinity HR2 can interact with the viral membrane most of the time due to the fact that it directly anchors the TM helix (Fig. 10D).

**6.3.4. Hemifusion.** The addition of HR2, originally anchored to the viral membrane by the TM fragment, recruits HR1 from the surface of the bilayer to form a C3-symmetrical 6HB structure, pointing to the mechanism by which 6HB formation is associated with membrane fusion. However, before reaching this postfusion state, hemifusion represents another obligatory intermediate step.[395] In this intermediate state, the two inner leafts of the bilayers come very close to each other, while the apposed proximal outer leaflets fuse (Fig. 10E). The hemifusion step is a transient and can either proceed to pore formation or dissociate and form two separate vesicles.[400] As with the membrane-bound intermediate, the highly-solution structure of S2 in the hemi-fusion state has not been resolved either experimentally or computationally.

Using fluorescence-based methodologies, Pattnaik *et al.*[371] found that the internal fusion peptide 1 (IFP1, GAALQIPFAMQMAYRF) of SARS-CoV-2 is far more efficient than its N-terminal counterpart (IYKTPTLKDFGGFNFSQIL) in inducing hemifusion between small unilamellar vesicles. The higher fusogenicity of IFP1 may be due to its higher hydrophobicity compared to N-terminal FP.

**6.3.5. Postfusion.** After hemifusion, when the outer leaflets of the virus and host membrane fuse, in postfusion the inner leaflets fuse, resulting in fusion core formation (Fig. 10F) and facilitating virus entry. This step occurs mainly due to folding back of HR2 and the formation of long central three helical strands.[76] Since the postfusion state is stable, the structure of the S2 trimer in this state was resolved by cryo–electron microscopy and cryo–electron tomography (Fig. 9D). The postfusion structure contains the unusually long central three-stranded coiled coil formed by HR1 and CH, making it a highly rigid structure.

Together with the connector domain, the 718–729 segment from the S1/S2–S2′ fragment forms a three-stranded β-sheet invariant between post- and pre-fusion structures. In the postfusion state, the 1127–1135 residues bind to the connector β-sheet, extending it to four strands, with HR2 projecting toward the viral membrane. Residues 737–769 of the S1/S2–S2′ fragment form three helical regions connected by two disulfide bonds that are stacked against the CH groove of the spiral coil, forming a bundle of six spirals (6HB-1 in Fig. 9D). The N-terminal region of HR2 has a single-turn helical shape and also fits against the groove of the helical coil HR1. The C-terminal region of HR2 constitutes a longer helix forming a second six-helix bundle structure with part of HR1 (6HB-2 in Fig. 9D). The post-fusion structure of S2 with glycans is displayed in Fig. 1D.

### 6.4. Effect of cholesterol on membrane fusion

Membrane fusion depends on the lipid composition of the host and viral membranes.[401] Due to an inverted cone-like structure, cholesterol can generate negative curvature to the membrane promoting the formation of fusion intermediates. Cholesterol might promote membrane fusion by modulating penetration depth,[402] peptide conformation,[403] and membrane stiffness.[404] According to the ''lipid rafts'' scenario, in both viral and host membranes, cholesterol and sphingolipid molecules tend to clump together and form microdomains called ''lipid rafts'' floating in a ''sea'' of phospholipids.[405] The high ordering of the lipid tail in rafts influences the distribution of proteins and other lipids.[406] It has been shown that viral transmembrane receptors can be concentrated within rafts serving as ''hot spots'' for virus entry, and cholesterol in rafts promotes fusion by reducing the energy required to form fusion intermediates.

Several attempts have been made to understand the interaction of SARS-CoV-1 with lipid rafts, but the location of its ACE2 receptor in rafts remains controversial. Earlier studies demonstrated that ACE2 was found in non-raft fractions in Vero E6 cells endogenously expressing it and in Chinese hamster ovary (CHO) cells transiently expressing it.[407,408] Other

 

studies have shown that ACE2 co-localizes with the raft proteins flotilin-2, ganglioside GM1, and caveolin-1 in Vero E6 cells,[409,410] with discrepancies between these results explaining different experimental techniques.[409] By examining the role of cholesterol in SARS-CoV-1 infectivity these studies have supported the notion that ACE2 is a raft protein. By disrupting raft formation with the cholesterol-chelating drug methyl-β-cyclodextrin (mβCD), ACE2 is no longer concentrated in rafts, reducing receptor availability and therefore SARS-CoV-1 binding efficiency.[410] Thus, these results confirm that lipid rafts can serve as an entry port for SARS-CoV-1.

An *in vitro* study of the molecular mechanism of spike/ACE2-driven membrane fusion by Sanders *et al.*[411] revealed that cholesterol is essential for SARS-CoV-2 to enter the host cell, but not *via* a raft-dependent mechanism, suggesting that, unlike in the case of SARS-CoV-1, ACE2 is not a raft protein. However, Li *et al.*[412] showed that the cholesterol-rich lipid raft is a platform for SARS-CoV-2 entry after engagement with ACE2. Formation of lipid rafts is also relevant for SARS-CoV-2 entry *via* other non-ACE2 receptors like HDL-scavenger receptor B type 1 (SR-B1) and CD-147.[413] Infection with SARS-CoV-2 was found to depend on membrane cholesterol of the virus, but not the host cell.[411] It would be interesting to test whether this observation holds true for SARS-CoV-1 and other coronaviruses.

Pattnaik *et al.*[371] explore the effect of cholesterol on the ability of IFP1 and the N-terminal FP (IYKTPTLKDFGGFNFSQIL) to modulate hemifusion of SARS-CoV-2. Namely, the ability of IFP1 to induce the formation of hemifusion state sharply increases with growing content of cholesterol in the membrane. Interestingly, IFP1 is able to induce semi-fusion but fails to open the pore.[371] It was demonstrated that the interaction of the fusion peptide with the transmembrane domain of the fusion protein is important for pore opening.[414] Therefore, the limited ability of fusion peptides to open up the pore observed by Pattnaik *et al.*[371] further supports the hypothesis of an interaction between transmembrane domain and fusion peptide to open the fusion pore.

### 6.5. Effect of $Ca^{2+}$ on membrane fusion

Since metal ions affect the membrane ordering, they have been shown to be important for membrane fusion process such as synaptic vesicle fusion.[361] Experimental studies discovered that the rubella virus[415] and Ebola virus[416,417] fusion machinery coordinates with $Ca^{2+}$ for proper orientation and insertion into the host membrane.

The functional role of $Ca^{2+}$ in activity of FPs was studied for other closely related viruses, such as MERS-CoV,[418] Ebola virus[416] and SARS-CoV-1.[377] For example, $Ca^{2+}$-induced enhancement of MERS-CoV fusion with host cells increases infectivity as reported by Straus *et al.*[418] Here we briefly discuss the SARS-CoV-2 case, which has been intensively studied experimentally[370,379] and computationally.[419] MD simulations with a POPC/POPG/Cholesterol membrane revealed that $Ca^{2+}$ ions prefer to bind to the E819/D820 and D830/D839 residue pairs (Fig. 11A).[419] Remarkably, FP insertion proceeds predominantly in the presence of these two $Ca^{2+}$ binding poses. Thus,

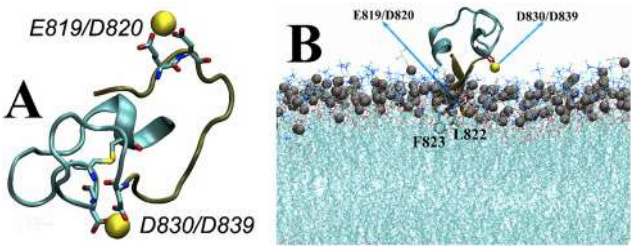


Fig. 11 (A) The most populated conformation of FP interacting with a membrane; $Ca^{2+}$ ions (lemon yellow) bind to E819/D820 and D830/D839. (B) $Ca^{2+}$ at E819/D820 and L822 and F823 of the LLF motif are embedded in the membrane. The results were obtained by all-atom MD simulations.[419] Reproduced from ref. 419 with permission from Elsevier, copyright 2021.

FP inserts the hydrophobic residues L822 and F823 of the LLF motif into the hydrophobic part of the membrane (Fig. 11B), and this predominant mode is stabilized by several factors, including the electrostatic interaction of E819/D820-bound $Ca^{2+}$ with lipid head groups. This theoretical conclusion is consistent with the experiment[370,379] showing that $Ca^{2+}$ ions can enhance the interaction of the membrane with FP and stabilize its insertion.

### 6.6. Effect of mutations on membrane fusion

SARS-CoV-2 D614G variant was recognized shortly after the emergence of COVID-19 in China and D614G is found in all variant of concern such as Alpha, Beta, Gamma, Delta and Omicron (Fig. 7). D614G is one of the most important mutations that increase the infectivity of SARS-CoV-2[420,421] has been extensively studied.[422] Here, we briefly discuss its role in virus-host membrane fusion, although it may alter viral activity through other mechanisms, including promoting an open conformation favorable for RBD-ACE2 interaction,[423–425] and stabilizing the prefusion spike trimer complex and amplifying spike protein incorporation into the virion.[426] The D614G mutation in the SARS-CoV-2 spike protein has a dual effect on the stability of the spike protein trimer, depending on ACE2 involvement.[427] Namely, this mutation promoted S-trimer stability in the absence of ACE2, but increased spike protein trimer dissociation upon engagement with ACE2 exposing the S2 subunit. The increased S2 production by the D614G mutant enhanced membrane fusion and high contagiousness. To test whether high Delta S transmissibility is associated with more efficient fusion, Zhang *et al.*[197] performed a time-course experiment with a cell–cell fusion assay and found that at high transfection levels of S and ACE2, differences in fusion activity between Alpha, Beta, Delta, Gamma, G614 and Kappa are not significant. However, at low levels of ACE2, the Delta spike protein can fuse membranes more efficiently than the other five variants, possibly explaining its increased transmissibility.

Two cleavage sites, S1/S2 (WT spike residues: 675–690) and S2′ (809–821), have been shown to promote host-virus membrane fusion. Cleavage at the S1/S2 site leads to shedding of the S1 unit and induces structural rearrangement that subsequently allows the S2′ site to become accessible to host

proteases.[149,428] Therefore, together with D614G, mutations at these cleavage sites may be critical for membrane fusion. The P681R mutation may boost membrane fusion of Delta by facilitating cleavage of the precursor protein S to the active S1/S2 conformation.[429] An important role of the P681R mutation in increased pathogenicity and fusogenicity in hamsters was also demonstrated by Saito *et al.*[430] Using bioinformatics tools, Beaudoin *et al.*[431] demonstrated that variants of concern and variants of interest display different membrane fusion capacity. Mutations at or near cleavage sites can alter interaction with host proteases and thus fusion potential. All mutations found at the S1/S2 site were predicted to increase affinity for furin protease but not for TMPRSS2.[431] This interesting prediction needs further verification in *in vitro* and *in vivo* experiments.

Mutations in HR1 and HR2 are expected to be critical for membrane fusion, as their refolding generates the energy needed to complete this process, allowing viral RNA to enter the host cell. Yang *et al.*[432] selected eight mutations (five mutations D936Y, L938F, S940F, A942S, V1176F from the SARS-CoV-2 variant and three mutations Q954H, N969K, L981F from the Omicron varian), in the postfusion HR1HR2 bundle for structural and functional studies. As shown by single particle cryoEM, these mutations have little effect on bundle structure but reduce fusion activity, with the exception of A942S, which increases fusion activity approximately threefold. For the D936Y and S940F mutants, the decrease in fusion activity is associated with disruption of the D936-R1185 salt bridge, while the A942S mutation results in the formation of one additional hydrogen bond between the HR1 residue S942 and the HR2 residue N1187, along with an increase in fusion activity.[432] The fusion activity of the Omicron triple mutant (Q954H-N969K-L981F) in HR1 is ~80% of that of WT.

Mutations do not occur in the SARS-CoV-2 FP (S816-F855) of the variants of concern (Fig. 7), but for Omicron BA.1, the N856K mutation[433] should affect the fusion process at it is adjacent to the FP. However, this effect has not been investigated.

# 7. Interaction of spike protein with antibodies and nanobodies

An antibody (Ab) in the immune systems, is produced and secreted by B cells, usually differentiated B cells, including plasma cells and memory B cells. Ab consists of a pair of polypeptide chains forming a flexible Y-shape (Fig. 12A). The Y-shape stem is made up of the ends of two identical heavy chains, and each arm is made up of the remainder of the heavy chain plus a smaller protein called a light chain. Within certain Ab classes, the stem and the bottom of the arms are quite similar and referred to as the constant region. The tips of the arms vary greatly in sequence and can bind antigens.[434,435] In detail, each antibody has two fragments, including a fragment of the antigen-binding site (Fab), one at the end of each arm, which allows the immune system to recognize an equally wide variety of antigens, and a fragment of the crystallizable region (Fc), composing of two heavy chains (Fig. 12A).[436]

Monoclonal antibody (mAb) is a type of protein that is made in a laboratory and can bind to certain targets in the body, for example, antigens on the surface of cancer cells. It has been discovered and developed using hybridoma technology, known as the first reliable source of Ab therapy.[437,438] The therapeutic and prophylactic efficacy of mAbs against cancer, neurological disorders, and infectious viruses (HIV, Ebola, MERS, SARS-CoV, SARS-CoV-2, *etc.*) has already been established.[439–442] However, they cause some side effects, mostly related to immunomodulation and therapeutic Abs, such as Ab-dependent enhancement and cytokine storm, which may be associated with infection.[443–445]

Nanobody (Nb) is an antigen-specific, single-domain and variable camelid heavy chain-only segment Abs that are produced recombinantly. This type of Ab exhibits a wide range of strong physical and chemical properties such as high solubility, and stability. Nb is a relatively new type of recombinant Ab derived from members of the Camelidae such as camels, llamas and alpacas (Fig. 12B).[446–448] Although Nb lacks a light chain, resulting in disadvantages in terms of antigen binding, it has intriguing properties including higher solubility, smaller size, greater resistance to denaturation under some special conditions, higher thermal stability and chemical stability than Ab. It can be administered with an inhaler directly into the most common site of SARS-CoV-2 infection, the respiratory tract.[449,450] For example, a camelid antibody of only heavy chain called VHH could offer a cheap and easy way to produce antiviral agents for passive immunization. Moreover, tissue penetration and extravasation of Nb are better classical Ab, which explains it greater therapeutic value.[451,452]

As mentioned in the previous section, the S protein consists of two functional subunits: S1 is responsible for adherence to the host cell and S2 promotes fusion of virus and host membranes.[127,453] Both Ab and Nb target S1 (RBD and NTD) and S2 (FP), but most Ab and Nb target RBD (Fig. 12C and D).[82,127,454]

In summary, Ab has been demonstrated to be a promising class of therapeutics against SARS-CoV-2 infection.[38,455–459] Since the convalescent plasma from recovered patients contains Abs elicited by the adaptive immune response, it may improve survival rate, but this issue is still under debate.[460–462] In addition, the large-scale production of plasma-based therapies presents significant challenges due to high costs. As a result, seeking potent Abs on an industrial scale is becoming one of the most feasible strategies to combat COVID-19. Another promising way is the use of Nb, which is small but very stable and easy to manufacture, and targets only RBD as therapeutic agents.[168,463] We will discuss the most representative therapeutic Abs and Nbs and their interaction with the host cell. A discussion of antibodies generated by the host immune system is beyond the scope of this review.

### 7.1. Neutralizing Abs targeting RBD

RBD is the target of a variety Abs and Nbs (Fig. 12D), which inhibit SARS-CoV-2 infection by disrupting the interaction between the spike protein and ACE2 (Fig. 12C). SARS-CoV-2 is

 

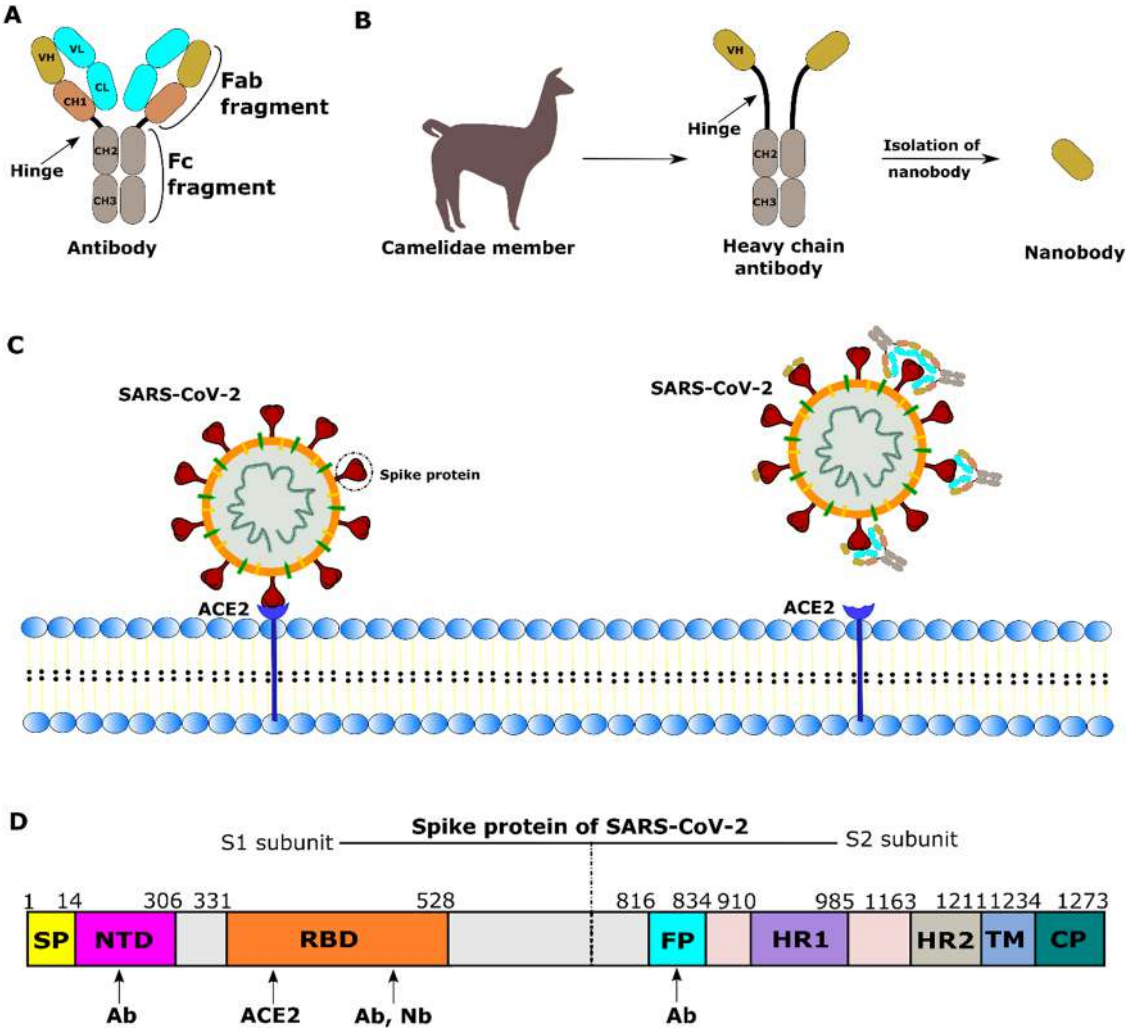


Fig. 12 (A) An antibody structure contains antigen binding sites (Fab) and crystallization region fragments (Fc), which include VH (heavy chain variable domain), VL (light chain variable domain), CH (heavy chain constant region), and CL (light chain constant region). (B) Nanobody isolated from the heavy chain of antibodies that are extracted from the Camelidae members. (C) SARS-CoV-2 binds to ACE2 to infect a human cell; Ab and Nb bind to the spike protein to prevent SARS-CoV-2 from entering the human cell. (D) The spike protein structure includes S1 and S2 domains; ACE2, Ab and Nb bind to RBD while Ab also binds to NTD and FP.

an asymmetric trimer and its RBD can sample open and closed conformations. Neutralizing Ab can bind to RBD in the closed, open or closed-open states,[158,464] but SARS-CoV-2 cannot recognize host cell ACE2 in the down state. Therefore, Ab binding to the inactive RBD conformation is not important for further discussion. RBD is composed of a core and RBM, the latter is responsible for binding to the SARS-CoV-2 receptor,[87] but Abs can bind to both of them. In this review, we only discuss some important Abs such as REGN-CoV (combination of REGN10933 and REGN10987), S309, LY-CoV555, LY-CoV016, AZD7442 (combination of AZD8895 and AZD1061), CT-P59, LY-CoV1404, and P2C-1F11 (Fig. 13), which have an emergency use authorization (EUA) as a therapeutic Ab targeting RBD. Table 3 lists their neutralization and binding characteristics. Here, neutralizing activity is characterized by either $IC_{50}$ or $EC_{50}$ of antibody, while binding activity is measured by the $K_D$ of the RBD-Ab complex in the absence of ACE2.

**7.1.1. REGEN-CoV (Casirivimab/Imdevimab).** REGEN-CoV is a mAb cocktail that is a combination of REGN10933 and REGN10987 (also known as casirivimab and imdevimab) that reduces viral load and the number of patients with COVID-19. REGEN-CoV is active *in vitro* against SARS-CoV-2 variants of concern. The REGN-COV2 is a combination of the antibodies REGN10933 and REGN10987, derived from humanized VelocImmune® mice in addition to blood samples from patients who have recovered from COVID-19.[92]

The market name of REGEN-CoV is Casirivimab/Imdevimab, which was produced by the American biotechnology firm Regeneron Pharmaceuticals for the treatment of SARS-CoV-2. The drug replaced two monoclonal drugs, casirivimab (REGN10933) and imdevimab (REGN10987). On November 21, 2020, the U.S. Food and Drug Administration (FDA) issued an Emergency Use Authorization (EUA) for the use of casirivimab/imdevimab in the treatment of mild to moderate COVID-19

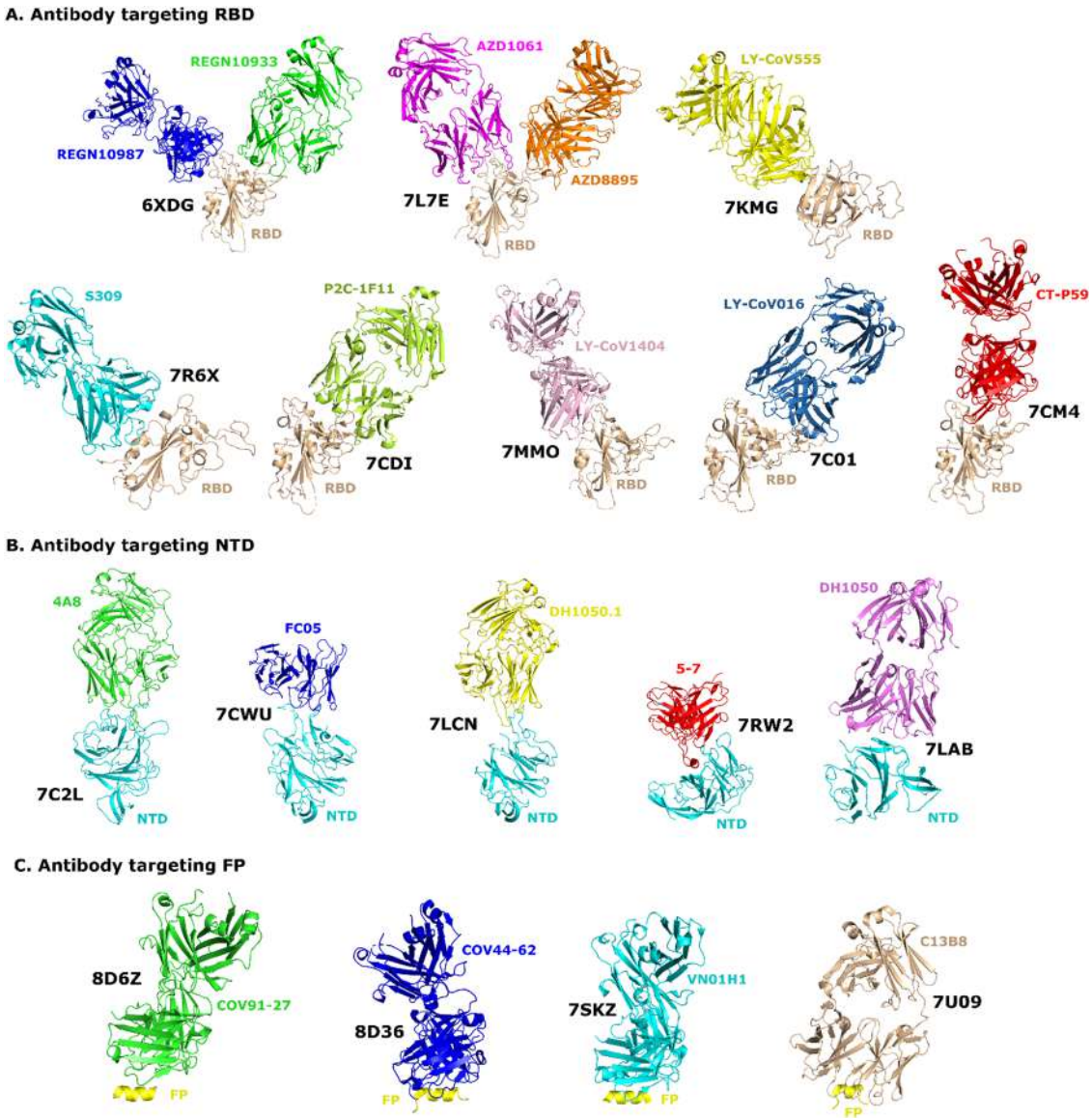


Fig. 13 3D structure of some antibodies targeting (A) RBD, (B) NTD and (C) FP. Their name and PDB ID are shown next to the image.

cases in adults and children aged min 12 years (**https://www.fda.gov/news-events/press-announcements/coronavirus-covid-19-update-fda-authorizes-monoclonal-antibodies-treatment-covid-19**).

REGN10933 and REGN10987 are attached to the top and side of RBD, respectively (Fig. 13A). The binding domain of REGN10933 to RBD overlaps to a large extent with the binding site of ACE2, while the binding region of REGN10987 overlap slightly with the binding site between RBD and ACE2. Thus, after binding to the spike protein, REGN10933 and REGN10987 occupy the RBD-ACE2 interaction interface, completely blocking the ACE2-S interaction.[465] The $K_D$ values of REGN10933 and REGN10987 are about 3.37 nM and 45.2 nM as estimated by experiment,[92] while they are about 1.73 and 16.38 nM as determined from MD simulations by Nguyen *et al.*[466] Thus both experiment and simulation ascertain that, in the absence of ACE2, REGN10933 binds to RBD more strongly than REGN10987. Despite the difference in binding activity, the neutralizing activity of REGN10933 (5.6 ng $mL^{-1}$) and REGN10987 (6.3 ng $mL^{-1}$) is almost the same,[92] implying the binding affinity alone does not determine neutralizing activity.

Recent reports have indicated that REGN10933 and REGN10987 can treat most escape mutants because they are a non-competing Ab cocktail. Beta and Gamma variants are fully resistant to REGN10933 and weakly resistant to REGN10987 in neutralization[467] while Alpha and Omicron are not refractory to the neutralizing activity of REGN-CoV.[468] The combination of REGN10933 and REGN10987 shows prophylactic and therapeutic efficacy against SARS-CoV-2 variants including Alpha, Beta, and Gamma but not against Omicron.[467,468]

For the Delta variant, although REGN10987 exhibits reduced neutralizing ability, REGN10933 and REGN10933 + REGN10987

 

Table 3 The list of antibodies targeting RBD, NTD and S2. Neutralizing activity is measured by either $IC_{50}$ or $EC_{50}$ of antibody, while binding activity is characterized by dissociation constant $K_D$ of the RBD-Antibody complex in the absence of ACE2. The methods used to obtain these characteristics are shown in the last column. BLI refers to biolayer interferometry, and SPR-surface plasmon resonance

| | | Antibody | PDB ID | Neutralizing activity ($IC_{50}$ or $EC_{50}$) | Binding activity ($K_D$) | Method |
|---|---|---|---|---|---|---|
| S1 | RBD | REGN10933 | 6XDG | 5.6 ng mL$^{-1}$[465] | 3.37 nM[92] | BLI, SPR |
| | | REGN10987 | | 6.3 ng mL$^{-1}$[465] | 45.2 nM[92] | BLI, SPR |
| | | S309 | 7R6X | 79.0 ng mL$^{-1}$[472] | 0.001 nM[472] | BLI |
| | | LY-CoV555 | 7KMG | 20 or 49 ng mL$^{-1}$[478] | N/A | SPR |
| | | LY-CoV016 | 7C01 | 0.036 μg mL$^{-1}$[479] | 2.49 nM[479] | BLI |
| | | AZD8895 | 7L7E | 47.7 ng mL$^{-1}$[483] | 0.003 nM[483] | BLI |
| | | AZD1061 | | 79.6 ng mL$^{-1}$[483] | 0.01 nM[483] | BLI |
| | | CT-P59 | 7CM4 | 8.4 ng mL$^{-1}$[484] | 0.03 nM[484] | SPR, BLI |
| | | P2C-1F11 | 7CDI | 0.03 μg mL$^{-1}$[488] | 2.12 nM[488] | SPR |
| | | LY-CoV1404 | 7MMO | 0.01 μg mL$^{-1}$[492] | 0.07 nM[492] | SPR |
| | NTD | 4A8 | 7C2L | 0.61 μg mL$^{-1}$[82] | 92.7 nM[82] | BLI |
| | | FC05 | 7CWU | NA | NA | SPR |
| | | DH1050.1 | 7LCN | 0.04 μg mL$^{-1}$[499] | NA | SPR |
| | | 5–7 | 7RW2 | NA | NA | SPR |
| FP of S2 | | COV91-27 | 8D6Z | NA | 0.49 nM[501] | SPR |
| | | COV44-62 | 8D36 | 9.8 μg mL$^{-1}$[501] | 0.95 nM[501] | SPR |
| | | C13B8 | 7U09 | NA | NA | NA |
| | | VN01H1 | 7SKZ | NA | NA | NA |

can still efficiently block spike protein entry into the host cell.[469] Verkhivker *et al.*[470] studied functional residues of the spike protein by targeting novel mutational variants and REGN-CoV escaping mutations. Using mutational sensitivity analysis and alanine scanning, they showed that residues K417, E484, and N501 correspond to key interacting centers with a significant degree of structural and energetic plasticity, allowing mutations at these positions to improve binding affinity for ACE2. Moreover, the functional centers in the spike protein can be exploited to manipulate the conformational landscape of the spike proteins, design allosteric modulators, and potential engineering, which could be useful for tailoring novel therapeutic interventions to combat potential antibody escaping resistance.

Using MD modeling Nguyen *et al.*[466] also showed that a cocktail of REGN10933 and REGN10987 binds to RBD more tightly than its components. The association of REGN10987 with RBD is driven by van der Waals interactions, whereas in the case of REGN10933 and the cocktail, electrostatic interactions predominate. They also demonstrated that Omicron reduced significantly the neutralizing activity of monoclonal antibodies REGN10933, REGN10987, and their combination, while Delta altered their activity slightly. This decrease in potency is mainly caused by the Q498R, L484A, N440K and K417N mutations in RBD.

**7.1.2. S309 (VIR-7831, Sotrovimab).** S309 is a mAb designed to prevent the progression of COVID-19 in patients at high risk in the early stages of the disease. It was first identified from the memory B cells of a person infected with SARS-CoV-1 in 2003 and was later found to be able to cross-neutralize SARS-CoV-2.[471] Cryo-EM analysis shows that S309 can attach to the open and closed states of the RBD in the spike trimer (Fig. 13A), with the neutralizing activity of 79.0 ng mL$^{-1}$[472] (Table 3).

Neutralization by S309 may be associated with the induction of spike trimer cross-linking, preventing RBD from interacting with ACE2 due to steric hindrance or causing virion aggregation.[473] S309 exhibited potent antibody-dependent cellular cytotoxicity and effector functions of antibody-dependent cellular phagocytosis.[472] The *in vitro* studies showed that S309 retains activity against circulating variants, including Gamma, Epsilon, Iota, and Delta[83,467,474] while it has lower neutralizing activity against Omicron than against the ancestral strain and other variants of concern.[474–476] Using accelerated MD simulation Marti *et al.*[477] showed that S309 binds to the spike protein more strongly than ACE2, which is consistent with the experiment[472] (Table 3).

**7.1.3. LY-CoV555 and LY-CoV016 (Bamlanivimab and Etesevimab).** LY-CoV555 and LY-CoV016 are RBD-targeting human IgG1 detected by high throughput microfluidic screen of antigen-specific B cells from a convalescent patient (Fig. 13A). A clinical trial for LY-CoV555 was conducted on hospitalized patients with COVID-19 in May 2020, with the neutralizing activity of 20 ng mL$^{-1}$.[478] This Ab then became the world's first SARS-CoV-2 specific Ab to be used for COVID-19 therapy. The activity of LY-CoV555 does not affect the Alpha variant, while its protective efficacy is lost against the Beta and Gamma variants by the E484-mutation point.[83,467] A complete loss of neutralizing activity against the Omicron variant has also been reported.[468]

According to X-ray crystallography data, the epitope LY-CoV016 on RBD largely overlaps with ACE2 binding residues. LY-CoV016 can neutralize SARS-CoV-2 with a neutralizing activity of 36 ng mL$^{-1}$.[479] Importantly, the combination of LY-CoV555 and LY-CoV016 more significantly reduces hospitalization and morality in high-risk patients compared to LY-CoV555 and LY-CoV016 alone.[480] The combination of LY-CoV555 and LY-CoV016 can neutralize Alpha, but does not protect Beta, Gamma, Delta and Omicron variants,[83,467–469] leading to their trials being paused by the US Department of Health and Human Services.

However, some contributions were made to a clear understanding of the interaction of this Ab with SARS-CoV-2. Liu *et al.*[481] reported that the E484Q/L452R mutations significantly reduced the binding affinity between Kappa and LY-CoV555. LY-CoV555 completely lost its neutralizing activity against Delta and Lambda variants due to the presence of L452R and L452Q mutations. Laurini *et al.*[482] predicted that E484A/G/K/Q/R/V, Q493K/L/R, S494A/P/R, L452R and F490S reduce the neutralizing capacity of LY-CoV555. Similarly, the K417E/N/T, D420A/G/N, N460I/K/S/T, T415P, and Y489C/S mutations confer the virus the advantage of escaping LY-CoV016. These findings provided essential structural information for the development of next-generation vaccines more resilient to viral evolution.

**7.1.4. AZD7442 (Tixagevimab and Cilgavimab).** AZD7442 is a combination of two mAbs, AZD8895 (Tixagevimab) and AZD1061 (Cilgavimab) isolated from convalescent patients after SARS-CoV-2 infection and later engineered as long acting IgG molecules. Both AZD8895 and AZD1061 bind to two distinct non-overlapping epitopes on the SARS-CoV-2 RBD in an up conformation[483] (Fig. 13A). The dissociation constant of AZD8895 and AZD1061 and AZD7442 is $K_D$ = 2.8, 13 and 13.7 pM, respectively (Table 3). The neutralizing ability is $IC_{50}$ = 47.7, 79.6 and 65.0 ng $mL^{-1}$ for AZD8895, AZD1061 and AZD7442, respectively. AZD7442 is known as a potential candidate to neutralize most SARS-CoV-2 variants.[483]

**7.1.5. CT-P59 (Regdanvimab).** CT-P59 is a monoclonal antibody being considered by the European Medicines Agency in October 2021 for marketing authorization for the treatment of patients with COVID-19 who do not require supplemental oxygen therapy and who are at high risk of developing severe COVID-19. CT-P59 can inhibit SARS-CoV-2 by blocking the interaction between RBD and ACE2 (Fig. 13A) at a dissociation constant $K_D$ = 0.027 nM and a neutralizing activity of 8.4 ng $mL^{-1}$[484] (Table 3). It is effective against the Alpha, Beta, Gamma, Delta, Epsilon and Kappa variants,[485,486] but has reduced inhibitory activity against the Omicron variant.[468]

Using FoldX, Mutabind2, mMCS-PPI2 and DS methods, Fung *et al.*[487] predicted the binding free energy for various variants targeting this convalescent antibody. RBD residues F456, F486, F490, G485, L452, L455, L492, Q493, S494, Y449, and Y453 have been identified as possible immune-escaping hotspots that are unfavorable for the virus binding to the CT-P59 post-mutation.

**7.1.6. P2C-1F11 (Amubarvimab).** P2C-1F11 is a mAb that exhibits the most potent neutralizing activity *in vitro* and confers strong protection against SARS-CoV-2 infection. It occupies a large binding surface area with RBD (Fig. 13A), resulting in strong neutralizing activity against SARS-CoV-2 ($IC_{50}$ = 0.03 μg $mL^{-1}$), and high binding affinity for RBD ($K_D$ = 2.12 nM)[488] (Table 3). Amubarvimab can maintain neutralization of Alpha, Beta, Gamma, and Delta variants, but its binding activity is completely reduced by the Omicron variant.[489–491]

**7.1.7. LY-CoV1404 (Bebtelovimab).** LY-CoV1404 can effectively neutralize WT and all known variants, such as D614G, Alpha, Beta, Gamma, Delta, Omicrons. Bebtelovimab exhibits strong neutralizing activity ($IC_{50}$ = 0.011 μg $mL^{-1}$), and high binding affinity ($K_D$ = 0.0745 nM) for SARS-CoV-2.[492] LY-CoV1404 binds to a region spanning the ACE2-interacting site of the spike protein, which is accessible in up' and down RBD conformations (Fig. 13A). Interestingly, the epitope of LY-CoV1404 is similar to REGN10987. LY-CoV1404 and REGN10987 share 92% amino acid sequence identity in the variable regions of their heavy and light chains. Both engage equally RBD through their heavy and light chains, but REGN10987 has a more divergent sequence, and almost all of its interactions with RBD are through its heavy chain. LY-CoV1404 received an emergency use authorization on February 11, 2022.[492]

**7.1.8. Efficacy of therapeutic antibodies against new Omicron subvariants.** Omicron subvariants appear to evade neutralization of REGN-10933, LY-CoV016, LY-CoV555, AZD8895, and P2C-1F11. Although these Abs have shown reduced activity against most of the Omicron subvariants, they still exhibit competitive efficacy against the BA.1 and BA.2 subvariants. REGN-10987, AZD1061, and LY-CoV1404 can neutralize BA.2, BA.4 and BA.5. BA.2 sublineage greatly reduced the effectiveness of S309, while BA.2, BA.3, BA.4 and BA.5 escaped neutralization of P2C-1F11. Especially, LY-CoV14044 demonstrated high activity against all Omicron subvariants.[84,493]

### 7.2. Abs targeting NTD

In addition to RBD, NTD from S1 of the spike protein of SARS-CoV-2 is also a target for Abs. The role of NTD is not fully understood, but it may recognize specific sugar moieties during initial attachment, helping the spike protein to transform from a pre-fusion state to a post-fusion state. Certain antibodies that bind to specific epitopes on the NTD can block SARS-CoV-2 infection.[81,344] However, some NTD-directed antibodies may actually increase viral infectivity and are found in patients with severe COVID-19.[494] Although NTD-targeting antibodies cannot prevent the virus from binding to ACE2, their ability to neutralize SARS-CoV-2 is of considerable interest for hindering viral entry and confirming the spike protein as a primary target for SARS-CoV-2 vaccine and drug development.

Antibodies targeting the NTD are mapped to their recognition at three sites on the NTD.[81] Several typical Abs of this class are shown in Fig. 13B. Most Abs with neutralizing activity are directly bound to a single site, namely the site-1 supersite, while other Abs are attached to another single site, coinciding with the site-1 supersite[81,495] and outside the site-1 supersite. For example, Abs 4A8, FC05, DH1050.1 bind to the site-1 supersite,[496–498] while Abs 5–7, DH1052 *etc.* bind to another single site and outside the site-1 supersite (Fig. 13B).[497] Chi *et al.*[82] determined the structure of 4A8 in complex with spike protein, revealing that its epitope is located in the NTD with $K_D$ = 92.7 nM and moderate neutralizing activity $IC_{50}$ = 0.61 μg $mL^{-1}$ (Table 3). Although 4A8 does not inhibit ACE2 interaction with the spike protein, it significantly neutralizes both pseudotyped and authentic SARS-CoV-2 *in vitro*. DH1050.1 has a higher neutralizing activity ($IC_{50}$ = 0.04 μg $mL^{-1}$[499]) compared to 4A8.

 

In general, the site-1 supersite is the only NTD mitigation site that is under high selection pressure for virus escape. However, Abs targeting the site-1 supersite appear to be particularly vulnerable to escape, with many losing all activity against the SARS-CoV-2 variants.[467] Although there are many Abs targeting NTD to prevent SARS-CoV-2 activity, they seem to be easily breached by certain mutations in the NTD, and the immune escape site has little to do with the RBD.[207,495]

### 7.3. Antibodies targeting FP

Abs can bind to FP from S2 (Fig. 13C), which is more conserved among coronaviruses than S1 because it elicits more cross-reactivity than S1. Cross-reactive anti-S2 Abs are more likely to preexist in populations due to previous exposure to SARS-CoV-2. S2 retention may be a potential target for vaccine development. Vaccines that include a FP site in their immunogens can induce the production of more widely active Abs, combat other beta coronaviruses, elicit a stronger and longer memory response, and reduce the likelihood of sequence-altering mutations that render the vaccine ineffective. Furthermore, since S2 is more structurally conserved, it is less prone to non-synonymous mutations, making FP-targeting Abs less sensitive to different SARS-CoV-2 variants.[127,500]

The neutralizing activity of Abs targeting S2 is weaker than that of Abs targeting S1 (Table 3). For example, while COV91-27, COV44-62, VN01H1, C13B8, *etc.* targeting FP are able to neutralize WT, Alpha, Beta, Gamma, Delta, Omicron (BA.2 and BA.4/5) variants, their neutralizing activity is limited in comparison with Abs targeting RBD and NTD. However, targeting-S2 Abs may provide some evidence for understanding immune defenses and identifying targets for vaccine development based on the conserved S2 subunit, and S2-specific Abs may be useful in inhibiting conformational changes necessary for membrane fusion to occur. FP is also known as a candidate epitope for the development of next-generation coronavirus vaccines.[501,502]

Although Abs and ACE2 bind to the spike protein with binding affinities in the same nM range, their molecular binding mechanisms are different. In contrast to the case of ACE2, where the stability of RBD-ACE2 is controlled by electrostatic interactions, the stability of RBD-Ab is determined by either electrostatic interactions or vdW interactions depending on the type of Ab. ACE2 binds only to RBD (Fig. 14A), while Abs can bind not only to RBD, but also to NTD and FP in the S2 subunit (Fig. 14B–D). ACE2 recognizes RBD in the active state, but Abs can interact with both RBD-up and RBD-down (Fig. 14B).

### 7.4. Interaction between nanobodies and spike protein

Nanobody (Nb) therapy has emerged as a promising tool for the COVID-19 treatment.[450] Nbs target RBD blocking the interaction between the spike protein and ACE2 and inhibiting the entry of the virus into host cells.[475,479,503] SARS-CoV-2 is neutralized with high affinity by Nb, making RBD an attractive target for vaccine development.[504] Nbs are either naïve or synthetic. Naïve NBs are extracted from camelids (llamas, alpacas, camels and dromedaries).[505] Synthetic Nbs are

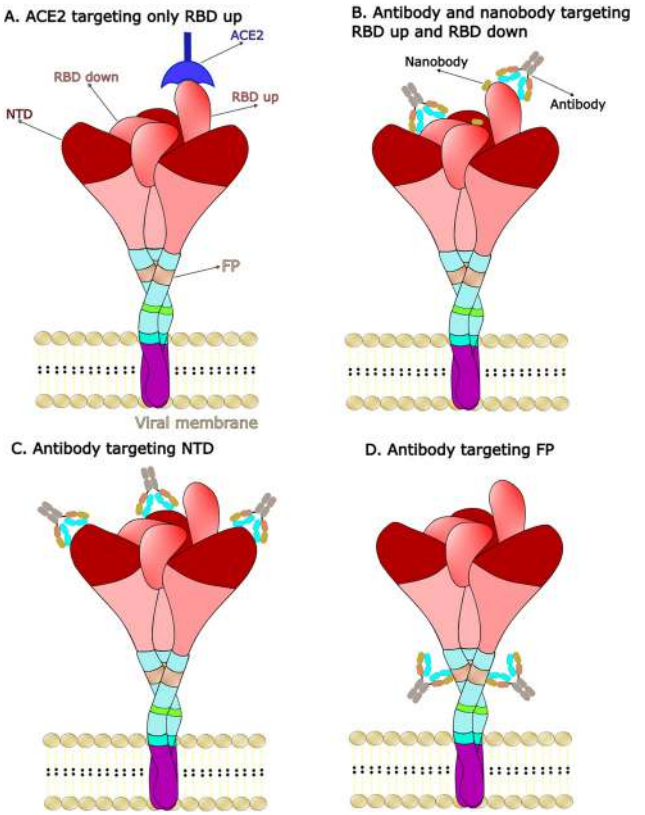


Fig. 14 (A) ACE2 only binds to RBD up. (B) Antibodies and nanobodies can bind to both open and closed RBD. (C) Antibodies target NTD. (D) Antibodies target FP.

produced by different methods and can be found in various libraries[506] such as humanized synthetic Nb library and the yeast surface display of synthetic Nb.[507,508]

Although synthetic Nbs exhibit high affinity for pre-fusion S glycoprotein and strong neutralizing activities,[509] they have limitations in meeting therapeutic needs. Nbs are able to bind to two RBD domains, including a binding epitope overlapping with the ACE2 binding region and a non-overlapping binding epitope with no overlap with ACE2 binding region. Moreover, Nb offers a faster way to exploit avidity to improve affinity and efficacy in the treatment of COVID-19.[510,511] Since SARS-CoV-2 is prone to rapid mutations that elude most potential Abs, Nbs may be good candidates for the treatment of dangerous variants.[512–514] Nb in combination with another Nb or Ab can increase the neutralizing activity.[208,508] Here we discuss important Nbs that can be used in COVID-19 therapy in the near future (Fig. 15 and Table 4).

**7.4.1. H11-H4, H11-D4, and Ty1.** H11–H4, H11–D4 and Ty1 are VHH Nbs identified as targeting RBD and disrupting its interaction with ACE2 (Fig. 15). These Nbs have been reported to be promising therapeutic agents to neutralize SARS-CoV-2 infection. Ty1 binding region overlaps with ACE2 binding region with binding activity $K_D$ = 5–10 nM and neutralizing activity $IC_{50}$ = 54 nM[508,515] (Table 4). Because Ty1 and ACE2 binding sites overlap on RBD, Ty1 prevents RBD from binding

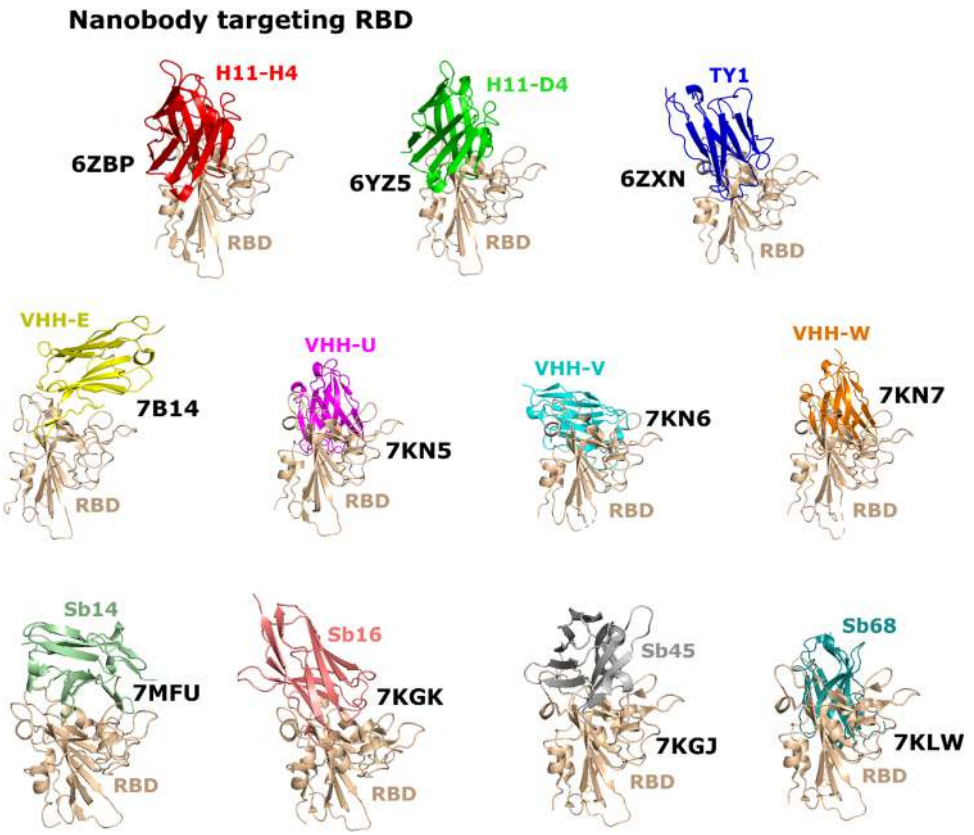


Fig. 15 3D structure of some important nanobodies targeting RBD. Their name and PDB ID are shown next to the image.

Table 4 Neutralizing and binding activity of nanobodies targeting RBD. The results were obtained experimentally

| Nanobody | PDB ID | Neutralizing activity (nM) | Binding activity, $K_D$ (nM) | Method | Library |
|---|---|---|---|---|---|
| H11-H4 | 6ZBP | NA | 12[508] | SPR | Naive llama single-domain antibody |
| H11-D4 | 6YZ5 | NA | 39[508] | SPR | Naive llama single-domain antibody |
| TY1 | 6ZXN | 54[515] | 5–10[515] | BLI | Immunized phage display |
| VHH-E | 7B14 | 60[520] | 1.86[520] | SPR | Immunized phage display |
| VHH-U | 7KN5 | 185[520] | 21.4[520] | SPR | Immunized phage display |
| VHH-V | 7KN6 | 142[520] | 8.92[520] | SPR | Immunized phage display |
| VHH-W | 7KN7 | 81[520] | 22.2[520] | SPR | Immunized phage display |
| Sb14 | 7MFU | 178.3[522] | 0.14[523] | SPR | Camelid-inspired synthetic |
| Sb16 | 7KGK | 1250[522] | 0.41[523] | SPR | Camelid-inspired synthetic |
| Sb45 | 7KGJ | 910[522] | 0.47[523] | SPR | Camelid-inspired synthetic |
| Sb68 | 7KLW | 137.7[522] | 0.63[523] | SPR | Camelid-inspired synthetic |

to ACE2 through steric exclusion. H11-H4 and H11-D4 bind to RBD with $K_D$ = 12 and 39 nM, respectively.[508,515]

H11–H4 and H11–D4 do not share a common binding region in RBD with ACE2. However, upon binding to RBD, H11–H4 can dislodge ACE2 from its RBD binding site due to repulsive electrostatic interaction because H11–H4 and ACE2 have similar-sign charged residues in close proximity when bound to RBD. H11–D4 was able to abolish ACE2 binding to a lesser extent. In short, both H11–H4 and Ty1 abrogate ACE2 binding through different mechanisms, while H11–D4 is perhaps the least effective inhibitor for RBD.[208,515–518]

For SARS-CoV-2 variants, the effect of H11–H4 on abrogating ACE2 binding was reduced by the N501Y and N501Y/E484K/K417N mutations on RBD for Alpha and Beta variants, while H11–D4 was much less effective in abolishing ACE2 binding to RBD with triple mutants. A significant decrease in binding strength of H11–H4 and H11–D4 to RBD was observed for mutations N501Y/E484K/K417N on RBD. Ty1 binds to the Beta variant twice as strongly as ACE2, meaning that Ty1 can neutralize this variant by sterically blocking ACE2 binding. For the Delta variant, because the L452R mutation is located at the binding interface of H11–H4, H11–D4, and Ty1, this may reduce their binding affinity.[518]

Using Martini coarse-grained umbrella sampling Nguyen *et al.*[208] obtained a binding affinity between H11-H4 and RBD, $\Delta G_{bind}$ = −19.8 kcal mol$^{-1}$, which is higher than

 

$\Delta G_{bind} = -21.4$ kcal mol$^{-1}$ for the CR3022-RBD complex. This *in silico* result is consistent with *in vitro* data[508,519] showing that the CR3022 antibody binds to RBD weaker than H11–H4. Importantly, if H11–H4 and CR3022 concurrently bind to RBD, their binding affinity is higher than when they each bind individually.[208] This indicates that their combination improves the SARS-CoV-2 neutralization, providing a promising approach in the treatment of COVID-19. SMD simulations[208] showed that H11–H4 yields a high ability to neutralize Alpha, Kappa, and dangerous Delta, while at the same time reducing the activity against Beta, Gamma, Lambda, and Mu variants.

**7.4.2. VHH-E, VHH-U, VHH-V, and VHH-W.** This is a set of rationally engineered Nbs with effective neutralizing capacity and resilience to mutational escape, including llama-derived Nb VHH-E ($IC_{50}$ = 60 nM, $K_D$ = 1.86 nM), three alpaca-derived Nb VHH-U ($IC_{50}$ = 185 nM, $K_D$ = 21.4 nM), VHH-V ($IC_{50}$ = 142 nM, $K_D$ = 8.92 nM) and VHH-W ($IC_{50}$ = 81 nM, $K_D$ = 22.2 nM) (Table 4). VHH-E binds to the ACE2 binding area, while the rest bind to a non-overlapping with ACE2 binding site (Fig. 15). Clearly, VHH-E binds to RBD more strongly than VHH-U, VHH-V, and VHH-W. VHH-E can bind to all RBDs in the three-up conformation, while VHH-V binds to the two-up conformation. These Nbs were found to be able to prevent infection through a synergistic effect.[520]

Various combinations of Nbs have been developed to improve the neutralization efficiency. While the neutralizing capacity of combinations of Nbs targeting different RBD epitopes (VHH-E and VHH-V, VHH-E and VHH-U, VHH-E and VHH-W) was increased, the combination of VHH-E and VHH-U, VHH-E and VHH-V, and VHH-E and VHH-W were not effective against mutants resistant to both Nbs alone.[521] The experiment showed that VHH-EEE (three VHH-E bind to RBD) most effectively suppressed infection without activation of viral fusion and can inactivate the virion by inhibiting its interaction with the receptor. VHH-VE (VHH-V and VHH-E) targets two independent epitopes simultaneously, preventing persistent escape mutants from appearing in evolution experiments.[520]

**7.4.3. Sb14, Sb16, Sb45, and Sb68.** This is a set of four synthetic Nbs that bind to RBD. Sb14, Sb16, and Sb45 competitively and directly block the ACE2 binding site, while Sb68 binding is non-competitive. Both Sb16 and Sb45 can associate with RBD in the up and down positions (Fig. 15), but the others cannot. In particular, Sb14 exhibits the highest binding affinity with $K_D$ of 0.14 nM, because for Sb16, Sb45, and Sb68 $K_D$ = 0.41, 0.47, and 0.63 nM, respectively.[523] Neutralizing capacity was also measured and $IC_{50}$ = 178.3, 1250, 910, and 137.7 nM for Sb14, Sb16, Sb45, and Sb68, respectively[522] (Table 4). Thus, Sb14 can suppress SARS-CoV-2 activity better than others. Sb68 can be combined with either Sb14 or Sb45 to increase the neutralizing activity.[523]

Alpha, Beta, and Gamma variants contain mutations in RBD that result in increased binding affinity for ACE2 and may reduce vaccine efficacy.[83,524] Sb14 binding was most affected by K417N, while this mutation did not influence the Sb16 binding. Both Sb14 and Sb16 showed reduced N501Y recognition and did not interact with E484K. Like Sb16, Sb45 also cannot bind to E484K and displayed reduced recognition of N501Y and K417N compared to WT. Because the Sb68 binding site is outside of the ACE2 binding region on the RBD, its binding affinity was not significantly affected by the three variants Alpha, Beta, and Gamma compared to WT.[523]

To date, Nbs that bind to RBD have been detected, but perhaps in the future Nbs capable of binding to other regions of the spike protein will be discovered. Like Abs, Nbs can target both open and closed RBDs (Fig. 14B). One of multiple benefits of Nbs is their small size ($\sim$15 KDa), which allows them most likely recognize more epitopes for neutralizing SARS-CoV-2 than conventional Abs. For example, glycans at sites N165, N234, and N343 of the spike protein shield RBD from conventional Abs, in particular, when RBD is in the down conformation,[134] but they leave sufficient space to accommodate small Nbs such as Ty1.[515] Additional advantages of Nbs over Abs are discussed in a recent review.[525]

# 8. Impact of SARS-CoV-2 on protein synthesis

SARS-CoV-2 contains a positive sense and single-stranded RNA composed of 50 UTR, two large overlapping open reading frames ORF1a and ORF1b, structural and accessory protein genes, and a 30-polyadenylated tail.[526] It can suppress the innate immune response of the host cell through an unspecified effect of non-structural proteins (NSPs), NSP1 to NSP16, on the protein synthesis process of the host cell.[527,528] Upon entering host cells, ORF1a and ORF1b are translated and proteolytically processed by virus-encoded proteinases to form functional NSPs, which play an essential roles in viral infection and RNA genome replication.[529] NSPs encode many crucial enzymes for RNA processing and viral replication.[530,531] mRNA splicing, mRNA translation, and protein trafficking are the three main steps in protein production, and understanding how SARS-CoV-2 NSPs affect these steps is important in finding different solutions in the treatment of COVID-19.[44,530,531]

## 8.1. NSP16 binds mRNA recognition domains of U1/U2 snRNAs and disrupts mRNA splicing

After transcription in the nucleus, the nascent pre-mRNAs are spliced to form mature mRNAs that are translated into protein (Fig. 16A). Splicing of pre-mRNA occurs on the spliceosome, which is composed of five snRNAs (U1, U2, U4, U5, and U6) and numerous proteins. snRNAs form small nuclear ribonucleoprotein complexes (snRNPs) by combining with specific proteins, and they work with pre-mRNA in the step-by-step process of spliceosome assembly. Assembly begins with U1 binding to the 5′ splice site and Msl5-Mud2 to the branch site, forming a commit complex.[532,533] Msl5 binding is then replaced by U2, forming a pre-spliceosome.[534] U5 is then added, resulting in a new base pairing between U2 and U6, and between U6 and the 5′ splicing site, and the release of U1 and U4. Other protein factors join the spliceosome to stabilize the interaction of U5 and U6 with pre-mRNA during the formation of an active

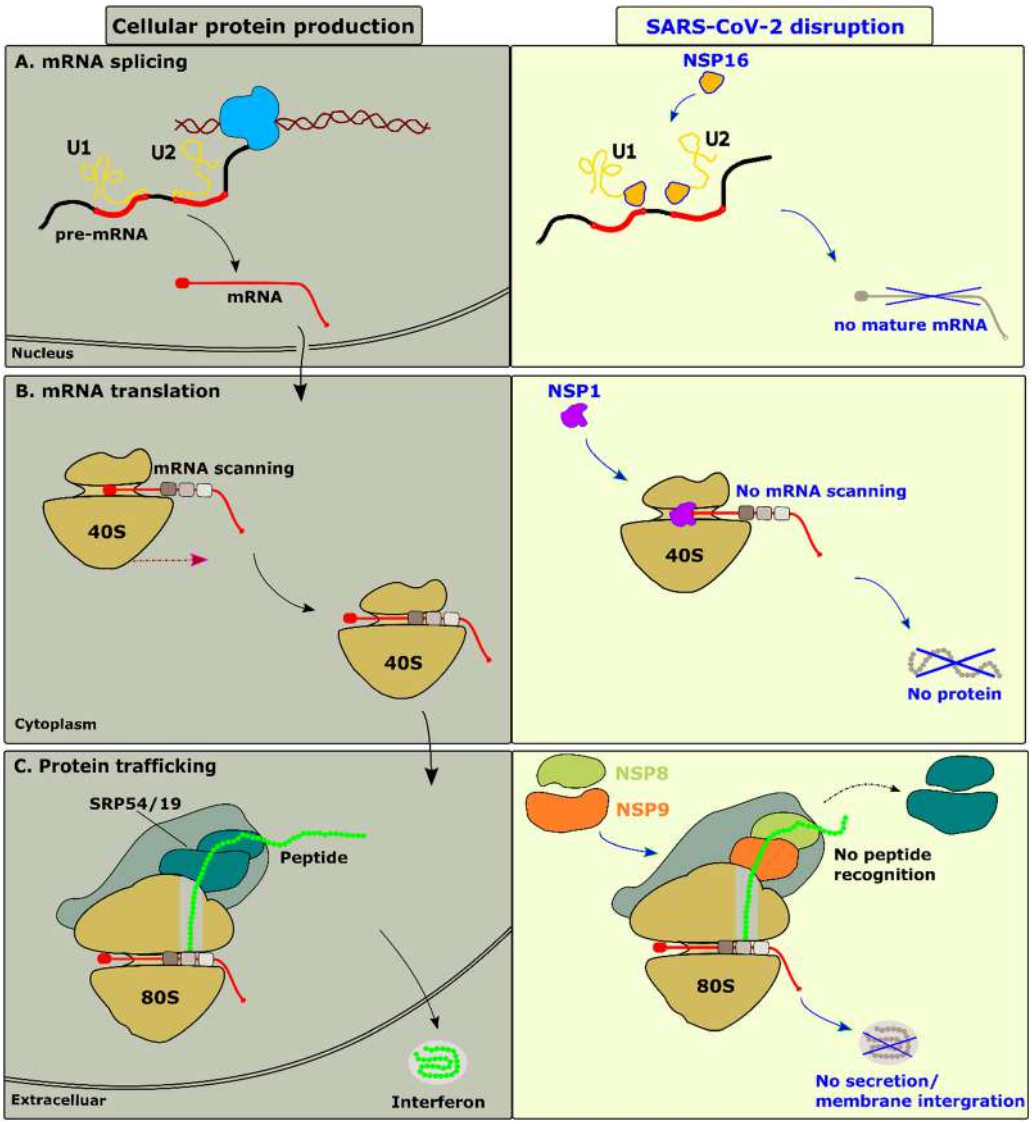


Fig. 16 (A) NSP16 binds to U1/U2 snRNAs to disrupts mRNA splicing, (B) NSP1 binds to the mRNA entry channel of the 40S ribosome to disrupt the protein translation, and (C) How NSP8 and NSP9 bind the signal recognition particle and disrupt protein trafficking. SRP54 and SRP19 are the domains of SRP.

spliceosome, which catalyzes the splicing process through two transesterification reactions.[535–537]

However, upon entry into the host cell, SARS-CoV-2 NSP16 binds to U1/U2 snRNAs and disrupts mRNA splicing, resulting in decrease of host protein and mRNA levels by triggering nonsense-mediated decay of improperly spliced mRNAs (Fig. 16A).[538] NSP16 binds to the 5′ splice site recognition sequence of U1 and the branchpoint recognition site of U2 (Fig. 17A).[44] These binding sites are uniquely specific for NSP16 compared to all other viral and human proteins. Here, NSP16 is an essential component of the coronavirus replication process as it helps the virus evade the immune system.[539,540] It includes 2′-*O*-methyltransferase (2′-*O*-MTase), which is part of the replication-transcription complex and resembles the human protein Cap-specific mRNA (nucleoside-2′-*O*-)-methyltransferase (CMTr1).[541] In particular, NSP16 is responsible for transferring a methyl group from its cofactor, *S*-adenosylmethionine (SAM), to viral mRNA, increasing the efficiency of translation and hiding it from detection by cellular pathogen recognition receptors.[541–543] Furthermore, although NSP16 is primarily known as an enzyme that adds 2′-*O*-methyl modifications to viral RNAs, it also plays the role of a host virulence factor.

Thus, mRNA plays a key role in carrying protein information from DNA in the cell nucleus to the cell cytoplasm, where the protein-making machinery reads the mRNA sequence and translates each three-base codon into the corresponding amino acid in a growing protein chain.[544] The disruption of mRNA splicing is consistent with the significant drop in steady-state mRNA levels observed during SARS-CoV-2 infection. The result of this effect is to reduce the host cell innate immune response to virus recognition.

 

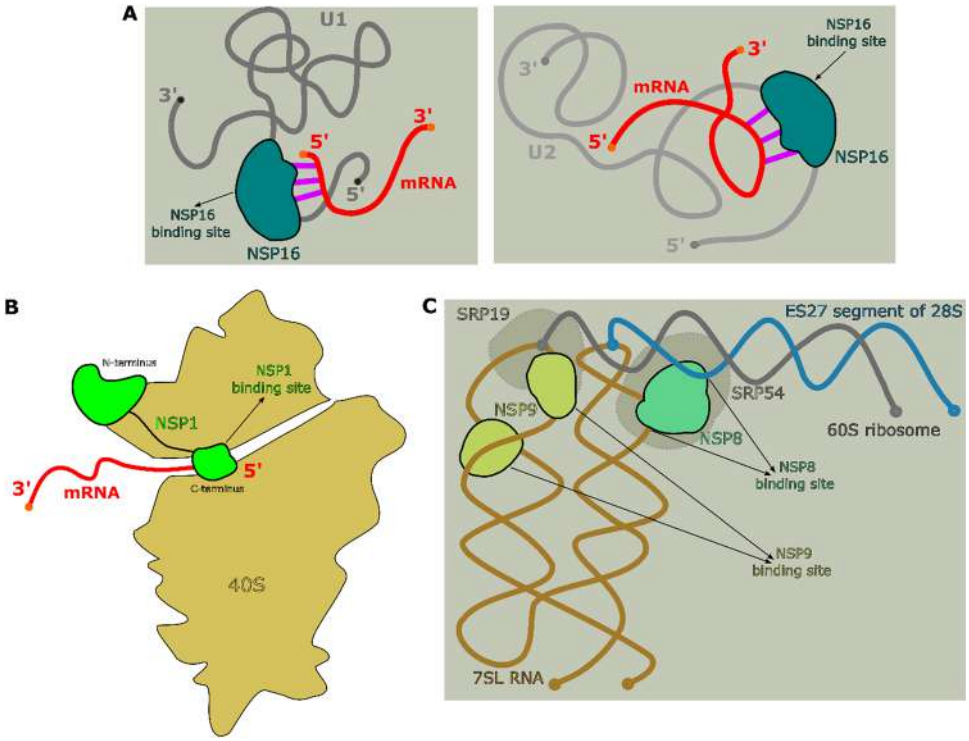


Fig. 17 (A) Left: NSP16 binding site (marine) relative to U1 (dark grey) and mRNA (red). Right: NSP16 binding site relative to U2 (grey) and mRNA. This shows how NSP16 binding can disrupt mRNA splicing. (B) The C-terminus of NSP1 (green) binds to the mRNA exit channel (red) in the 40S ribosome (olive). This describes how NSP1 binding can block mRNA entry. (C) Binding sites of NSP8 (green cyan) and NSP9 (citric) to the7SL RNA (dark olive) of SRP, ES27 segment of 28S (marine), and 60S rRNA (dark gray) complex. Upon binding of NSP8 and NSP9, SRP19 and SRP54 are displaced, disrupting protein trafficking.

### 8.2. NSP1 binds to the mRNA entry channel of the 40S ribosome to disrupt protein translation

The 40S subunit is responsible for the interaction between mRNA codons and transfer RNA (tRNA) anti-codons, which transfer amino acids to form polypeptides.[545] In the absence of NSP1, mRNA translation occurs normally and proteins are synthesized (Fig. 16B). Upon NSP1 binding to the mRNA entry channel of the 40S ribosome, the interaction of about 30 codons at the 5′ terminus of the mRNA sequence and NSP1 results in blocking of human mRNA translation.[527,546,547] This means that NSP1 can block protein production and all mechanisms of cellular antiviral defense that depend on the expression of host factors. Turning off important parts of the innate immune system can facilitate viral replication and effective immune evasion. NSP1 plays a critical role in weakening the antiviral immune response, making it a promising therapeutic target.

SARS-CoV-2 NSP1 consists of 180 amino acids with three domains, including an N-terminal domain, a linker domain, and a C-terminal domain. The C-terminal binds to the 40S subunit of the human ribosome (Fig. 17B), which leads to the inhibition of the translation of mRNA, including IFN proteins *in vitro* and in the cell.[548] The N-terminal and linker regions of NSP1 are not docked to the 40S mRNA entry channel, however, they stabilize its association with the ribosome and mRNA.[549] Drugs targeting either the C-terminal or the N-terminal of NSP1 may be good for antiviral therapy. A recent study demonstrated that montelukast sodium hydrate, an FDA-approved drug, binds to the C-terminal domain reducing the inhibitory effect of host protein synthesis. It shows an antiviral effect against SARS-CoV-2 by interfering with virus replication in HEK cells that express Vero-E6 cells and ACE2, which means that montelukast sodium hydrate can be used as an inhibitor to combat SARS-CoV-2 infection.[550] Using fragment-based X-ray screening Ma *et al.*[551] identified potential inhibitors that can bind to two binding sites of the NSP1 N-terminal, reducing the possibility of generating new virions.

Several mutations in NSP1 can change its structural and functional characteristics with respect to SARS-CoV-2. The double mutant K164A/H165A in the C-terminal domain eliminates the ability to bind to the 40S ribosome.[546,552] Mutations Y154A/F157A and R171E/R175E also abolished ribosome binding.[549] R124A/K124A mutations in the linker domain impaired the mRNA endonucleolytic cleavage guided by NSP1. The R99A mutation, located in the N-terminal domain, abolishes not only NSP1 evasion but also NSP1-guided mRNA cleavage.[549] Furthermore, a small deletion of the essential amino acids of NSP1 is also sufficient to eliminate NSP1 evasion.[553,554]

Using MD simulations, Borišek *et al.*[555] investigated the interaction of SARS-CoV/SARS-CoV-2 NSP1 with the 40S ribosome. They found that SARS-CoV-2 NSP1 hijacks the ribosome

more efficiently than SARS-CoV-1 NSP1 due to a critical switch of Q/E158 and E/Q159 residues that occurred during virus evolution. This switch predominantly alters the interaction of NSP1 with neighboring ribosomal proteins uS3 and uS5, as well as with helix 18 of rRNA lining the exit tunnel. Although this finding provides a clear picture of the role of SARS-CoV-2 in human cell invasion and diversion, the effect of NSP1 binding to the 40S ribosome on mRNA translation has not been theoretically studied. To solve this problem, Nguyen *et al.*[556] used SMD in conjunction with alchemical free energy calculations. NSP1 binding was found to significantly increase the mRNA binding affinity to the 40S ribosome, consistent with the experimental fact that in the presence of NSP1, the mRNA translation is completely halted after entering host cells. NSP1 residues Asn162, Trp161, Asn160, Glu159, Gln158, Phe157, and Asp156 located at the border with mRNA are most important for triggering translational blockade of the host immune system. In addition, the mRNA translation process is controlled by electrostatic interactions between mRNA and the 40S ribosome.

### 8.3. NSP8 and NSP9 bind to the signal recognition particle and disrupt protein trafficking

To start mRNA translation, the 60S subunit binds the 40S subunit forming the 80S ribosome. Then, a signal recognition particle (SRP), known as the universally conserved complex, binds to the 80S ribosome and co-translationally scans the nascent peptide to identify hydrophobic signal peptides present in integral membrane proteins and proteins secreted from the plasma membrane (Fig. 16C, left).[44]

SRP is a ribonucleoprotein complex with dual functions. It co-translationally targets proteins with a signal sequence to the endoplasmic reticulum (ER) and protects their mRNA from degradation. When SRP is unable to recognize the signal sequence or is depleted, regulation of aberrant protein production (RAPP) is triggered, resulting in the loss of secretory protein mRNA. If SRP can identify the substrates but fails to direct them to the ER, they may end up in the wrong location or be destroyed. All of these events lead to dramatic consequences for protein biogenesis, activating protein quality control pathways, and creating pressure on cell physiology, and may lead to disease pathogenesis.[557]

In general, the co-translational translocation of nascent peptides/proteins into the ER lumen for protein folding is initiated by the binding of SRP to a signal sequence (SS), which is a short 16–30 amino acid peptide predominantly present at the N-terminus of newly synthesized proteins destined toward the secretory pathway. SRP contains SRP54, a protein responsible for signal peptide recognition, SRP-receptor binding, and translocation through ribosomes, and 7SL RNA, which is a RNA component of SRP.[558] The interaction of SRP with SS on the nascent peptide stops translational elongation on ribosomes and the peptide associated with the SRP complex enters the ER lumen through the translocation, followed by removal of the SRP complex. Signal peptidases then cleave SS and the nascent peptides in the ER lumen undergo folding and enter the secretory pathway destined for secretion or targeting a different location in cells. SRP triggers the ribosome translocation to the ER to ensure proper folding and trafficking of these proteins to the cell membrane.[559]

However, this standard scenario may change in the presence of coronaviruses, as the SARS-CoV-2 NSP8 and NSP9 proteins have been found to bind to SRP (Fig. 16C, right).[44] NSP8 interacts with the 7SL RNA of SRP in the region bound by SRP54, while NSP9 binds 7SL in the region associated with the SRP19 protein (Fig. 17C), interfering with protein trafficking to the cell membrane upon viral infection.[44]

NSP8 includes an N-terminal positively charged α-helix optimized for RNA binding, followed by another α-helix linked by a long loop with half a β-barrel-like domain consisting of five antiparallel β-strands.[560] NSP8 plays a critical role in expanding the template RNA-binding surface. The disordered N-terminal regions are hypothesized to act as molecular handles for the recruiting additional viral factors and organizing the viral replication complex.[561] NSP9 consists of a central core of a six-stranded barrel surrounded by a C-terminal helix and an N-terminal extension. The function of RNA binding is achieved through the β-barrel loop structure, while dimerization and interaction with other proteins are likely preserved by the C-terminal β-hairpin and helix across different coronaviruses.[562] NSP9 is believed to play a role in creating viral RNA. It is dimeric and forms a solitary structure, a nucleic acid-binding site for efficient virus replication.[563] Binding of both NSP8 and NSP9 to SRP leads to failure of translocation of the nascent peptide to the ER lumen, causing protein mislocalization and degradation of the protein in the cytoplasm, and, ultimately, protein secretion.

Another interesting problem with protein production is that SARS-CoV-2, like other coronaviruses, uses a programmed ribosome −1 frameshift (−1 PRF) mechanism to directly synthesize its replicase proteins.[49,564] Therefore, −1 PRF may be therapeutically targeted to arrest virus replication.[49,564] The molecular mechanism of the critical switch in the SARS-CoV-2 replication program and the development of appropriate inhibitors are interesting issues, but are beyond the scope of this review.

## 9. Conclusions and perspectives

Our detailed analysis showed that the binding free energy of the RBD-ACE2 complex predicted by the MM-P/GBSA method is well below the experimental values. One possible reason is that this method does not work well for complexes with a large number of charged residues at the interface, such as RBD-ACE2, which makes improving the MM-P/GBSA method in this area a difficult task for future research. The machine learning approach provides reasonable agreement with experiment, but cannot provide insight into the mechanism of molecular interactions due to the large number of parameters used. Coarse-grained models combined with replica exchange and umbrella sampling provide a reasonable estimate of the dissociation

 

constant, but it is not clear whether this approach works for different variants, as coarse-graining may be insensitive to mutations. It is worth trying the same approach, but with all-atom models, which requires significant computational resources. Single molecule force spectroscopy has been successfully used to decipher the free energy landscape of virus-host complexes, but a corresponding theoretical description is still lacking, which motivates new work in this direction.

It has been recognized that inhibition of the farnesoid X receptor (FXR) can resist SARS-CoV-2 infection by reducing ACE2.[565] Thus, it would be interesting to investigate the binding affinity of FXR with ACE2. So far it was generally believed that the activity of various SARS-CoV-2 variants is driven by mutations in the spike protein, in particular, in the receptor binding region. However, the pathogenicity of Omicron appears to be controlled not only by mutations within the spike protein, but also by mutations in NSP6,[566] prompting additional studies to better understand the role of mutations outside the spike protein.

Experiments have identified many co-receptors for SARS-CoV-2 such as NRP1, but the mechanism of their interaction with the virus is poorly understood, especially compared to the ACE2 case. In addition, to the best of our best knowledge, the binding affinity and neutralizing activity of antibodies with respect to these receptors has not been explored. Since the presence of co-receptors may be essential for viral infection and antibody effectiveness it is important to study their molecular interaction mechanism experimentally and theoretically.

It has been almost 3 years since the COVID-19 outbreak in Wuhan we have been through four infective waves and are now entering our fifth with fast-spreading Omicron subvariants. Vaccines, especially RNA vaccines, have been beneficial, saving millions of lives, but due to immune escape we still need to consider new complementary approaches including large-scale antibody/nanobody development. In particular, nanobodies are an attractive option due to their advantages over traditional antibodies, including smaller size, higher stability, easier administration *etc.* The binding affinity of antibodies to the virus has been thoroughly investigated both in experiment and in simulations. However, their neutralizing activity has been extensively studied experimentally, but not theoretically. One of possible reasons is that quantifying the neutralizing capacity, which can be characterized by the binding free energy of host cell to a virus in the presence of an antibody, is not a trivial task, since one has to deal with a three-body problem instead of the standard two-body problem. Appropriate methods need to be developed to calculate the binding free energy in a three-body system, but a simple way to characterize neutralizing activity based on the distances between an antibody and its two antigens can be tried. In other words, the reach of an antibody can be used to describe its ability to neutralize its antigen, which is a valuable means of predicting antibody effectiveness.

Stable prefusion and postfusion SARS-CoV-2 S structures have been obtained by cryo-EM and cryo-ET, but due to transient nature the fusion intermediates have not been resolved. Marcink *et al.*[567] have used an antiviral lipopeptide entry inhibitor to arrest spike protein refolding and thus capture intermediates along the fusion pathway as spike proteins interact with fusion-activating proteases and ACE2. It remains unclear to what extent the inhibitor used affects the intermediate structure identified by this method, leaving the problem of determining the structure of fusion intermediates a major challenge for experiments and modeling. Estimation of the free energy barriers between prefusion, intermediate and postfusion states using experiment and simulation would be of great interest.

Since lung cells express TMPRSS2, it is believed that the surface pathway of entry of the virus into host cells is more clinically relevant than the endosomal pathway. Therefore, additional *in vivo* experiments are needed to test whether other proteases, such as cathepsin L, can activate the virus, and that the endosomal route may be of clinical relevance. From this point of view, identification of the elusive cathepsin L cleavage sites should provide further insight into additional fusion-related domains in the spike protein.

The emergence of SARS-CoV-2 variants that evade the immune response necessitates the development of new vaccine constructs. Rational design of vaccines based on the spike protein structure could address this challenge by designing non-overlapping, variant-aware epitopes that are harder for the virus to evade.[92] Significant efforts have been invested in generating such constructs for SARS-CoV-2 spike protein using bioinformatic tools, MD simulations and machine learning to predict and optimize epitopes.[568–571] While glycan shielding emerges as key obstacle in triggering immune response, glycan-aware methods are only beginning to emerge,[572] either treating glycosylation as static ''shielding spots'',[573] or including full glycoprotein dynamics.[574] Variant mutations are located mainly within such predicted epitopes, which corroborates these findings and sets glycan dynamics as a key factor in predicting B-cell epitopes on highly glycosylated fusion proteins like spike. It will be interesting to see how faithful representation of glycans surrounding the epitopes will aid epitope predictions, possibly allowing for rational glycoengineering of glycan shields in the vaccine constructs in the future.

Recent studies shed light on the complex mechanisms employed by SARS-CoV-2 to evade the host's immune response. The virus utilizes a multi-pronged strategy to suppress essential cellular functions, including global mRNA splicing, mRNA translation, and protein trafficking. While the termination of mRNA translation due to binding of NSP1 to the 40S ribosome has been studied both experimentally and by simulation, the effect of other NSPs on mRNA splicing and protein transport has not been theoretically considered. Thus, it would be important to perform molecular modeling of the NSP16 binding to the mRNA recognition domains of U1 and U2 splicing RNAs, and the association of NSP8 and NSP9 with 7SL RNA, which leads to disruption of the relevant processes. This will provide invaluable information for the development of effective therapies and vaccines to combat COVID-19. Another potentially interesting line of research is investigating the role of other SARS-CoV-2 NSPs in the production of host proteins.

One of limitations of this review is that we did not discussed molecular analyses that provide a basis for predicting novel variants that would be of concern. A discussion of this important problem can be found elsewhere.

In summary, our review provides valuable information that will facilitate more effective anti-viral drug design, vaccine and antibody/nanobody development. Understanding complex processes such as membrane fusion, RNA splicing, mRNA translation, and protein trafficking in the presence of nonstructured proteins in the ribosome requires the development of several innovative biophysical methods and accurate models, ranging from all-atom to coarse-grained representations. The field of research of COVID-19 is rapidly expanding and raises issues in the full spectrum of academic disciplines ranging from biochemistry, biophysics, chemistry, physics, theory, simulations, biology, and genetics to medicine and therapeutics. Thus, our review will be useful to people working in these areas.

## Author contributions

Hung Nguyen: writing – original draft, writing – review & editing, visualization; Hoang Linh Nguyen: writing – original draft, writing – review & editing, visualization; Pham Dang Lan: writing – original draft, writing – review & editing, visualization, Nguyen Quoc Thai: writing – original draft, visualization writing; Mateusz Sikora: writing – original draft, writing – review & editing, visualization; Mai Suan Li: conceptualisation, writing – review & editing, supervision.

## Conflicts of interest

There are no conflicts to declare.

## Acknowledgements

Financial support is acknowledged from Narodowe Centrum Nauki in Poland (grant 2019/35/B/ST4/02086). MS was supported by a project financed under Dioscuri, a programme initiated by the Max Planck Society, jointly managed with the National Science Centre in Poland, and mutually funded by Polish the Ministry of Education and Science and the German Federal Ministry of Education and Research.

## References

1 D. S. Hui, E. I Azhar, T. A. Madani, F. Ntoumi, R. Kock, O. Dar, G. Ippolito, T. D. McHugh, Z. A. Memish, C. Drosten, A. Zumla and E. Petersen, *Int. J. Infect. Dis.*, 2020, **91**, 264–266.
2 W. H. Organization, Naming the coronavirus disease (COVID-19) and the virus that causes it, 2020, 2.
3 M. Worobey, J. I. Levy, L. Malpica Serrano, A. Crits-Christoph, J. E. Pekar, S. A. Goldstein, A. L. Rasmussen, M. U. G. Kraemer, C. Newman, M. P. G. Koopmans, M. A. Suchard, J. O. Wertheim, P. Lemey, D. L. Robertson, R. F. Garry, E. C. Holmes, A. Rambaut and K. G. Andersen, *Science*, 2022, **377**, 951–959.
4 A. E. Gorbalenya, S. C. Baker, R. S. Baric, R. J. de Groot, C. Drosten, A. A. Gulyaeva, B. L. Haagmans, C. Lauber, A. M. Leontovich, B. W. Neuman, D. Penzar, S. Perlman, L. L. M. Poon, D. V. Samborskiy, I. A. Sidorov, I. Sola and J. Ziebuhr, *Nat. Microbiol.*, 2020, **5**, 536–544.
5 E. Dong, H. Du and L. Gardner, *Lancet Infect. Dis.*, 2020, **20**, 533–534.
6 J. E. Pekar, A. Magee, E. Parker, N. Moshiri, K. Izhikevich, J. L. Havens, K. Gangavarapu, L. M. Malpica Serrano, A. Crits-Christoph, N. L. Matteson, M. Zeller, J. I. Levy, J. C. Wang, S. Hughes, J. Lee, H. Park, M. S. Park, K. Ching Zi Yan, R. T. P. Lin, M. N. Mat Isa, Y. M. Noor, T. I. Vasylyeva, R. F. Garry, E. C. Holmes, A. Rambaut, M. A. Suchard, K. G. Andersen, M. Worobey and J. O. Wertheim, *Science*, 2022, **377**, 960–966.
7 M. Coccia, *Environ. Res.*, 2022, **211**, 113062.
8 R. Frutos, O. Pliez, L. Gavotte and C. A. Devaux, *Environ. Res.*, 2022, **207**, 112173.
9 M. Di Fusco, J. Lin, S. Vaghela, M. Lingohr-Smith, J. L. Nguyen, T. Scassellati Sforzolini, J. Judy, A. Cane and M. M. Moran, *Expert Rev. Vaccines*, 2022, **21**, 435–451.
10 C. Zheng, W. Shao, X. Chen, B. Zhang, G. Wang and W. Zhang, *Int. J. Infect. Dis.*, 2022, **114**, 252–260.
11 D. B. Naidoo and A. A. Chuturgoon, *Mol. Diagn. Ther.*, 2023, **27**, 193–226.
12 Q. Peng, R. Peng, B. Yuan, M. Wang, J. Zhao, L. Fu, J. Qi and Y. Shi, *Innovation*, 2021, **2**, 100080.
13 G. Kokic, H. S. Hillen, D. Tegunov, C. Dienemann, F. Seitz, J. Schmitzova, L. Farnung, A. Siewert, C. Hobartner and P. Cramer, *Nat. Commun.*, 2021, **12**, 279.
14 F. Kabinger, C. Stiller, J. Schmitzova, C. Dienemann, G. Kokic, H. S. Hillen, C. Hobartner and P. Cramer, *Nat. Struct. Mol. Biol.*, 2021, **28**, 740–746.
15 W. Wen, C. Chen, J. Tang, C. Wang, M. Zhou, Y. Cheng, X. Zhou, Q. Wu, X. Zhang, Z. Feng, M. Wang and Q. Mao, *Ann. Med.*, 2022, **54**, 516–523.
16 R. M. El-Shabasy, M. A. Nayel, M. M. Taher, R. Abdelmonem, K. R. Shoueir and E. R. Kenawy, *Int. J. Biol. Macromol.*, 2022, **204**, 161–168.
17 E. Callaway, *Nature*, 2022, **605**, 204–206.
18 K. Kupferschmidt and M. Wadman, *Science*, 2021, **372**, 1375–1376.
19 E. Mostafavi, A. K. Dubey, L. Teodori, S. Ramakrishna and A. Kaushik, *MedComm*, 2022, **3**, e119.
20 S. Xia, L. Wang, Y. Zhu, L. Lu and S. Jiang, *Signal Transduction Targeted Ther.*, 2022, **7**, 241.
21 C. Kurhade, J. Zou, H. Xia, M. Liu, H. C. Chang, P. Ren, X. Xie and P. Y. Shi, *Nat. Med.*, 2023, **29**, 344–347.
22 Q. Wang, S. Iketani, Z. Li, L. Liu, Y. Guo, Y. Huang, A. D. Bowen, M. Liu, M. Wang, J. Yu, R. Valdez, A. S. Lauring, Z. Sheng, H. H. Wang, A. Gordon, L. Liu and D. D. Ho, *Cell*, 2023, **186**, 279–286 e278.
23 M. E. Davis-Gardner, L. Lai, B. Wali, H. Samaha, D. Solis, M. Lee, A. Porter-Morrison, I. T. Hentenaar, F. Yamamoto,

 

S. Godbole, Y. Liu, D. C. Douek, F. E. Lee, N. Rouphael, A. Moreno, B. A. Pinsky and M. S. Suthar, *N. Engl. J. Med.*, 2023, **388**, 183–185.

24 K. C. Entzminger, J. K. Fleming, P. D. Entzminger, L. Y. Espinosa, A. Samadi, Y. Hiramoto, S. C. J. Okumura and T. Maruyama, *Antibody Ther.*, 2023, **6**, 108–118.

25 C. Liu, Q. Zhou, Y. Li, L. V. Garner, S. P. Watkins, L. J. Carter, J. Smoot, A. C. Gregg, A. D. Daniels, S. Jervey and D. Albaiu, *ACS Cent. Sci.*, 2020, **6**, 315–331.

26 B. Hu, H. Guo, P. Zhou and Z. L. Shi, *Nat. Rev. Microbiol.*, 2021, **19**, 141–154.

27 P. V'Kovski, A. Kratzel, S. Steiner, H. Stalder and V. Thiel, *Nat. Rev. Microbiol.*, 2021, **19**, 155–170.

28 H. Yang and Z. Rao, *Nat. Rev. Microbiol.*, 2021, **19**, 685–700.

29 J. M. Minkoff and B. tenOever, *Nat. Rev. Microbiol.*, 2023, **21**, 178–194.

30 W. T. Harvey, A. M. Carabelli, B. Jackson, R. K. Gupta, E. C. Thomson, E. M. Harrison, C. Ludden, R. Reeve, A. Rambaut, C.-G. U. Consortium, S. J. Peacock and D. L. Robertson, *Nat. Rev. Microbiol.*, 2021, **19**, 409–424.

31 J. W. Saville, A. M. Berezuk, S. S. Srivastava and S. Subramaniam, *Chem. Rev.*, 2022, **122**, 14066–14084.

32 C. B. Jackson, M. Farzan, B. Chen and H. Choe, *Nat. Rev. Mol. Cell Biol.*, 2022, **23**, 3–20.

33 A. I. Abulsoud, H. M. El-Husseiny, A. A. El-Husseiny, H. A. El-Mahdy, A. Ismail, S. Y. Elkhawaga, E. G. Khidr, D. Fathi, E. A. Mady, A. Najda, M. Algahtani, A. Theyab, K. F. Alsharif, A. Albrakati, R. Bayram, M. M. Abdel-Daim and A. S. Doghish, *Biomed. Pharmacother.*, 2023, **157**, 113977.

34 M. Cox, T. P. Peacock, W. T. Harvey, J. Hughes, D. W. Wright, C.-G. U. Consortium, B. J. Willett, E. Thomson, R. K. Gupta, S. J. Peacock, D. L. Robertson and A. M. Carabelli, *Nat. Rev. Microbiol.*, 2023, **21**, 112–124.

35 Y. Fan, X. Li, L. Zhang, S. Wan, L. Zhang and F. Zhou, *Signal Transduction Targeted Ther.*, 2022, **7**, 141.

36 A. K. Padhi, S. L. Rath and T. Tripathi, *J. Phys. Chem. B*, 2021, **125**, 9078–9091.

37 K. Gao, R. Wang, J. Chen, L. Cheng, J. Frishcosy, Y. Huzumi, Y. Qiu, T. Schluckbier, X. Wei and G. W. Wei, *Chem. Rev.*, 2022, **122**, 11287–11368.

38 Y. Chen, X. Zhao, H. Zhou, H. Zhu, S. Jiang and P. Wang, *Nat. Rev. Immunol.*, 2023, **23**, 189–199.

39 M. Bhattacharya, S. Chatterjee, S. S. Lee and C. Chakraborty, *Int. J. Biol. Macromol.*, 2023, **229**, 70–80.

40 A. Mittal, A. Khattri and V. Verma, *PLoS Pathog.*, 2022, **18**, e1010260.

41 G. Negi, A. Sharma, M. Dey, G. Dhanawat and N. Parveen, *Biophys. Rev.*, 2022, **14**, 1109–1140.

42 T. Tang, M. Bidon, J. A. Jaimes, G. R. Whittaker and S. Daniel, *Antiviral Res.*, 2020, **178**, 104792.

43 S. C. Chiliveri, J. M. Louis, R. Ghirlando and A. Bax, *Sci. Adv.*, 2021, **7**, eabk2226.

44 A. K. Banerjee, M. R. Blanco, E. A. Bruce, D. D. Honson, L. M. Chen, A. Chow, P. Bhat, N. Ollikainen, S. A. Quinodoz, C. Loney, J. Thai, Z. D. Miller, A. E. Lin, M. M. Schmidt, D. G. Stewart, D. Goldfarb, G. De Lorenzo, S. J. Rihn, R. M. Voorhees, J. W. Botten, D. Majumdar and M. Guttman, *Cell*, 2020, **183**, 1325–1339 e1321.

45 R. Lu, X. Zhao, J. Li, P. Niu, B. Yang, H. Wu, W. Wang, H. Song, B. Huang, N. Zhu, Y. Bi, X. Ma, F. Zhan, L. Wang, T. Hu, H. Zhou, Z. Hu, W. Zhou, L. Zhao, J. Chen, Y. Meng, J. Wang, Y. Lin, J. Yuan, Z. Xie, J. Ma, W. J. Liu, D. Wang, W. Xu, E. C. Holmes, G. F. Gao, G. Wu, W. Chen, W. Shi and W. Tan, *Lancet*, 2020, **395**, 565–574.

46 A. Banerjee, A. C. Doxey, K. Mossman and A. T. Irving, *Trends Ecol. Evol.*, 2021, **36**, 180–184.

47 P. C. Woo, S. K. Lau, Y. Huang and K. Y. Yuen, *Exp. Biol. Med.*, 2009, **234**, 1117–1127.

48 R. Arya, S. Kumari, B. Pandey, H. Mistry, S. C. Bihani, A. Das, V. Prashar, G. D. Gupta, L. Panicker and M. Kumar, *J. Mol. Biol.*, 2021, **433**, 166725.

49 P. R. Bhatt, A. Scaiola, G. Loughran, M. Leibundgut, A. Kratzel, R. Meurs, R. Dreos, K. M. O'Connor, A. McMillan, J. W. Bode, V. Thiel, D. Gatfield, J. F. Atkins and N. Ban, *Science*, 2021, **372**, 1306–1313.

50 E. J. Snijder, R. Limpens, A. H. de Wilde, A. W. M. de Jong, J. C. Zevenhoven-Dobbe, H. J. Maier, F. Faas, A. J. Koster and M. Barcena, *PLoS Biol.*, 2020, **18**, e3000715.

51 S. Klein, M. Cortese, S. L. Winter, M. Wachsmuth-Melm, C. J. Neufeldt, B. Cerikan, M. L. Stanifer, S. Boulant, R. Bartenschlager and P. Chlanda, *Nat. Commun.*, 2020, **11**, 5885.

52 S. Stertz, M. Reichelt, M. Spiegel, T. Kuri, L. Martinez-Sobrido, A. Garcia-Sastre, F. Weber and G. Kochs, *Virology*, 2007, **361**, 304–315.

53 D. Casares, P. V. Escriba and C. A. Rossello, *Int. J. Mol. Sci.*, 2019, **20**, 2167.

54 Z. Saud, V. J. Tyrrell, A. Zaragkoulias, M. B. Protty, E. Statkute, A. Rubina, K. Bentley, D. A. White, P. D. S. Rodrigues and R. C. Murphy, *J. Lipid Res.*, 2022, 100208.

55 S. Eymieux, R. Uzbekov, Y. Rouille, E. Blanchard, C. Hourioux, J. Dubuisson, S. Belouzard and P. Roingeard, *Cells*, 2021, **10**, 2047.

56 S. Ghosh, T. A. Dellibovi-Ragheb, A. Kerviel, E. Pak, Q. Qiu, M. Fisher, P. M. Takvorian, C. Bleck, V. W. Hsu, A. R. Fehr, S. Perlman, S. R. Achar, M. R. Straus, G. R. Whittaker, C. A. M. de Haan, J. Kehrl, G. Altan-Bonnet and N. Altan-Bonnet, *Cell*, 2020, **183**, 1520–1535 e1514.

57 Z. Ke, J. Oton, K. Qu, M. Cortese, V. Zila, L. McKeane, T. Nakane, J. Zivanov, C. J. Neufeldt, B. Cerikan, J. M. Lu, J. Peukes, X. Xiong, H. G. Krausslich, S. H. W. Scheres, R. Bartenschlager and J. A. G. Briggs, *Nature*, 2020, **588**, 498–502.

58 H. Yao, Y. Song, Y. Chen, N. Wu, J. Xu, C. Sun, J. Zhang, T. Weng, Z. Zhang, Z. Wu, L. Cheng, D. Shi, X. Lu, J. Lei, M. Crispin, Y. Shi, L. Li and S. Li, *Cell*, 2020, **183**, 730–738 e713.

59 C. Liu, L. Mendonca, Y. Yang, Y. Gao, C. Shen, J. Liu, T. Ni, B. Ju, C. Liu, X. Tang, J. Wei, X. Ma, Y. Zhu, W. Liu, S. Xu, Y. Liu, J. Yuan, J. Wu, Z. Liu, Z. Zhang, L. Liu, P. Wang and P. Zhang, *Structure*, 2020, **28**, 1218–1224 e1214.

60 B. Turonova, M. Sikora, C. Schurmann, W. J. H. Hagen, S. Welsch, F. E. C. Blanc, S. von Bulow, M. Gecht, K. Bagola, C. Horner, G. van Zandbergen, J. Landry, N. T. D. de Azevedo, S. Mosalaganti, A. Schwarz, R. Covino, M. D. Muhlebach, G. Hummer, J. Krijnse Locker and M. Beck, *Science*, 2020, **370**, 203–208.
61 A. L. Pinto, R. K. Rai, J. C. Brown, P. Griffin, J. R. Edgar, A. Shah, A. Singanayagam, C. Hogg, W. S. Barclay, C. E. Futter and T. Burgoyne, *Nat. Commun.*, 2022, **13**, 1609.
62 J. L. Nieto-Torres, M. L. Dediego, E. Alvarez, J. M. Jimenez-Guardeno, J. A. Regla-Nava, M. Llorente, L. Kremer, S. Shuo and L. Enjuanes, *Virology*, 2011, **415**, 69–82.
63 R. Arya, S. Kumari, B. Pandey, H. Mistry, S. C. Bihani, A. Das, V. Prashar, G. D. Gupta, L. Panicker and M. Kumar, *J. Mol. Biol.*, 2021, **433**, 166725.
64 M. Barcena, C. O. Barnes, M. Beck, P. J. Bjorkman, B. Canard, G. F. Gao, Y. Gao, R. Hilgenfeld, G. Hummer, A. Patwardhan, G. Santoni, E. O. Saphire, C. Schaffitzel, S. L. Schendel, J. L. Smith, A. Thorn, D. Veesler, P. Zhang and Q. Zhou, *Nat. Struct. Mol. Biol.*, 2021, **28**, 2–7.
65 A. C. Walls, Y. J. Park, M. A. Tortorici, A. Wall, A. T. McGuire and D. Veesler, *Cell*, 2020, **181**, 281–292 e286.
66 M. Hoffmann, H. Kleine-Weber, S. Schroeder, N. Kruger, T. Herrler, S. Erichsen, T. S. Schiergens, G. Herrler, N. H. Wu, A. Nitsche, M. A. Muller, C. Drosten and S. Pohlmann, *Cell*, 2020, **181**, 271–280 e278.
67 M. M. Zhao, W. L. Yang, F. Y. Yang, L. Zhang, W. J. Huang, W. Hou, C. F. Fan, R. H. Jin, Y. M. Feng, Y. C. Wang and J. K. Yang, *Signal Transduction Targeted Ther.*, 2021, **6**, 134.
68 D. Bestle, M. R. Heindl, H. Limburg, T. Van Lam van, O. Pilgram, H. Moulton, D. A. Stein, K. Hardes, M. Eickmann, O. Dolnik, C. Rohde, H. D. Klenk, W. Garten, T. Steinmetzer and E. Bottcher-Friebertshauser, *Life Sci. Alliance*, 2020, **3**, e202000786.
69 M. G. Hossain, Y. D. Tang, S. Akter and C. Zheng, *J. Med. Virol.*, 2022, **94**, 1815–1820.
70 B. A. Johnson, X. Xie, A. L. Bailey, B. Kalveram, K. G. Lokugamage, A. Muruato, J. Zou, X. Zhang, T. Juelich, J. K. Smith, L. Zhang, N. Bopp, C. Schindewolf, M. Vu, A. Vanderheiden, E. S. Winkler, D. Swetnam, J. A. Plante, P. Aguilar, K. S. Plante, V. Popov, B. Lee, S. C. Weaver, M. S. Suthar, A. L. Routh, P. Ren, Z. Ku, Z. An, K. Debbink, M. S. Diamond, P. Y. Shi, A. N. Freiberg and V. D. Menachery, *Nature*, 2021, **591**, 293–299.
71 M. Sikora, S. von Bulow, F. E. C. Blanc, M. Gecht, R. Covino and G. Hummer, *PLoS Comput. Biol.*, 2021, **17**, e1008790.
72 M. Gecht, S. von Bülow, C. Penet, G. Hummer, C. Hanus and M. Sikora, *bioRxiv*, 2022, preprint, DOI: **10.1101/2021.08.04.455134**.
73 D. Wrapp, N. Wang, K. S. Corbett, J. A. Goldsmith, C.-L. Hsieh, O. Abiona, B. S. Graham and J. S. McLellan, *Science*, 2020, **367**, 1260–1263.
74 J. Shang, G. Ye, K. Shi, Y. Wan, C. Luo, H. Aihara, Q. Geng, A. Auerbach and F. Li, *Nature*, 2020, **581**, 221–224.
75 Q. Wang, Y. Zhang, L. Wu, S. Niu, C. Song, Z. Zhang, G. Lu, C. Qiao, Y. Hu, K. Y. Yuen, Q. Wang, H. Zhou, J. Yan and J. Qi, *Cell*, 2020, **181**, 894–904 e899.
76 Y. Cai, J. Zhang, T. Xiao, H. Peng, S. M. Sterling, R. M. Walsh, S. Rawson, S. Rits-Volloch and B. Chen, *Science*, 2020, **369**, 1586–1592.
77 G. Cerutti, Y. Guo, T. Zhou, J. Gorman, M. Lee, M. Rapp, E. R. Reddem, J. Yu, F. Bahna, J. Bimela, Y. Huang, P. S. Katsamba, L. Liu, M. S. Nair, R. Rawi, A. S. Olia, P. Wang, B. Zhang, G. Y. Chuang, D. D. Ho, Z. Sheng, P. D. Kwong and L. Shapiro, *Cell Host Microbe*, 2021, **29**, 819–833 e817.
78 Y. Yuan, D. Cao, Y. Zhang, J. Ma, J. Qi, Q. Wang, G. Lu, Y. Wu, J. Yan, Y. Shi, X. Zhang and G. F. Gao, *Nat. Commun.*, 2017, **8**, 15092.
79 H. Zhou, Y. Chen, S. Zhang, P. Niu, K. Qin, W. Jia, B. Huang, S. Zhang, J. Lan, L. Zhang, W. Tan and X. Wang, *Nat. Commun.*, 2019, **10**, 3068.
80 X. L. Sun, *Glycobiology*, 2021, **31**, 1245–1253.
81 M. McCallum, A. De Marco, F. A. Lempp, M. A. Tortorici, D. Pinto, A. C. Walls, M. Beltramello, A. Chen, Z. Liu, F. Zatta, S. Zepeda, J. di Iulio, J. E. Bowen, M. Montiel-Ruiz, J. Zhou, L. E. Rosen, S. Bianchi, B. Guarino, C. S. Fregni, R. Abdelnabi, S. C. Foo, P. W. Rothlauf, L. M. Bloyet, F. Benigni, E. Cameroni, J. Neyts, A. Riva, G. Snell, A. Telenti, S. P. J. Whelan, H. W. Virgin, D. Corti, M. S. Pizzuto and D. Veesler, *Cell*, 2021, **184**, 2332–2347 e2316.
82 X. Chi, R. Yan, J. Zhang, G. Zhang, Y. Zhang, M. Hao, Z. Zhang, P. Fan, Y. Dong, Y. Yang, Z. Chen, Y. Guo, J. Zhang, Y. Li, X. Song, Y. Chen, L. Xia, L. Fu, L. Hou, J. Xu, C. Yu, J. Li, Q. Zhou and W. Chen, *Science*, 2020, **369**, 650–655.
83 P. Wang, M. S. Nair, L. Liu, S. Iketani, Y. Luo, Y. Guo, M. Wang, J. Yu, B. Zhang, P. D. Kwong, B. S. Graham, J. R. Mascola, J. Y. Chang, M. T. Yin, M. Sobieszczyk, C. A. Kyratsous, L. Shapiro, Z. Sheng, Y. Huang and D. D. Ho, *Nature*, 2021, **593**, 130–135.
84 Y. Cao, J. Wang, F. Jian, T. Xiao, W. Song, A. Yisimayi, W. Huang, Q. Li, P. Wang, R. An, J. Wang, Y. Wang, X. Niu, S. Yang, H. Liang, H. Sun, T. Li, Y. Yu, Q. Cui, S. Liu, X. Yang, S. Du, Z. Zhang, X. Hao, F. Shao, R. Jin, X. Wang, J. Xiao, Y. Wang and X. S. Xie, *Nature*, 2022, **602**, 657–663.
85 R. Yan, Y. Zhang, Y. Li, F. Ye, Y. Guo, L. Xia, X. Zhong, X. Chi and Q. Zhou, *Cell Res.*, 2021, **31**, 717–719.
86 T. Zhou, Y. Tsybovsky, J. Gorman, M. Rapp, G. Cerutti, G. Y. Chuang, P. S. Katsamba, J. M. Sampson, A. Schon, J. Bimela, J. C. Boyington, A. Nazzari, A. S. Olia, W. Shi, M. Sastry, T. Stephens, J. Stuckey, I. T. Teng, P. Wang, S. Wang, B. Zhang, R. A. Friesner, D. D. Ho, J. R. Mascola, L. Shapiro and P. D. Kwong, *Cell Host Microbe*, 2020, **28**, 867–879 e865.
87 J. Lan, J. Ge, J. Yu, S. Shan, H. Zhou, S. Fan, Q. Zhang, X. Shi, Q. Wang, L. Zhang and X. Wang, *Nature*, 2020, **581**, 215–220.
88 R. Zhu, D. Canena, M. Sikora, M. Klausberger, H. Seferovic, A. R. Mehdipour, L. Hain, E. Laurent, V. Monteil, G. Wirnsberger, R. Wieneke, R. Tampe, N. F. Kienzl, L. Mach, A. Mirazimi, Y. J. Oh, J. M. Penninger,

 

G. Hummer and P. Hinterdorfer, *Nat. Commun.*, 2022, **13**, 7926.
89 A. R. Mehdipour and G. Hummer, *Proc. Natl. Acad. Sci. U. S. A.*, 2021, **118**, e2100425118.
90 H. Liu, P. Wei, J. W. Kappler, P. Marrack and G. Zhang, *Front. Immunol.*, 2022, **13**, 825256.
91 M. F. Bachmann, M. O. Mohsen and D. E. Speiser, *npj Vaccines*, 2022, **7**, 56.
92 J. Hansen, A. Baum, K. E. Pascal, V. Russo, S. Giordano, E. Wloga, B. O. Fulton, Y. Yan, K. Koon, K. Patel, K. M. Chung, A. Hermann, E. Ullman, J. Cruz, A. Rafique, T. Huang, J. Fairhurst, C. Libertiny, M. Malbec, W. Y. Lee, R. Welsh, G. Farr, S. Pennington, D. Deshpande, J. Cheng, A. Watty, P. Bouffard, R. Babb, N. Levenkova, C. Chen, B. Zhang, A. Romero Hernandez, K. Saotome, Y. Zhou, M. Franklin, S. Sivapalasingam, D. C. Lye, S. Weston, J. Logue, R. Haupt, M. Frieman, G. Chen, W. Olson, A. J. Murphy, N. Stahl, G. D. Yancopoulos and C. A. Kyratsous, *Science*, 2020, **369**, 1010–1014.
93 C. O. Barnes, C. A. Jette, M. E. Abernathy, K. A. Dam, S. R. Esswein, H. B. Gristick, A. G. Malyutin, N. G. Sharaf, K. E. Huey-Tubman, Y. E. Lee, D. F. Robbiani, M. C. Nussenzweig, A. P. West, Jr. and P. J. Bjorkman, *Nature*, 2020, **588**, 682–687.
94 J. Huo, Y. Zhao, J. Ren, D. Zhou, H. M. E. Duyvesteyn, H. M. Ginn, L. Carrique, T. Malinauskas, R. R. Ruza, P. N. M. Shah, T. K. Tan, P. Rijal, N. Coombes, K. R. Bewley, J. A. Tree, J. Radecke, N. G. Paterson, P. Supasa, J. Mongkolsapaya, G. R. Screaton, M. Carroll, A. Townsend, E. E. Fry, R. J. Owens and D. I. Stuart, *Cell Host Microbe*, 2020, **28**, 445–454 e446.
95 S. M. Gobeil, R. Henderson, V. Stalls, K. Janowska, X. Huang, A. May, M. Speakman, E. Beaudoin, K. Manne, D. Li, R. Parks, M. Barr, M. Deyton, M. Martin, K. Mansouri, R. J. Edwards, A. Eaton, D. C. Montefiori, G. D. Sempowski, K. O. Saunders, K. Wiehe, W. Williams, B. Korber, B. F. Haynes and P. Acharya, *Mol. Cell*, 2022, **82**, 2050–2068.e2056.
96 I. Berger and C. Schaffitzel, *Cell Res.*, 2020, **30**, 1059–1060.
97 S. M. Gobeil, K. Janowska, S. McDowell, K. Mansouri, R. Parks, K. Manne, V. Stalls, M. F. Kopp, R. Henderson, R. J. Edwards, B. F. Haynes and P. Acharya, *Cell Rep.*, 2021, **34**, 108630.
98 M. Lu, P. D. Uchil, W. Li, D. Zheng, D. S. Terry, J. Gorman, W. Shi, B. Zhang, T. Zhou and S. Ding, *Cell Host Microbe*, 2020, **28**, 880–891 e888.
99 C. Xu, Y. Wang, C. Liu, C. Zhang, W. Han, X. Hong, Y. Wang, Q. Hong, S. Wang, Q. Zhao, Y. Wang, Y. Yang, K. Chen, W. Zheng, L. Kong, F. Wang, Q. Zuo, Z. Huang and Y. Cong, *Sci. Adv.*, 2021, **7**, eabe5575.
100 Z. Yang, Y. Han, S. Ding, W. Shi, T. Zhou, A. Finzi, P. D. Kwong, W. Mothes and M. Lu, *Mbio*, 2022, **13**, e03227–e03221.
101 M. Gur, E. Taka, S. Z. Yilmaz, C. Kilinc, U. Aktas and M. Golcuk, *J. Chem. Phys.*, 2020, **153**, 075101.
102 M. I. Zimmerman, J. R. Porter, M. D. Ward, S. Singh, N. Vithani, A. Meller, U. L. Mallimadugula, C. E. Kuhn, J. H. Borowsky, R. P. Wiewiora, M. F. D. Hurley, A. M. Harbison, C. A. Fogarty, J. E. Coffland, E. Fadda, V. A. Voelz, J. D. Chodera and G. R. Bowman, *Nat. Chem. Biol.*, 2021, **13**, 651–659.
103 L. Fallon, K. A. Belfon, L. Raguette, Y. Wang, D. Stepanenko, A. Cuomo, J. Guerra, S. Budhan, S. Varghese and C. P. Corbo, *J. Am. Chem. Soc.*, 2021, **143**, 11349–11360.
104 Y. T. Pang, A. Acharya, D. L. Lynch, A. Pavlova and J. C. Gumbart, *Commun. Biol*, 2022, **5**, 1–11.
105 H. M. Dokainish, S. Re, T. Mori, C. Kobayashi, J. Jung and Y. Sugita, *Elife*, 2022, **11**, e75720.
106 W. Song, M. Gui, X. Wang and Y. Xiang, *PLoS Pathog.*, 2018, **14**, e1007236.
107 C. Peng, Z. Zhu, Y. Shi, X. Wang, K. Mu, Y. Yang, X. Zhang, Z. Xu and W. Zhu, *J. Phys. Chem. Lett*, 2020, **11**, 10482–10488.
108 V. G. Kumar, D. S. Ogden, U. H. Isu, A. Polasa, J. Losey and M. Moradi, *J. Biol. Chem.*, 2022, **298**, 101814.
109 Y. Wu, R. Qian, Y. Yang, Y. Sheng, W. Li and W. Wang, *ACS Omega*, 2021, **6**, 23432–23441.
110 J. Shang, Y. Wan, C. Luo, G. Ye, Q. Geng, A. Auerbach and F. Li, *Proc. Natl. Acad. Sci. U. S. A.*, 2020, **117**, 11727–11734.
111 L. Casalino, Z. Gaieb, J. A. Goldsmith, C. K. Hjorth, A. C. Dommer, A. M. Harbison, C. A. Fogarty, E. P. Barros, B. C. Taylor and J. S. McLellan, *ACS Cent. Sci.*, 2020, **6**, 1722–1734.
112 A. M. Harbison, C. A. Fogarty, T. K. Phung, A. Satheesan, B. L. Schulz and E. Fadda, *Chem Sci*, 2022, **13**, 386–395.
113 T. Sztain, S.-H. Ahn, A. T. Bogetti, L. Casalino, J. A. Goldsmith, E. Seitz, R. S. McCool, F. L. Kearns, F. Acosta-Reyes and S. Maji, *Nat. Chem.*, 2021, **13**, 963–968.
114 P. B. Harbury, J. J. Plecs, B. Tidor, T. Alber and P. S. Kim, *Science*, 1998, **282**, 1462–1467.
115 X. Xia, *Viruses*, 2021, **13**, 109.
116 P. Shah, G. A. Canziani, E. P. Carter and I. Chaiken, *Front. Immunol.*, 2021, **12**, 637651.
117 Q. Li, Q. Huang and C. Kang, *Int. J. Mol. Sci.*, 2022, **23**, 1040.
118 D. Pinto, C. Fenwick, C. Caillat, C. Silacci, S. Guseva, F. Dehez, C. Chipot, S. Barbieri, A. Minola, D. Jarrossay, G. D. Tomaras, X. Shen, A. Riva, M. Tarkowski, O. Schwartz, T. Bruel, J. Dufloo, M. S. Seaman, D. C. Montefiori, A. Lanzavecchia, D. Corti, G. Pantaleo and W. Weissenhorn, *Cell Host Microbe*, 2019, **26**, 623–637 e628.
119 S. De Cae, I. Van Molle, L. van Schie, S. R. Shoemaker, J. Deckers, N. Debeuf, S. Lameire, W. Nerinckx, K. Roose, D. Fijalkowska, S. Devos, A.-S. Desmet, J. C. Zavala Marchan, T. Venneman, G. H. Ghassabeh, K. Sedeyn, M. Ballegeer, M. Vanheerswynghels, C. De Wolf, H. Demol, P. Vanhaverbeke, C. Lonigro, V. Bockstal, M. Rinaldi, R. Abdelnabi, J. Neyts, S. Marqusee, B. N. Lambrecht, N. Callewaert, H. Remaut, X. Saelens and B. Schepens, *bioRxiv*, 2023, preprint, DOI: 10.1101/2023.03.10.531533.
120 R. Broer, B. Boson, W. Spaan, F. L. Cosset and J. Corver, *J. Virol.*, 2006, **80**, 1302–1310.
121 J. Corver, R. Broer, P. van Kasteren and W. Spaan, *Virol. J.*, 2009, **6**, 230.

122 C. M. Petit, V. N. Chouljenko, A. Iyer, R. Colgrove, M. Farzan, D. M. Knipe and K. G. Kousoulas, *Virology*, 2007, **360**, 264–274.
123 P. Kumar, T. Bhardwaj, N. Garg and R. Giri, *Virology*, 2022, **566**, 42–55.
124 M. E. Dieterle, D. Haslwanter, R. H. Bortz, 3rd, A. S. Wirchnianski, G. Lasso, O. Vergnolle, S. A. Abbasi, J. M. Fels, E. Laudermilch, C. Florez, A. Mengotto, D. Kimmel, R. J. Malonis, G. Georgiev, J. Quiroz, J. Barnhill, L. A. Pirofski, J. P. Daily, J. M. Dye, J. R. Lai, A. S. Herbert, K. Chandran and R. K. Jangra, *Cell Host Microbe*, 2020, **28**, 486–496 e486.
125 S. Belouzard, V. C. Chu and G. R. Whittaker, *Proc. Natl. Acad. Sci. U. S. A.*, 2009, **106**, 5871–5876.
126 D. J. Benton, S. J. Gamblin, P. B. Rosenthal and J. J. Skehel, *Nature*, 2020, **583**, 150–153.
127 A. C. Walls, M. A. Tortorici, J. Snijder, X. Xiong, B. J. Bosch, F. A. Rey and D. Veesler, *Proc. Natl. Acad. Sci. U. S. A.*, 2017, **114**, 11157–11162.
128 S. L. Schaefer, H. Jung and G. Hummer, *J. Phys. Chem. B*, 2021, **125**, 7732–7741.
129 S. Liu, G. Xiao, Y. Chen, Y. He, J. Niu, C. R. Escalante, H. Xiong, J. Farmar, A. K. Debnath, P. Tien and S. Jiang, *Lancet*, 2004, **363**, 938–947.
130 A. Casas-Sanchez, A. Romero-Ramirez, E. Hargreaves, C. C. Ellis, B. I. Grajeda, I. L. Estevao, E. I. Patterson, G. L. Hughes, I. C. Almeida, T. Zech and A. Acosta-Serrano, *mBio*, 2021, **13**, e0371821.
131 Y. Li, D. Liu, Y. Wang, W. Su, G. Liu and W. Dong, *Front. Immunol.*, 2021, **12**, 638573.
132 J. D. Allen, H. Chawla, F. Samsudin, L. Zuzic, A. T. Shivgan, Y. Watanabe, W. T. He, S. Callaghan, G. Song, P. Yong, P. J. M. Brouwer, Y. Song, Y. Cai, H. M. E. Duyvesteyn, T. Malinauskas, J. Kint, P. Pino, M. J. Wurm, M. Frank, B. Chen, D. I. Stuart, R. W. Sanders, R. Andrabi, D. R. Burton, S. Li, P. J. Bond and M. Crispin, *Biochem*, 2021, **60**, 2153–2169.
133 P. Zhao, J. L. Praissman, O. C. Grant, Y. Cai, T. Xiao, K. E. Rosenbalm, K. Aoki, B. P. Kellman, R. Bridger, D. H. Barouch, M. A. Brindley, N. E. Lewis, M. Tiemeyer, B. Chen, R. J. Woods and L. Wells, *Cell Host Microbe*, 2020, **28**, 586–601 e586.
134 Y. Watanabe, J. D. Allen, D. Wrapp, J. S. McLellan and M. Crispin, *Science*, 2020, **369**, 330–333.
135 W. Tian, D. Li, N. Zhang, G. Bai, K. Yuan, H. Xiao, F. Gao, Y. Chen, C. C. L. Wong and G. F. Gao, *Cell Res.*, 2021, **31**, 1123–1125.
136 L. Zhang, M. Mann, Z. A. Syed, H. M. Reynolds, E. Tian, N. L. Samara, D. C. Zeldin, L. A. Tabak and K. G. Ten Hagen, *Proc. Natl. Acad. Sci. U. S. A.*, 2021, **118**, e2109905118.
137 J. Brun, S. Vasiljevic, B. Gangadharan, M. Hensen, V. C. A, M. L. Hill, J. L. Kiappes, R. A. Dwek, D. S. Alonzi, W. B. Struwe and N. Zitzmann, *ACS Cent. Sci.*, 2021, **7**, 586–593.
138 O. C. Grant, D. Montgomery, K. Ito and R. J. Woods, *Sci. Rep.*, 2020, **10**, 14991.
139 H. Y. Huang, H. Y. Liao, X. Chen, S. W. Wang, C. W. Cheng, M. Shahed-Al-Mahmud, Y. M. Liu, A. Mohapatra, T. H. Chen, J. M. Lo, Y. M. Wu, H. H. Ma, Y. H. Chang, H. Y. Tsai, Y. C. Chou, Y. P. Hsueh, C. Y. Tsai, P. Y. Huang, S. Y. Chang, T. L. Chao, H. C. Kao, Y. M. Tsai, Y. H. Chen, C. Y. Wu, J. T. Jan, T. R. Cheng, K. I. Lin, C. Ma and C. H. Wong, *Sci. Transl. Med.*, 2022, **14**, eabm0899.
140 H. Chawla, E. Fadda and M. Crispin, *Curr. Opin. Struct. Biol.*, 2022, **75**, 102402.
141 S. Zhang, Q. Liang, X. He, C. Zhao, W. Ren, Z. Yang, Z. Wang, Q. Ding, H. Deng, T. Wang, L. Zhang and X. Wang, *Cell Res.*, 2022, **32**, 315–318.
142 J. D. Allen, D. Ivory, S. Ge Song, W. T. He, T. Capozzola, P. Yong, D. R. Burton, R. Andrabi and M. Crispin, *Cell Rep.*, 2023, **42**, 112307.
143 R. Yan, Y. Zhang, Y. Li, L. Xia, Y. Guo and Q. Zhou, *Science*, 2020, **367**, 1444–1448.
144 M. m M. Hatmal, W. Alshaer, M. A. I. Al-Hatamleh, M. Hatmal, O. Smadi, M. O. Taha, A. J. Oweida, J. C. Boer, R. Mohamud and M. Plebanski, *Cells*, 2020, **9**, 2638.
145 Y. Wang, M. Liu and J. Gao, *Proc. Natl. Acad. Sci. U. S. A.*, 2020, **117**, 13967–13974.
146 A. Ali and R. Vijayan, *Sci. Rep.*, 2020, **10**, 14214.
147 T. P. Peacock, D. H. Goldhill, J. Zhou, L. Baillon, R. Frise, O. C. Swann, R. Kugathasan, R. Penn, J. C. Brown, R. Y. Sanchez-David, L. Braga, M. K. Williamson, J. A. Hassard, E. Staller, B. Hanley, M. Osborn, M. Giacca, A. D. Davidson, D. A. Matthews and W. S. Barclay, *Nat. Microbiol.*, 2021, **6**, 899–909.
148 J. M. White and G. R. Whittaker, *Traffic*, 2016, **17**, 593–614.
149 S. Belouzard, V. C. Chu and G. R. Whittaker, *Proc. Natl. Acad. Sci. U. S. A.*, 2009, **106**, 5871–5876.
150 B. Coutard, C. Valle, X. de Lamballerie, B. Canard, N. G. Seidah and E. Decroly, *Antiviral Res.*, 2020, **176**, 104742.
151 P. Zhou, X. L. Yang, X. G. Wang, B. Hu, L. Zhang, W. Zhang, H. R. Si, Y. Zhu, B. Li, C. L. Huang, H. D. Chen, J. Chen, Y. Luo, H. Guo, R. D. Jiang, M. Q. Liu, Y. Chen, X. R. Shen, X. Wang, X. S. Zheng, K. Zhao, Q. J. Chen, F. Deng, L. L. Liu, B. Yan, F. X. Zhan, Y. Y. Wang, G. F. Xiao and Z. L. Shi, *Nature*, 2020, **579**, 270–273.
152 G. R. Whittaker, S. Daniel and J. K. Millet, *Curr. Opin. Virol.*, 2021, **47**, 113–120.
153 D. Cyranoski, *Nature*, 2020, **581**, 22–26.
154 W. Li, M. J. Moore, N. Vasilieva, J. Sui, S. K. Wong, M. A. Berne, M. Somasundaran, J. L. Sullivan, K. Luzuriaga, T. C. Greenough, H. Choe and M. Farzan, *Nature*, 2003, **426**, 450–454.
155 S. K. Wong, W. Li, M. J. Moore, H. Choe and M. Farzan, *J. Biol. Chem.*, 2004, **279**, 3197–3201.
156 X. Y. Ge, J. L. Li, X. L. Yang, A. A. Chmura, G. Zhu, J. H. Epstein, J. K. Mazet, B. Hu, W. Zhang, C. Peng, Y. J. Zhang, C. M. Luo, B. Tan, N. Wang, Y. Zhu, G. Crameri, S. Y. Zhang, L. F. Wang, P. Daszak and Z. L. Shi, *Nature*, 2013, **503**, 535–538.

 

157 W. Li, M. J. Moore, N. Vasilieva, J. Sui, S. K. Wong, M. A. Berne, M. Somasundaran, J. L. Sullivan, K. Luzuriaga, T. C. Greenough, H. Choe and M. Farzan, *Nature*, 2003, **426**, 450–454.
158 D. Wrapp, N. Wang, K. S. Corbett, J. A. Goldsmith, C. L. Hsieh, O. Abiona, B. S. Graham and J. S. McLellan, *Science*, 2020, **367**, 1260–1263.
159 J. Yang, S. J. L. Petitjean, M. Koehler, Q. Zhang, A. C. Dumitru, W. Chen, S. Derclaye, S. P. Vincent, P. Soumillion and D. Alsteens, *Nat. Commun.*, 2020, **11**, 4541.
160 Y. Wan, J. Shang, R. Graham, R. S. Baric and F. Li, *J. Virol.*, 2020, **94**, JVI.00127-00120.
161 G. R. Bullock, I. Steyaert, G. Bilbe, R. M. Carey, J. Kips, B. De Paepe, R. Pauwels, M. Praet, H. M. Siragy and M. de Gasparo, *Histochem. Cell Biol.*, 2001, **115**, 117–124.
162 F. Silhol, G. Sarlon, J. C. Deharo and B. Vaisse, *Hypertens. Res.*, 2020, **43**, 854–856.
163 D. Batlle, J. Wysocki, M. J. Soler and K. Ranganath, *Kidney Int.*, 2012, **81**, 520–528.
164 Y. Imai, K. Kuba and J. M. Penninger, *Exp Physiol*, 2008, **93**, 543–548.
165 Y. Imai, K. Kuba, S. Rao, Y. Huan, F. Guo, B. Guan, P. Yang, R. Sarao, T. Wada, H. Leong-Poi, M. A. Crackower, A. Fukamizu, C. C. Hui, L. Hein, S. Uhlig, A. S. Slutsky, C. Jiang and J. M. Penninger, *Nature*, 2005, **436**, 112–116.
166 D. Chen, X. Li, Q. Song, C. Hu, F. Su, J. Dai, Y. Ye, J. Huang and X. Zhang, *JAMA Netw. Open*, 2020, **3**, e2011122.
167 M. Donoghue, F. Hsieh, E. Baronas, K. Godbout, M. Gosselin, N. Stagliano, M. Donovan, B. Woolf, K. Robison, R. Jeyaseelan, R. E. Breitbart and S. Acton, *Circ. Res.*, 2000, **87**, E1–E9.
168 F. Li, W. Li, M. Farzan and S. C. Harrison, *Science*, 2005, **309**, 1864–1868.
169 G. Y. Oudit, K. Wang, A. Viveiros, M. J. Kellner and J. M. Penninger, *Cell*, 2023, **186**, 906–922.
170 D. J. Muller, A. C. Dumitru, C. Lo Giudice, H. E. Gaub, P. Hinterdorfer, G. Hummer, J. J. De Yoreo, Y. F. Dufrene and D. Alsteens, *Chem. Rev.*, 2021, **121**, 11701–11725.
171 M. S. Li and B. K. Mai, *Curr. Bioinf.*, 2012, **7**, 342–351.
172 W. Cao, C. Dong, S. Kim, D. Hou, W. Tai, L. Du, W. Im and X. F. Zhang, *Biophys. J.*, 2021, **120**, 1011–1019.
173 J. Yang, S. J. Petitjean, M. Koehler, Q. Zhang, A. C. Dumitru, W. Chen, S. Derclaye, S. P. Vincent, P. Soumillion and D. Alsteens, *Nat. Commun.*, 2020, **11**, 1–10.
174 M. Koehler, A. Ray, R. A. Moreira, B. Juniku, A. B. Poma and D. Alsteens, *Nat. Commun.*, 2021, **12**, 6977.
175 E. Evans and K. Ritchie, *Biophys. J.*, 1997, **72**, 1541–1555.
176 G. I. Bell, *Science*, 1978, **200**, 618–627.
177 X. Zhang, B. Hong, P. Wei, P. Pei, H. Xu, L. Chen, Y. Tong, J. Chen, S. Z. Luo, H. Fan and C. He, *Emerging Microbes Infect.*, 2022, **11**, 2658–2669.
178 J. D. Simpson, A. Ray, C. Marcon, R. Dos Santos Natividade, G. M. Dorrazehi, K. Durlet, M. Koehler and D. Alsteens, *Nano Lett.*, 2023, **23**, 1496–1504.
179 R. N. Kirchdoerfer, N. Wang, J. Pallesen, D. Wrapp, H. L. Turner, C. A. Cottrell, K. S. Corbett, B. S. Graham, J. S. McLellan and A. B. Ward, *Sci. Rep.*, 2018, **8**, 15701.
180 C. Lei, K. Qian, T. Li, S. Zhang, W. Fu, M. Ding and S. Hu, *Nat. Commun.*, 2020, **11**, 2070.
181 H. L. Nguyen, P. D. Lan, N. Q. Thai, D. A. Nissley, E. P. O'Brien and M. S. Li, *J. Phys. Chem. B*, 2020, **124**, 7336–7347.
182 H. Liu, Q. Zhang, P. Wei, Z. Chen, K. Aviszus, J. Yang, W. Downing, C. Jiang, B. Liang, L. Reynoso, G. P. Downey, S. K. Frankel, J. Kappler, P. Marrack and G. Zhang, *Cell Res.*, 2021, **31**, 720–722.
183 P. Supasa, D. Zhou, W. Dejnirattisai, C. Liu, A. J. Mentzer, H. M. Ginn, Y. Zhao, H. M. E. Duyvesteyn, R. Nutalai, A. Tuekprakhon, B. Wang, G. C. Paesen, J. Slon-Campos, C. Lopez-Camacho, B. Hallis, N. Coombes, K. R. Bewley, S. Charlton, T. S. Walter, E. Barnes, S. J. Dunachie, D. Skelly, S. F. Lumley, N. Baker, I. Shaik, H. E. Humphries, K. Godwin, N. Gent, A. Sienkiewicz, C. Dold, R. Levin, T. Dong, A. J. Pollard, J. C. Knight, P. Klenerman, D. Crook, T. Lambe, E. Clutterbuck, S. Bibi, A. Flaxman, M. Bittaye, S. Belij-Rammerstorfer, S. Gilbert, D. R. Hall, M. A. Williams, N. G. Paterson, W. James, M. W. Carroll, E. E. Fry, J. Mongkolsapaya, J. Ren, D. I. Stuart and G. R. Screaton, *Cell*, 2021, **184**, 2201–2211 e2207.
184 E. Cameroni, J. E. Bowen, L. E. Rosen, C. Saliba, S. K. Zepeda, K. Culap, D. Pinto, L. A. VanBlargan, A. De Marco, J. di Iulio, F. Zatta, H. Kaiser, J. Noack, N. Farhat, N. Czudnochowski, C. Havenar-Daughton, K. R. Sprouse, J. R. Dillen, A. E. Powell, A. Chen, C. Maher, L. Yin, D. Sun, L. Soriaga, J. Bassi, C. Silacci-Fregni, C. Gustafsson, N. M. Franko, J. Logue, N. T. Iqbal, I. Mazzitelli, J. Geffner, R. Grifantini, H. Chu, A. Gori, A. Riva, O. Giannini, A. Ceschi, P. Ferrari, P. E. Cippa, A. Franzetti-Pellanda, C. Garzoni, P. J. Halfmann, Y. Kawaoka, C. Hebner, L. A. Purcell, L. Piccoli, M. S. Pizzuto, A. C. Walls, M. S. Diamond, A. Telenti, H. W. Virgin, A. Lanzavecchia, G. Snell, D. Veesler and D. Corti, *Nature*, 2022, **602**, 664–670.
185 X. Zhang, S. Wu, B. Wu, Q. Yang, A. Chen, Y. Li, Y. Zhang, T. Pan, H. Zhang and X. He, *Signal Transduction Targeted Ther.*, 2021, **6**, 430.
186 K. K. Chan, D. Dorosky, P. Sharma, S. A. Abbasi, J. M. Dye, D. M. Kranz, A. S. Herbert and E. Procko, *Science*, 2020, **369**, 1261–1265.
187 W. Dejnirattisai, J. Huo, D. Zhou, J. Zahradnik, P. Supasa, C. Liu, H. M. E. Duyvesteyn, H. M. Ginn, A. J. Mentzer, A. Tuekprakhon, R. Nutalai, B. Wang, A. Dijokaite, S. Khan, O. Avinoam, M. Bahar, D. Skelly, S. Adele, S. A. Johnson, A. Amini, T. G. Ritter, C. Mason, C. Dold, D. Pan, S. Assadi, A. Bellass, N. Omo-Dare, D. Koeckerling, A. Flaxman, D. Jenkin, P. K. Aley, M. Voysey, S. A. Costa Clemens, F. G. Naveca, V. Nascimento, F. Nascimento, C. Fernandes da Costa, P. C. Resende, A. Pauvolid-Correa, M. M. Siqueira, V. Baillie, N. Serafin, G. Kwatra, K. Da Silva, S. A. Madhi, M. C. Nunes, T. Malik, P. J. M. Openshaw, J. K. Baillie, M. G. Semple, A. R. Townsend, K. A. Huang, T. K. Tan, M. W. Carroll, P. Klenerman, E. Barnes, S. J. Dunachie, B. Constantinides, H. Webster, D. Crook, A. J. Pollard, T. Lambe, O. Consortium, I. C. Consortium, N. G. Paterson,

M. A. Williams, D. R. Hall, E. E. Fry, J. Mongkolsapaya, J. Ren, G. Schreiber, D. I. Stuart and G. R. Screaton, *Cell*, 2022, **185**, 467–484 e415.

188 F. Tian, B. Tong, L. Sun, S. Shi, B. Zheng, Z. Wang, X. Dong and P. Zheng, *Elife*, 2021, **10**, e69091.

189 W. Yin, Y. Xu, P. Xu, X. Cao, C. Wu, C. Gu, X. He, X. Wang, S. Huang, Q. Yuan, K. Wu, W. Hu, Z. Huang, J. Liu, Z. Wang, F. Jia, K. Xia, P. Liu, X. Wang, B. Song, J. Zheng, H. Jiang, X. Cheng, Y. Jiang, S. J. Deng and H. E. Xu, *Science*, 2022, **375**, 1048–1053.

190 Q. Wang, Y. Guo, S. Iketani, M. S. Nair, Z. Li, H. Mohri, M. Wang, J. Yu, A. D. Bowen, J. Y. Chang, J. G. Shah, N. Nguyen, Z. Chen, K. Meyers, M. T. Yin, M. E. Sobieszczyk, Z. Sheng, Y. Huang, L. Liu and D. D. Ho, *Nature*, 2022, **608**, 603–608.

191 P. Han, C. Su, Y. Zhang, C. Bai, A. Zheng, C. Qiao, Q. Wang, S. Niu, Q. Chen, Y. Zhang, W. Li, H. Liao, J. Li, Z. Zhang, H. Cho, M. Yang, X. Rong, Y. Hu, N. Huang, J. Yan, Q. Wang, X. Zhao, G. F. Gao and J. Qi, *Nat. Commun.*, 2021, **12**, 6103.

192 J. Zhang, Y. Cai, C. L. Lavine, H. Peng, H. Zhu, K. Anand, P. Tong, A. Gautam, M. L. Mayer, S. Rits-Volloch, S. Wang, P. Sliz, D. R. Wesemann, W. Yang, M. S. Seaman, J. Lu, T. Xiao and B. Chen, *Cell Rep.*, 2022, **39**, 110729.

193 M. I. Barton, S. A. MacGowan, M. A. Kutuzov, O. Dushek, G. J. Barton and P. A. van der Merwe, *Elife*, 2021, **10**, e70658.

194 T. J. Yang, P. Y. Yu, Y. C. Chang, K. H. Liang, H. C. Tso, M. R. Ho, W. Y. Chen, H. T. Lin, H. C. Wu and S. D. Hsu, *Nat. Struct. Mol. Biol.*, 2021, **28**, 731–739.

195 D. A. Collier, A. De Marco, I. Ferreira, B. Meng, R. P. Datir, A. C. Walls, S. A. Kemp, J. Bassi, D. Pinto, C. Silacci-Fregni, S. Bianchi, M. A. Tortorici, J. Bowen, K. Culap, S. Jaconi, E. Cameroni, G. Snell, M. S. Pizzuto, A. F. Pellanda, C. Garzoni, A. Riva, C.-N. B. C. Collaboration, A. Elmer, N. Kingston, B. Graves, L. E. McCoy, K. G. C. Smith, J. R. Bradley, N. Temperton, L. Ceron-Gutierrez, G. Barcenas-Morales, C.-G. U. Consortium, W. Harvey, H. W. Virgin, A. Lanzavecchia, L. Piccoli, R. Doffinger, M. Wills, D. Veesler, D. Corti and R. K. Gupta, *Nature*, 2021, **593**, 136–141.

196 C. Laffeber, K. de Koning, R. Kanaar and J. H. G. Lebbink, *J. Mol. Biol.*, 2021, **433**, 167058.

197 J. Zhang, T. Xiao, Y. Cai, C. L. Lavine, H. Peng, H. Zhu, K. Anand, P. Tong, A. Gautam, M. L. Mayer, R. M. Walsh, Jr., S. Rits-Volloch, D. R. Wesemann, W. Yang, M. S. Seaman, J. Lu and B. Chen, *Science*, 2021, **374**, 1353–1360.

198 M. McCallum, A. C. Walls, K. R. Sprouse, J. E. Bowen, L. E. Rosen, H. V. Dang, A. De Marco, N. Franko, S. W. Tilles, J. Logue, M. C. Miranda, M. Ahlrichs, L. Carter, G. Snell, M. S. Pizzuto, H. Y. Chu, W. C. Van Voorhis, D. Corti and D. Veesler, *Science*, 2021, **374**, 1621–1626.

199 Y. Wang, C. Liu, C. Zhang, Y. Wang, Q. Hong, S. Xu, Z. Li, Y. Yang, Z. Huang and Y. Cong, *Nat. Commun.*, 2022, **13**, 871.

200 D. Mannar, J. W. Saville, Z. Sun, X. Zhu, M. M. Marti, S. S. Srivastava, A. M. Berezuk, S. Zhou, K. S. Tuttle, M. D. Sobolewski, A. Kim, B. R. Treat, P. M. Da Silva Castanha, J. L. Jacobs, S. M. Barratt-Boyes, J. W. Mellors, D. S. Dimitrov, W. Li and S. Subramaniam, *Nat. Commun.*, 2022, **13**, 4696.

201 R. Bayarri-Olmos, L. B. Johnsen, M. Idorn, L. S. Reinert, A. Rosbjerg, S. Vang, C. B. Hansen, C. Helgstrand, J. R. Bjelke, T. Bak-Thomsen, S. R. Paludan, P. Garred and M. O. Skjoedt, *Elife*, 2021, **10**, e70002.

202 Z. Cui, P. Liu, N. Wang, L. Wang, K. Fan, Q. Zhu, K. Wang, R. Chen, R. Feng, Z. Jia, M. Yang, G. Xu, B. Zhu, W. Fu, T. Chu, L. Feng, Y. Wang, X. Pei, P. Yang, X. S. Xie, L. Cao, Y. Cao and X. Wang, *Cell*, 2022, **185**, 860–871 e813.

203 Y. Cao, W. Song, L. Wang, P. Liu, C. Yue, F. Jian, Y. Yu, A. Yisimayi, P. Wang, Y. Wang, Q. Zhu, J. Deng, W. Fu, L. Yu, N. Zhang, J. Wang, T. Xiao, R. An, J. Wang, L. Liu, S. Yang, X. Niu, Q. Gu, F. Shao, X. Hao, R. Jin, Y. Wang, X. S. Xie and X. Wang, *Cell Host Microbe*, 2022, **30**, 1527–1539.e5.

204 H. Grubmuller, B. Heymann and P. Tavan, *Science*, 1996, **271**, 997–999.

205 M. Koehler, A. Ray, R. A. Moreira, B. Juniku, A. B. Poma and D. Alsteens, *Nat. Commun.*, 2021, **12**, 1–13.

206 H. Nguyen, P. D. Lan, D. A. Nissley, E. P. O'Brien and M. S. Li, *J. Phys. Chem. B*, 2022, **126**, 2812–2823.

207 H. Nguyen, P. D. Lan, D. A. Nissley, E. P. O'Brien and M. S. Li, *J. Phys. Chem. B*, 2021, **125**, 7368–7379.

208 H. Nguyen and M. S. Li, *Sci. Rep.*, 2022, **12**, 9701.

209 J. Aqvist, C. Medina and J. E. Samuelsson, *Protein Eng.*, 1994, **7**, 385–391.

210 R. Zhou, R. A. Friesner, A. Ghosh, R. C. Rizzo, W. L. Jorgensen and R. Levy, *J. Phys. Chem. B*, 2001, **105**, 10388–10397.

211 V. Durmaz, K. Kochl, A. Krassnigg, L. Parigger, M. Hetmann, A. Singh, D. Nutz, A. Korsunsky, U. Kahler, C. Konig, L. Chang, M. Krebs, R. Bassetto, T. Pavkov-Keller, V. Resch, K. Gruber, G. Steinkellner and C. C. Gruber, *Sci. Rep.*, 2022, **12**, 14534.

212 J. Zahradnik, S. Marciano, M. Shemesh, E. Zoler, D. Harari, J. Chiaravalli, B. Meyer, Y. Rudich, C. Li, I. Marton, O. Dym, N. Elad, M. G. Lewis, H. Andersen, M. Gagne, R. A. Seder, D. C. Douek and G. Schreiber, *Nat. Microbiol.*, 2021, **6**, 1188–1198.

213 M. I. Barton, S. A. MacGowan, M. A. Kutuzov, O. Dushek, G. J. Barton and P. A. Van Der Merwe, *Elife*, 2021, **10**, e70658.

214 M. Naim, S. Bhat, K. N. Rankin, S. Dennis, S. F. Chowdhury, I. Siddiqi, P. Drabik, T. Sulea, C. I. Bayly, A. Jakalian and E. O. Purisima, *J. Chem. Inf. Model.*, 2007, **47**, 122–133.

215 T. Sulea, Q. Cui and E. O. Purisima, *J. Chem. Inf. Model.*, 2011, **51**, 2066–2081.

216 F. F. Yan and F. Gao, *Briefings Bioinf.*, 2021, **22**, 1122–1136.

217 G. Naresh and L. Guruprasad, *J. Biomol. Struct. Dyn.*, 2023, **41**, 2368–2381.

218 P. A. Kollman, I. Massova, C. Reyes, B. Kuhn, S. Huo, L. Chong, M. Lee, T. Lee, Y. Duan, W. Wang, O. Donini,

 

P. Cieplak, J. Srinivasan, D. A. Case and T. E. Cheatham, 3rd, *Acc. Chem. Res.*, 2000, **33**, 889–897.
219 J. Srinivasan, T. E. Cheatham, P. Cieplak, P. A. Kollman and D. A. Case, *J. Am. Chem. Soc.*, 1998, **120**, 9401–9409.
220 F. Eisenhaber, P. Lijnzaad, P. Argos, C. Sander and M. Scharf, *J. Comput. Chem.*, 1995, **16**, 273–284.
221 E. Wang, H. Sun, J. Wang, Z. Wang, H. Liu, J. Z. H. Zhang and T. Hou, *Chem. Rev.*, 2019, **119**, 9478–9508.
222 H.-m Ding, Y.-w Yin, Y.-j Sheng and Y.-q Ma, *Chin. Phys. Lett.*, 2021, **38**, 018701.
223 M. Shah, B. Ahmad, S. Choi and H. G. Woo, *Comput. Struct. Biotechnol. J.*, 2020, **18**, 3402–3414.
224 N. Forouzesh and N. Mishra, *Molecules*, 2021, **26**, 2383.
225 L. Duan, X. Liu and J. Z. Zhang, *J. Am. Chem. Soc.*, 2016, **138**, 5722–5728.
226 H. L. Nguyen, N. Q. Thai, P. H. Nguyen and M. S. Li, *J. Phys. Chem. B*, 2022, **126**, 4669–4678.
227 Y. Zhang, X. He, J. Zhai, B. Ji, V. H. Man and J. Wang, *Briefings Bioinf.*, 2021, **22**, bbab188.
228 K. Nguyen, S. Chakraborty, R. Mansbach, B. Korber and S. Gnanakaran, *Viruses*, 2021, **13**, 927.
229 C. E. Chang, W. Chen and M. K. Gilson, *J. Chem. Theory Comput.*, 2005, **1**, 1017–1028.
230 J. Wang and T. Hou, *J. Chem. Inf. Model.*, 2012, **52**, 1199–1212.
231 B. Jawad, P. Adhikari, R. Podgornik and W.-Y. Ching, *J. Mol. Graphics Modell.*, 2021, **61**, 4425–4441.
232 F. Jafary, S. Jafari and M. R. Ganjalikhany, *Sci. Rep.*, 2021, **11**, 6927.
233 L. Wu, L. Zhou, M. Mo, T. Liu, C. Wu, C. Gong, K. Lu, L. Gong, W. Zhu and Z. Xu, *Signal Transduction Targeted Ther.*, 2022, **7**, 1–3.
234 J. de Andrade, P. F. B. Gonçalves and P. A. Netz, *ChemBioChem*, 2021, **22**, 865–875.
235 S. Ma, H. Li, J. Yang and K. Yu, *Biochimie*, 2021, **187**, 1–13.
236 S. Piplani, P. K. Singh, D. A. Winkler and N. Petrovsky, *Sci. Rep.*, 2021, **11**, 1–13.
237 A. Khan, J. Gui, W. Ahmad, I. Haq, M. Shahid, A. A. Khan, A. Shah, A. Khan, L. Ali and Z. Anwar, *RSC Adv.*, 2021, **11**, 30132–30147.
238 W. B. Wang, Y. Liang, Y. Q. Jin, J. Zhang, J. G. Su and Q. M. Li, *J. Mol. Graphics Modell.*, 2021, **109**, 108035.
239 C. S. Lupala, Y. Ye, H. Chen, X.-D. Su and H. Liu, *Biochem. Biophys. Res. Commun.*, 2022, **590**, 34–41.
240 N. Mandal, A. K. Padhi and S. L. Rath, *J. Mol. Graphics Modell.*, 2022, **114**, 108194.
241 W. Zhou, C. Xu, P. Wang, M. Luo, Z. Xu, R. Cheng, X. Jin, Y. Guo, G. Xue, L. Juan, A. A. Anashkina, H. Nie and Q. Jiang, *Front. Cell Dev. Biol.*, 2021, **9**, 697035.
242 E. S. Istifli, P. A. Netz, A. Sihoglu Tepe, C. Sarikurkcu and B. Tepe, *J. Biomol. Struct. Dyn.*, 2022, **40**, 12760–12771.
243 S. Guo, J. Yang, Y. Lei, B. Liu, W. Zhang, L. Zhang and Z. Zuo, *J. Mol. Graphics Modell.*, 2021, **105**, 107893.
244 J. D. Allen, Y. Watanabe, H. Chawla, M. L. Newby and M. Crispin, *J. Mol. Biol.*, 2021, **433**, 166762.
245 E. P. Barros, L. Casalino, Z. Gaieb, A. C. Dommer, Y. Wang, L. Fallon, L. Raguette, K. Belfon, C. Simmerling and R. E. Amaro, *Biophys. J.*, 2021, **120**, 1072–1084.
246 S. Rahnama, M. Azimzadeh Irani, M. Amininasab and M. R. Ejtehadi, *Sci. Rep.*, 2021, **11**, 15162.
247 B. Ma, Z. Zhang, Y. Li, X. Lin and N. Gu, *J. Mol. Graphics Modell.*, 2022, **62**, 936–944.
248 S. Vicatos, A. Rychkova, S. Mukherjee and A. Warshel, *Proteins*, 2014, **82**, 1168–1185.
249 M. Lee, V. Kolev and A. Warshel, *J. Phys. Chem. B*, 2017, **121**, 11284–11291.
250 C. Bai and A. Warshel, *J. Phys. Chem. B*, 2020, **124**, 5907–5912.
251 C. Bai, J. Wang, G. Chen, H. Zhang, K. An, P. Xu, Y. Du, R. D. Ye, A. Saha, A. Zhang and A. Warshel, *J. Am. Chem. Soc.*, 2021, **143**, 17646–17654.
252 D. A. Nissley, Q. V. Vu, F. Trovato, N. Ahmed, Y. Jiang, M. S. Li and E. P. O'Brien, *J. Am. Chem. Soc.*, 2020, **142**, 6103–6110.
253 J. Karanicolas and C. L. Brooks, 3rd, *Protein Sci.*, 2002, **11**, 2351–2361.
254 D. V. Parums, *Med. Sci. Monit.*, 2022, **28**, e937676.
255 V. Parums, *Med. Sci. Monit.*, 2021, **27**, e933622.
256 S. S. Abdool Karim and T. de Oliveira, *N. Engl. J. Med.*, 2021, **384**, 1866–1868.
257 A. Sanyaolu, A. Marinkovic, S. Prakash, N. Haider, M. Williams, C. Okorie, O. Badaru and S. Smith, *World J. Virol.*, 2022, **11**, 137–143.
258 R. Uraki, P. J. Halfmann, S. Iida, S. Yamayoshi, Y. Furusawa, M. Kiso, M. Ito, K. Iwatsuki-Horimoto, S. Mine, M. Kuroda, T. Maemura, Y. Sakai-Tagawa, H. Ueki, R. Li, Y. Liu, D. Larson, S. Fukushi, S. Watanabe, K. Maeda, A. Pekosz, A. Kandeil, R. J. Webby, Z. Wang, M. Imai, T. Suzuki and Y. Kawaoka, *Nature*, 2022, **612**, 540–545.
259 M. Kidd, A. Richter, A. Best, N. Cumley, J. Mirza, B. Percival, M. Mayhew, O. Megram, F. Ashford, T. White, E. Moles-Garcia, L. Crawford, A. Bosworth, S. F. Atabani, T. Plant and A. McNally, *J. Infect. Dis.*, 2021, **223**, 1666–1670.
260 P. Calistri, L. Amato, I. Puglia, F. Cito, A. Di Giuseppe, M. L. Danzetta, D. Morelli, M. Di Domenico, M. Caporale, S. Scialabba, O. Portanti, V. Curini, F. Perletta, C. Camma, M. Ancora, G. Savini, G. Migliorati, N. D'Alterio and A. Lorusso, *Int. J. Infect. Dis.*, 2021, **105**, 753–755.
261 J. R. Port, C. K. Yinda, V. A. Avanzato, J. E. Schulz, M. G. Holbrook, N. van Doremalen, C. Shaia, R. J. Fischer and V. J. Munster, *Nat. Microbiol.*, 2022, **7**, 213–223.
262 N. G. Davies, C. I. Jarvis, C. C.-W. Group, W. J. Edmunds, N. P. Jewell, K. Diaz-Ordaz and R. H. Keogh, *Nature*, 2021, **593**, 270–274.
263 N. G. Davies, S. Abbott, R. C. Barnard, C. I. Jarvis, A. J. Kucharski, J. D. Munday, C. A. B. Pearson, T. W. Russell, D. C. Tully, A. D. Washburne, T. Wenseleers, A. Gimma, W. Waites, K. L. M. Wong, K. van Zandvoort, J. D. Silverman, C. C.-W. Group, C.-G. U. Consortium, K. Diaz-Ordaz, R. Keogh, R. M. Eggo, S. Funk, M. Jit, K. E. Atkins and W. J. Edmunds, *Science*, 2021, **372**, eabg3055.

264 B. Meng, S. A. Kemp, G. Papa, R. Datir, I. Ferreira, S. Marelli, W. T. Harvey, S. Lytras, A. Mohamed, G. Gallo, N. Thakur, D. A. Collier, P. Mlcochova, C.-G. U. Consortium, L. M. Duncan, A. M. Carabelli, J. C. Kenyon, A. M. Lever, A. De Marco, C. Saliba, K. Culap, E. Cameroni, N. J. Matheson, L. Piccoli, D. Corti, L. C. James, D. L. Robertson, D. Bailey and R. K. Gupta, *Cell Rep.*, 2021, **35**, 109292.

265 Y. Liu, J. Liu, B. A. Johnson, H. Xia, Z. Ku, C. Schindewolf, S. G. Widen, Z. An, S. C. Weaver, V. D. Menachery, X. Xie and P. Y. Shi, *Cell Rep.*, 2022, **39**, 110829.

266 B. Lubinski, M. H. V. Fernandes, L. Frazier, T. Tang, S. Daniel, D. G. Diel, J. A. Jaimes and G. R. Whittaker, *iScience*, 2022, **25**, 103589.

267 A. Khan, T. Zia, M. Suleman, T. Khan, S. S. Ali, A. A. Abbasi, A. Mohammad and D. Q. Wei, *J. Cell. Physiol.*, 2021, **236**, 7045–7057.

268 H. Fu, H. Chen, W. Cai, X. Shao and C. Chipot, *J. Chem. Inf. Model.*, 2021, **61**, 2116–2123.

269 S. Dutta, B. Panthi and A. Chandra, *J. Phys. Chem. B*, 2022, **126**, 5375–5389.

270 N. A. Murugan, P. S. Javali, C. J. Pandianb, M. A. Ali, V. Srivastava and J. Jeyaraman, *Phys. Chem. Chem. Phys.*, 2022, **24**, 20371–20380.

271 N. Bhattarai, P. Baral, B. S. Gerstman and P. P. Chapagain, *J. Phys. Chem. B*, 2021, **125**, 7101–7107.

272 P. Mlcochova, S. A. Kemp, M. S. Dhar, G. Papa, B. Meng, I. Ferreira, R. Datir, D. A. Collier, A. Albecka, S. Singh, R. Pandey, J. Brown, J. Zhou, N. Goonawardane, S. Mishra, C. Whittaker, T. Mellan, R. Marwal, M. Datta, S. Sengupta, K. Ponnusamy, V. S. Radhakrishnan, A. Abdullahi, O. Charles, P. Chattopadhyay, P. Devi, D. Caputo, T. Peacock, C. Wattal, N. Goel, A. Satwik, R. Vaishya, M. Agarwal, S.-C.-G. C. Indian, C. Genotype To Phenotype Japan, C.-N. B. C.- Collaboration, A. Mavousian, J. H. Lee, J. Bassi, C. Silacci-Fegni, C. Saliba, D. Pinto, T. Irie, I. Yoshida, W. L. Hamilton, K. Sato, S. Bhatt, S. Flaxman, L. C. James, D. Corti, L. Piccoli, W. S. Barclay, P. Rakshit, A. Agrawal and R. K. Gupta, *Nature*, 2021, **599**, 114–119.

273 A. Saito, T. Irie, R. Suzuki, T. Maemura, H. Nasser, K. Uriu, Y. Kosugi, K. Shirakawa, K. Sadamasu, I. Kimura, J. Ito, J. Wu, K. Iwatsuki-Horimoto, M. Ito, S. Yamayoshi, S. Loeber, M. Tsuda, L. Wang, S. Ozono, E. P. Butlertanaka, Y. L. Tanaka, R. Shimizu, K. Shimizu, K. Yoshimatsu, R. Kawabata, T. Sakaguchi, K. Tokunaga, I. Yoshida, H. Asakura, M. Nagashima, Y. Kazuma, R. Nomura, Y. Horisawa, K. Yoshimura, A. Takaori-Kondo, M. Imai, C. Genotype to Phenotype Japan, S. Tanaka, S. Nakagawa, T. Ikeda, T. Fukuhara, Y. Kawaoka and K. Sato, *Nature*, 2022, **602**, 300–306.

274 C. Liu, H. M. Ginn, W. Dejnirattisai, P. Supasa, B. Wang, A. Tuekprakhon, R. Nutalai, D. Zhou, A. J. Mentzer, Y. Zhao, H. M. E. Duyvesteyn, C. Lopez-Camacho, J. Slon-Campos, T. S. Walter, D. Skelly, S. A. Johnson, T. G. Ritter, C. Mason, S. A. Costa Clemens, F. Gomes Naveca, V. Nascimento, F. Nascimento, C. Fernandes da Costa, P. C. Resende, A. Pauvolid-Correa, M. M. Siqueira, C. Dold, N. Temperton, T. Dong, A. J. Pollard, J. C. Knight, D. Crook, T. Lambe, E. Clutterbuck, S. Bibi, A. Flaxman, M. Bittaye, S. Belij-Rammerstorfer, S. C. Gilbert, T. Malik, M. W. Carroll, P. Klenerman, E. Barnes, S. J. Dunachie, V. Baillie, N. Serafin, Z. Ditse, K. Da Silva, N. G. Paterson, M. A. Williams, D. R. Hall, S. Madhi, M. C. Nunes, P. Goulder, E. E. Fry, J. Mongkolsapaya, J. Ren, D. I. Stuart and G. R. Screaton, *Cell*, 2021, **184**, 4220–4236 e4213.

275 L. Wu, L. Zhou, M. Mo, T. Liu, C. Wu, C. Gong, K. Lu, L. Gong, W. Zhu and Z. Xu, *Signal Transduction Targeted Ther.*, 2022, **7**, 8.

276 E. Socher, L. Heger, F. Paulsen, F. Zunke and P. Arnold, *Comput. Struct. Biotechnol. J.*, 2022, **20**, 1168–1176.

277 M. Romero-Durana, B. Jimenez-Garcia and J. Fernandez-Recio, *J. Bioinform.*, 2020, **36**, 2284–2285.

278 E. Pitsillou, J. J. Liang, R. C. Beh, A. Hung and T. C. Karagiannis, *Comput. Biol. Med.*, 2022, **149**, 106035.

279 K. Ito, C. Piantham and H. Nishiura, *J. Med. Virol.*, 2022, **94**, 2265–2268.

280 R. Karyakarte, R. Das, N. Taji, S. Yanamandra, S. Shende, S. Joshi, B. Karekar, R. Bawale, R. Tiwari, M. Jadhav, S. Sakalkar, G. Chaudhari, S. Rane, J. Agarasen, P. Pillai, S. Dudhate, P. Chandankhede, R. Labhshetwar, Y. Gadiyal, M. Rajmane, S. Mukade and P. Kulkarni, *Cureus*, 2022, **14**, e31352.

281 D. Mannar, J. W. Saville, X. Zhu, S. S. Srivastava, A. M. Berezuk, K. S. Tuttle, A. C. Marquez, I. Sekirov and S. Subramaniam, *Science*, 2022, **375**, 760–764.

282 V. Stalls, J. Lindenberger, S. M. Gobeil, R. Henderson, R. Parks, M. Barr, M. Deyton, M. Martin, K. Janowska, X. Huang, A. May, M. Speakman, E. Beaudoin, B. Kraft, X. Lu, R. J. Edwards, A. Eaton, D. C. Montefiori, W. B. Williams, K. O. Saunders, K. Wiehe, B. F. Haynes and P. Acharya, *Cell Rep.*, 2022, **39**, 111009.

283 A. Saito, T. Tamura, J. Zahradnik, S. Deguchi, K. Tabata, I. Kimura, J. Ito, H. Nasser, M. Toyoda, K. Nagata, K. Uriu, Y. Kosugi, S. Fujita, D. Yamasoba, M. Shofa, M. S. T. M. Begum, Y. Oda, R. Suzuki, H. Ito, N. Nao, L. Wang, M. Tsuda, K. Yoshimatsu, Y. Yamamoto, T. Nagamoto, H. Asakura, M. Nagashima, K. Sadamasu, K. Yoshimura, T. Ueno, G. Schreiber, A. Takaori-Kondo, K. Shirakawa, H. Sawa, T. Irie, K. Takayama, K. Matsuno, S. Tanaka, T. Ikeda, T. Fukuhara and K. Sato, *Cell Host Microbe*, 2022, **30**, 1540–1555.e1515.

284 T. Tamura, J. Ito, K. Uriu, J. Zahradnik, I. Kida, H. Nasser, M. Shofa, Y. Oda, S. Lytras, N. Nao, Y. Itakura, S. Deguchi, R. Suzuki, L. Wang, M. S. T. M. Begum, M. Tsuda, Y. Kosugi, S. Fujita, K. Yoshimatsu, S. Suzuki, H. Asakura, M. Nagashima, K. Sadamasu, K. Yoshimura, Y. Yamamoto, T. Nagamoto, G. Schreiber, T. Ikeda, T. Fukuhara, A. Saito, S. Tanaka, K. Matsuno, K. Takayama, K. Sato and C. The Genotype to Phenotype Japan, *Nat. Commun.*, 2023, **14**, 2800.

285 C. Yue, W. Song, L. Wang, F. Jian, X. Chen, F. Gao, Z. Shen, Y. Wang, X. Wang and Y. Cao, *Lancet Infect. Dis.*, 2023, **23**, 278–280.

286 J. Ito, R. Suzuki, K. Uriu, Y. Itakura, J. Zahradnik, S. Deguchi, L. Wang, S. Lytras, T. Tamura, I. Kida,

 

H. Nasser, M. Shofa, M. S. T. M. Begum, M. Tsuda, Y. Oda, S. Fujita, K. Yoshimatsu, H. Ito, N. Nao, H. Asakura, M. Nagashima, K. Sadamasu, K. Yoshimura, Y. Yamamoto, T. Nagamoto, G. Schreiber, A. Saito, K. Matsuno, K. Takayama, S. Tanaka, T. Fukuhara, T. Ikeda, K. Sato and C. The Genotype to Phenotype Japan, *Nat. Commun.*, 2023, **14**, 2671.

287 Y. Cao, F. Jian, J. Wang, Y. Yu, W. Song, A. Yisimayi, J. Wang, R. An, X. Chen, N. Zhang, Y. Wang, P. Wang, L. Zhao, H. Sun, L. Yu, S. Yang, X. Niu, T. Xiao, Q. Gu, F. Shao, X. Hao, Y. Xu, R. Jin, Z. Shen, Y. Wang and X. S. Xie, *Nature*, 2023, **614**, 521–529.

288 H. L. Nguyen, N. Q. Thai, P. H. Nguyen and M. S. Li, *J. Phys. Chem. B*, 2022, **126**, 4669–4678.

289 B. Jawad, P. Adhikari, R. Podgornik and W. Y. Ching, *J. Phys. Chem. Lett.*, 2022, **13**, 3915–3921.

290 C. S. Lupala, Y. Ye, H. Chen, X. D. Su and H. Liu, *Biochem. Biophys. Res. Commun.*, 2022, **590**, 34–41.

291 J. Chen and G. W. Wei, *J. Phys. Chem. Lett.*, 2022, **13**, 3840–3849.

292 A. Khan, H. Waris, M. Rafique, M. Suleman, A. Mohammad, S. S. Ali, T. Khan, Y. Waheed, C. Liao and D. Q. Wei, *Int. J. Biol. Macromol.*, 2022, **200**, 438–448.

293 J. Lan, X. He, Y. Ren, Z. Wang, H. Zhou, S. Fan, C. Zhu, D. Liu, B. Shao, T. Y. Liu, Q. Wang, L. Zhang, J. Ge, T. Wang and X. Wang, *Cell Res.*, 2022, **32**, 593–595.

294 M. Golcuk, A. Yildiz and M. Gur, *J. Mol. Graphics Modell.*, 2022, **117**, 108286.

295 S. L. Rath, A. K. Padhi and N. Mandal, *Biochem. Biophys. Res. Commun.*, 2022, **592**, 18–23.

296 M. Shah and H. G. Woo, *Front. Immunol.*, 2021, **12**, 830527.

297 S. Hwang, S. H. Baek and D. Park, *J. Chem. Inf. Model.*, 2022, **62**, 1771–1782.

298 S. Yamacli and M. Avci, *Adv. Theory Simul.*, 2022, 2200337, DOI: **10.1002/adts.202200337**.

299 Y. Cao, F. Jian, J. Wang, Y. Yu, W. Song, A. Yisimayi, J. Wang, R. An, X. Chen, N. Zhang, Y. Wang, P. Wang, L. Zhao, H. Sun, L. Yu, S. Yang, X. Niu, T. Xiao, Q. Gu, F. Shao, X. Hao, Y. Xu, R. Jin, Z. Shen, Y. Wang and X. S. Xie, *Nature*, 2023, **614**, 521–529.

300 C. Chen, V. S. Boorla, D. Banerjee, R. Chowdhury, V. S. Cavener, R. H. Nissly, A. Gontu, N. R. Boyle, K. Vandegrift and M. S. Nair, *Proc. Natl. Acad. Sci. U. S. A.*, 2021, **118**, e2106480118.

301 T. N. Starr, A. J. Greaney, S. K. Hilton, D. Ellis, K. H. Crawford, A. S. Dingens, M. J. Navarro, J. E. Bowen, M. A. Tortorici and A. C. Walls, *Cell*, 2020, **182**, 1295–1310. e1220.

302 A. Pavlova, Z. Zhang, A. Acharya, D. L. Lynch, Y. T. Pang, Z. Mou, J. M. Parks, C. Chipot and J. C. Gumbart, *J. Phys. Chem. Lett.*, 2021, **12**, 5494–5502.

303 J. Chen, R. Wang, M. Wang and G. W. Wei, *J. Mol. Biol.*, 2020, **432**, 5212–5226.

304 A. H. Williams and C. G. Zhan, *J. Phys. Chem. B*, 2021, **125**, 4330–4336.

305 A. H. Williams and C. G. Zhan, *J. Phys. Chem. B*, 2022, **126**, 2353–2360.

306 E. K. Makowski, J. S. Schardt, M. D. Smith and P. M. Tessier, *PLoS Comput. Biol.*, 2022, **18**, e1010160.

307 A. H. Williams and C. G. Zhan, *J. Phys. Chem. B*, 2022, **126**, 5194–5206.

308 Y. Meng, D. S. Dashti and A. E. Roitberg, *J. Chem. Theory Comput.*, 2011, **7**, 2721–2727.

309 M. Macchiagodena, M. Pagliai, M. Karrenbrock, G. Guarnieri, F. Iannone and P. Procacci, *J. Chem. Theory Comput.*, 2020, **16**, 7160–7172.

310 E. Awoonor-Williams and A. A. A. Abu-Saleh, *Phys. Chem. Chem. Phys.*, 2021, **23**, 6746–6757.

311 J. Aranda, M. Wieczor, M. Terrazas, I. Brun-Heath and M. Orozco, *Chem Catal.*, 2022, **2**, 1084–1099.

312 J. Li, Y. Wang, Y. Liu, Z. Zhang, Y. Zhai, Y. Dai, Z. Wu, X. Nie and L. Du, *Eur. J. Med.Res.*, 2022, **27**, 26.

313 K. Suryamohan, D. Diwanji, E. W. Stawiski, R. Gupta, S. Miersch, J. Liu, C. Chen, Y. P. Jiang, F. A. Fellouse, J. F. Sathirapongsasuti, P. K. Albers, T. Deepak, R. Saberianfar, A. Ratan, G. Washburn, M. Mis, D. Santhosh, S. Somasekar, G. H. Hiranjith, D. Vargas, S. Mohan, S. Phalke, B. Kuriakose, A. Antony, M. Ustav, Jr., S. C. Schuster, S. Sidhu, J. R. Junutula, N. Jura and S. Seshagiri, *Commun. Biol.*, 2021, **4**, 475.

314 M. J. Bhattacharjee, J. J. Lin, C. Y. Chang, Y. T. Chiou, T. N. Li, C. W. Tai, T. F. Shiu, C. A. Chen, C. Y. Chou, P. Chakraborty, Y. Y. Tseng, L. H. Wang and W. H. Li, *Mol. Biol. Evol.*, 2021, **38**, 2715–2731.

315 T. Hattori, T. Saito, K. Okuya, Y. Takahashi, H. Miyamoto, M. Kajihara, M. Igarashi and A. Takada, *Microbiol. Spectrum*, 2022, **10**, e0087022.

316 M. Cevik, K. Kuppalli, J. Kindrachuk and M. Peiris, *BMJ*, 2020, **371**, m3862.

317 F. Hikmet, L. Mear, A. Edvinsson, P. Micke, M. Uhlen and C. Lindskog, *Mol. Syst. Biol.*, 2020, **16**, e9610.

318 L. Cantuti-Castelvetri, R. Ojha, L. D. Pedro, M. Djannatian, J. Franz, S. Kuivanen, F. van der Meer, K. Kallio, T. Kaya, M. Anastasina, T. Smura, L. Levanov, L. Szirovicza, A. Tobi, H. Kallio-Kokko, P. Osterlund, M. Joensuu, F. A. Meunier, S. J. Butcher, M. S. Winkler, B. Mollenhauer, A. Helenius, O. Gokce, T. Teesalu, J. Hepojoki, O. Vapalahti, C. Stadelmann, G. Balistreri and M. Simons, *Science*, 2020, **370**, 856–860.

319 D. R. Bielenberg, C. A. Pettaway, S. Takashima and M. Klagsbrun, *Exp. Cell Res.*, 2006, **312**, 584–593.

320 C. Pellet-Many, P. Frankel, H. Jia and I. Zachary, *Biochem. J.*, 2008, **411**, 211–226.

321 C. C. Lee, A. Kreusch, D. McMullan, K. Ng and G. Spraggon, *Structure*, 2003, **11**, 99–108.

322 T. Teesalu, K. N. Sugahara, V. R. Kotamraju and E. Ruoslahti, *Proc. Natl. Acad. Sci. U. S. A.*, 2009, **106**, 16157–16162.

323 J. L. Daly, B. Simonetti, K. Klein, K.-E. Chen, M. K. Williamson, C. Antón-Plágaro, D. K. Shoemark, L. Simón-Gracia, M. Bauer and R. Hollandi, *Science*, 2020, **370**, 861–865.

324 H. B. Pang, G. B. Braun, T. Friman, P. Aza-Blanc, M. E. Ruidiaz, K. N. Sugahara, T. Teesalu and E. Ruoslahti, *Nat. Commun.*, 2014, **5**, 4904.

325 Z. L. Li and M. Buck, *Biophys. J.*, 2021, **120**, 2828–2837.
326 M. L. Saiz, M. L. DeDiego, D. Lopez-Garcia, V. Corte-Iglesias, A. Baragano Raneros, I. Astola, V. Asensi, C. Lopez-Larrea and B. Suarez-Alvarez, *Clin. Epigenet.*, 2021, **13**, 187.
327 A. Starzec, R. Vassy, A. Martin, M. Lecouvey, M. Di Benedetto, M. Crepin and G. Y. Perret, *Life Sci.*, 2006, **79**, 2370–2381.
328 D. Zanuy, R. Kotla, R. Nussinov, T. Teesalu, K. N. Sugahara, C. Aleman and N. Haspel, *J. Struct. Biol.*, 2013, **182**, 78–86.
329 A. Starzec, P. Ladam, R. Vassy, S. Badache, N. Bouchemal, A. Navaza, C. H. du Penhoat and G. Y. Perret, *Peptides*, 2007, **28**, 2397–2402.
330 H. Jia, A. Bagherzadeh, B. Hartzoulakis, A. Jarvis, M. Lohr, S. Shaikh, R. Aqil, L. Cheng, M. Tickner, D. Esposito, R. Harris, P. C. Driscoll, D. L. Selwood and I. C. Zachary, *J. Biol. Chem.*, 2006, **281**, 13493–13502.
331 H. F. Guo, X. Li, M. W. Parker, J. Waltenberger, P. M. Becker and C. W. Vander Kooi, *Biochem*, 2013, **52**, 7551–7558.
332 K. Bedjeguelal, H. Bienayme, A. Dumoulin, S. Poigny, P. Schmitt and E. Tam, *Bioorg. Med. Chem. Lett.*, 2006, **16**, 3998–4001.
333 S. Perez-Miller, M. Patek, A. Moutal, P. Duran, C. R. Cabel, C. A. Thorne, S. K. Campos and R. Khanna, *ACS Chem. Neurosci.*, 2021, **12**, 1299–1312.
334 C. D. Weekes, M. Beeram, A. W. Tolcher, K. P. Papadopoulos, L. Gore, P. Hegde, Y. Xin, R. Yu, L. M. Shih, H. Xiang, R. K. Brachmann and A. Patnaik, *Invest. New Drugs*, 2014, **32**, 653–660.
335 A. Moutal, L. F. Martin, L. Boinon, K. Gomez, D. Ran, Y. Zhou, H. J. Stratton, S. Cai, S. Luo, K. B. Gonzalez, S. Perez-Miller, A. Patwardhan, M. M. Ibrahim and R. Khanna, *Pain*, 2021, **162**, 243–252.
336 Y. L. Gao, C. X. Wang, Z. Y. Wang, W. J. Li, Y. C. Liu, S. T. Shou and Y. F. Chai, *Infect. Immun.*, 2021, **89**, e00399.
337 T. Kawasaki, T. Kitsukawa, Y. Bekku, Y. Matsuda, M. Sanbo, T. Yagi and H. Fujisawa, *Development*, 1999, **126**, 4895–4902.
338 K. Wang, W. Chen, Z. Zhang, Y. Deng, J.-Q. Lian, P. Du, D. Wei, Y. Zhang, X.-X. Sun and L. Gong, *Signal Transduction Targeted Ther.*, 2020, **5**, 1–10.
339 J. Geng, L. Chen, Y. Yuan, K. Wang, Y. Wang, C. Qin, G. Wu, R. Chen, Z. Zhang, D. Wei, P. Du, J. Zhang, P. Lin, K. Zhang, Y. Deng, K. Xu, J. Liu, X. Sun, T. Guo, X. Yang, J. Wu, J. Jiang, L. Li, K. Zhang, Z. Wang, J. Zhang, Q. Yan, H. Zhu, Z. Zheng, J. Miao, X. Fu, F. Yang, X. Chen, H. Tang, Y. Zhang, Y. Shi, Y. Zhu, Z. Pei, F. Huo, X. Liang, Y. Wang, Q. Wang, W. Xie, Y. Li, M. Shi, H. Bian, P. Zhu and Z. N. Chen, *Signal Transduction Targeted Ther.*, 2021, **6**, 347.
340 R. J. Ragotte, D. Pulido, F. R. Donnellan, M. L. Hill, G. Gorini, H. Davies, J. Brun, K. McHugh, L. D. W. King, K. Skinner, K. Miura, C. A. Long, N. Zitzmann and S. J. Draper, *mSphere*, 2021, **6**, e0064721.
341 J. Shilts, T. W. M. Crozier, E. J. D. Greenwood, P. J. Lehner and G. J. Wright, *Sci. Rep.*, 2021, **11**, 413.
342 Y. Gu, J. Cao, X. Zhang, H. Gao, Y. Wang, J. Wang, J. He, X. Jiang, J. Zhang, G. Shen, J. Yang, X. Zheng, G. Hu, Y. Zhu, S. Du, Y. Zhu, R. Zhang, J. Xu, F. Lan, D. Qu, G. Xu, Y. Zhao, D. Gao, Y. Xie, M. Luo and Z. Lu, *Cell Res.*, 2022, **32**, 24–37.
343 S. Wang, Z. Qiu, Y. Hou, X. Deng, W. Xu, T. Zheng, P. Wu, S. Xie, W. Bian, C. Zhang, Z. Sun, K. Liu, C. Shan, A. Lin, S. Jiang, Y. Xie, Q. Zhou, L. Lu, J. Huang and X. Li, *Cell Res.*, 2021, **31**, 126–140.
344 N. Suryadevara, S. Shrihari, P. Gilchuk, L. A. VanBlargan, E. Binshtein, S. J. Zost, R. S. Nargi, R. E. Sutton, E. S. Winkler, E. C. Chen, M. E. Fouch, E. Davidson, B. J. Doranz, R. E. Chen, P. Y. Shi, R. H. Carnahan, L. B. Thackray, M. S. Diamond and J. E. Crowe, Jr., *Cell*, 2021, **184**, 2316–2331 e2315.
345 O. O. Glebov, *FEBS J.*, 2020, **287**, 3664–3671.
346 J. Gu, E. Gong, B. Zhang, J. Zheng, Z. Gao, Y. Zhong, W. Zou, J. Zhan, S. Wang, Z. Xie, H. Zhuang, B. Wu, H. Zhong, H. Shao, W. Fang, D. Gao, F. Pei, X. Li, Z. He, D. Xu, X. Shi, V. M. Anderson and A. S. Leong, *J. Exp. Med.*, 2005, **202**, 415–424.
347 J. E. Kim, J. H. Heo, H. O. Kim, S. H. Song, S. S. Park, T. H. Park, J. Y. Ahn, M. K. Kim and J. P. Choi, *J. Clin. Neurol.*, 2017, **13**, 227–233.
348 R. Chen, K. Wang, J. Yu, D. Howard, L. French, Z. Chen, C. Wen and Z. Xu, *Front. Neurol.*, 2020, **11**, 573095.
349 A. Pepe, S. Pietropaoli, M. Vos, G. Barba-Spaeth and C. Zurzolo, *Sci. Adv.*, 2022, **8**, eabo0171.
350 C. Wei, L. Wan, Q. Yan, X. Wang, J. Zhang, X. Yang, Y. Zhang, C. Fan, D. Li, Y. Deng, J. Sun, J. Gong, X. Yang, Y. Wang, X. Wang, J. Li, H. Yang, H. Li, Z. Zhang, R. Wang, P. Du, Y. Zong, F. Yin, W. Zhang, N. Wang, Y. Peng, H. Lin, J. Feng, C. Qin, W. Chen, Q. Gao, R. Zhang, Y. Cao and H. Zhong, *Nat. Metab.*, 2020, **2**, 1391–1400.
351 K. Drickamer and M. E. Taylor, *Curr. Opin. Struct. Biol.*, 2015, **34**, 26–34.
352 S. Pohlmann, E. J. Soilleux, F. Baribaud, G. J. Leslie, L. S. Morris, J. Trowsdale, B. Lee, N. Coleman and R. W. Doms, *Proc. Natl. Acad. Sci. U. S. A.*, 2001, **98**, 2670–2675.
353 L. Tailleux, N. Pham-Thi, A. Bergeron-Lafaurie, J. L. Herrmann, P. Charles, O. Schwartz, P. Scheinmann, P. H. Lagrange, J. de Blic, A. Tazi, B. Gicquel and O. Neyrolles, *PLoS Med*, 2005, **2**, e381.
354 R. Amraei, W. Yin, M. A. Napoleon, E. L. Suder, J. Berrigan, Q. Zhao, J. Olejnik, K. B. Chandler, C. Xia, J. Feldman, B. M. Hauser, T. M. Caradonna, A. G. Schmidt, S. Gummuluru, E. Muhlberger, V. Chitalia, C. E. Costello and N. Rahimi, *ACS Cent. Sci.*, 2021, **7**, 1156–1165.
355 M. Thepaut, J. Luczkowiak, C. Vives, N. Labiod, I. Bally, F. Lasala, Y. Grimoire, D. Fenel, S. Sattin, N. Thielens, G. Schoehn, A. Bernardi, R. Delgado and F. Fieschi, *PLoS Pathog.*, 2021, **17**, e1009576.
356 B. Husain, K. Yuen, D. Sun, S. Cao, J. Payandeh and N. Martinez-Martin, *Commun. Biol.*, 2022, **5**, 788.
357 T. M. Clausen, D. R. Sandoval, C. B. Spliid, J. Pihl, H. R. Perrett, C. D. Painter, A. Narayanan, S. A. Majowicz,

 

E. M. Kwong, R. N. McVicar, B. E. Thacker, C. A. Glass, Z. Yang, J. L. Torres, G. J. Golden, P. L. Bartels, R. N. Porell, A. F. Garretson, L. Laubach, J. Feldman, X. Yin, Y. Pu, B. M. Hauser, T. M. Caradonna, B. P. Kellman, C. Martino, P. Gordts, S. K. Chanda, A. G. Schmidt, K. Godula, S. L. Leibel, J. Jose, K. D. Corbett, A. B. Ward, A. F. Carlin and J. D. Esko, *Cell*, 2020, **183**, 1043–1057 e1015.

358 R. Amraei, C. Xia, J. Olejnik, M. R. White, M. A. Napoleon, S. Lotfollahzadeh, B. M. Hauser, A. G. Schmidt, V. Chitalia, E. Muhlberger, C. E. Costello and N. Rahimi, *Proc. Natl. Acad. Sci. U. S. A.*, 2022, **119**, e2113874119.

359 J. Arrindell, P. Abou Atmeh, L. Jayet, Y. Sereme, J. L. Mege and B. Desnues, *iScience*, 2022, **25**, 105463.

360 S. C. Harrison, *Virology*, 2015, **479–480**, 498–507.

361 S. Martens and H. T. McMahon, *Nat. Rev. Mol. Cell Biol.*, 2008, **9**, 543–556.

362 M. Kielian, *Annu. Rev. Virol.*, 2014, **1**, 171–189.

363 X. Sun, S. Belouzard and G. R. Whittaker, *J. Biol. Chem.*, 2008, **283**, 6418–6427.

364 S. Cao and W. Zhang, *Proc. Natl. Acad. Sci. U. S. A.*, 2013, **110**, 13362–13367.

365 D. Birtles and J. Lee, *Biochem*, 2021, **60**, 2978–2986.

366 J. H. Nunberg and J. York, *Viruses*, 2012, **4**, 83–101.

367 I. G. Madu, S. L. Roth, S. Belouzard and G. R. Whittaker, *J. Virol.*, 2009, **83**, 7411–7421.

368 R. N. Kirchdoerfer, C. A. Cottrell, N. Wang, J. Pallesen, H. M. Yassine, H. L. Turner, K. S. Corbett, B. S. Graham, J. S. McLellan and A. B. Ward, *Nature*, 2016, **531**, 118–121.

369 R. K. Koppisetti, Y. G. Fulcher and S. R. Van Doren, *J. Am. Chem. Soc.*, 2021, **143**, 13205–13211.

370 A. L. Lai and J. H. Freed, *J. Mol. Biol.*, 2021, **433**, 166946.

371 G. P. Pattnaik, S. Bhattacharjya and H. Chakraborty, *Biochem*, 2021, **60**, 559–562.

372 L. G. M. Basso, A. E. Zeraik, A. P. Felizatti and A. J. Costa-Filho, *Biochim. Biophys. Acta, Biomembr.*, 2021, **1863**, 183697.

373 B. J. Bosch, B. E. Martina, R. Van Der Zee, J. Lepault, B. J. Haijema, C. Versluis, A. J. Heck, R. De Groot, A. D. Osterhaus and P. J. Rottier, *Proc. Natl. Acad. Sci. U. S. A.*, 2004, **101**, 8455–8460.

374 B. Sainz, Jr., J. M. Rausch, W. R. Gallaher, R. F. Garry and W. C. Wimley, *J. Virol.*, 2005, **79**, 7195–7206.

375 J. Guillen, A. J. Perez-Berna, M. R. Moreno and J. Villalain, *Biochem*, 2008, **47**, 8214–8224.

376 G. P. Pattnaik, G. Meher and H. Chakraborty, *Adv. Exp. Med. Biol.*, 2018, **1112**, 69–78.

377 A. L. Lai, J. K. Millet, S. Daniel, J. H. Freed and G. R. Whittaker, *J. Mol. Biol.*, 2017, **429**, 3875–3892.

378 H. Shen, Z. Wu and L. Chen, *J. Phys. Chem. B*, 2022, **126**, 4261–4271.

379 A. Santamaria, K. C. Batchu, O. Matsarskaia, S. F. Prevost, D. Russo, F. Natali, T. Seydel, I. Hoffmann, V. Laux, M. Haertlein, T. A. Darwish, R. A. Russell, G. Corucci, G. Fragneto, A. Maestro and N. R. Zaccai, *J. Am. Chem. Soc.*, 2022, **144**, 2968–2979.

380 F. A. Rey and S. M. Lok, *Cell*, 2018, **172**, 1319–1334.

381 X. Ou, Y. Liu, X. Lei, P. Li, D. Mi, L. Ren, L. Guo, R. Guo, T. Chen, J. Hu, Z. Xiang, Z. Mu, X. Chen, J. Chen, K. Hu, Q. Jin, J. Wang and Z. Qian, *Nat. Commun.*, 2020, **11**, 1620.

382 H. Kleine-Weber, M. T. Elzayat, M. Hoffmann and S. Pohlmann, *Sci. Rep.*, 2018, **8**, 16597.

383 M. Hoffmann, H. Kleine-Weber and S. Pohlmann, *Mol. Cell*, 2020, **78**, 779–784 e775.

384 N. Vankadari, N. N. Jeyasankar and W. J. Lopes, *J. Phys. Chem. Lett.*, 2020, **11**, 9659–9668.

385 A. J. Pak, A. Yu, Z. Ke, J. A. G. Briggs and G. A. Voth, *Nat. Commun.*, 2022, **13**, 1002.

386 X. Fan, D. Cao, L. Kong and X. Zhang, *Nat. Commun.*, 2020, **11**, 3618.

387 J. M. Remington, K. T. McKay, J. B. Ferrell, S. T. Schneebeli and J. Li, *Biophys. J.*, 2021, **120**, 2848–2858.

388 S. Borkotoky, D. Dey and M. Banerjee, *J. Chem. Inf. Model.*, 2021, **61**, 423–431.

389 D. Gorgun, M. Lihan, K. Kapoor and E. Tajkhorshid, *Biophys. J.*, 2021, **120**, 2914–2926.

390 I. G. Madu, S. Belouzard and G. R. Whittaker, *Virology*, 2009, **393**, 265–271.

391 M. Gui, W. Song, H. Zhou, J. Xu, S. Chen, Y. Xiang and X. Wang, *Cell Res.*, 2017, **27**, 119–129.

392 S. C. Harrison, *Nat. Struct. Mol. Biol.*, 2008, **15**, 690–698.

393 Y. G. Yu, D. S. King and Y. K. Shin, *Science*, 1994, **266**, 274–276.

394 O. Korazim, K. Sackett and Y. Shai, *J. Mol. Biol.*, 2006, **364**, 1103–1117.

395 K. Sackett and Y. Shai, *Biochem*, 2002, **41**, 4678–4685.

396 J. Roche, J. M. Louis, A. Grishaev, J. Ying and A. Bax, *Proc. Natl. Acad. Sci. U. S. A.*, 2014, **111**, 3425–3430.

397 C. Aisenbrey and B. Bechinger, *Biochim. Biophys. Acta, Biomembr.*, 2020, **1862**, 183274.

398 B. Tripet, M. W. Howard, M. Jobling, R. K. Holmes, K. V. Holmes and R. S. Hodges, *J. Biol. Chem.*, 2004, **279**, 20836–20849.

399 M. K. Lawless, S. Barney, K. I. Guthrie, T. B. Bucy, S. R. Petteway and G. Merutka, *Biochem*, 1996, **35**, 13697–13708.

400 B. R. Lentz, V. Malinin, M. E. Haque and K. Evans, *Curr. Opin. Struct. Biol.*, 2000, **10**, 607–615.

401 L. V. Chernomordik and M. M. Kozlov, *Annu. Rev. Biochem.*, 2003, **72**, 175–207.

402 G. P. Pattnaik and H. Chakraborty, *Biochim. Biophys. Acta, Biomembr.*, 2019, **1861**, 183056.

403 W. Qiang, M. L. Bodner and D. P. Weliky, *J. Am. Chem. Soc.*, 2008, **130**, 5459–5471.

404 H. T. McMahon and E. Boucrot, *J. Cell Sci.*, 2015, **128**, 1065–1070.

405 K. Simons and E. Ikonen, *Nature*, 1997, **387**, 569–572.

406 S. Munro, *Cell*, 2003, **115**, 377–388.

407 G. M. Li, Y. G. Li, M. Yamate, S. M. Li and K. Ikuta, *Microbes Infect.*, 2007, **9**, 96–102.

408 F. J. Warner, R. A. Lew, A. I. Smith, D. W. Lambert, N. M. Hooper and A. J. Turner, *J. Biol. Chem.*, 2005, **280**, 39353–39362.

409 J. Glende, C. Schwegmann-Wessels, M. Al-Falah, S. Pfefferle, X. Qu, H. Deng, C. Drosten, H. Y. Naim and G. Herrler, *Virology*, 2008, **381**, 215–221.
410 Y. Lu, D. X. Liu and J. P. Tam, *Biochem. Biophys. Res. Commun.*, 2008, **369**, 344–349.
411 D. W. Sanders, C. C. Jumper, P. J. Ackerman, D. Bracha, A. Donlic, H. Kim, D. Kenney, I. Castello-Serrano, S. Suzuki, T. Tamura, A. H. Tavares, M. Saeed, A. S. Holehouse, A. Ploss, I. Levental, F. Douam, R. F. Padera, B. D. Levy and C. P. Brangwynne, *Elife*, 2021, **10**, e65962.
412 X. Li, W. Zhu, M. Fan, J. Zhang, Y. Peng, F. Huang, N. Wang, L. He, L. Zhang, R. Holmdahl, L. Meng and S. Lu, *Comput. Struct. Biotechnol. J.*, 2021, **19**, 1933–1943.
413 S. N. Palacios-Rapalo, L. A. De Jesus-Gonzalez, C. D. Cordero-Rivera, C. N. Farfan-Morales, J. F. Osuna-Ramos, G. Martinez-Mier, J. Quistian-Galvan, A. Munoz-Perez, V. Bernal-Dolores, R. M. Del Angel and J. M. Reyes-Ruiz, *Front. Immunol.*, 2021, **12**, 796855.
414 E. M. Reuven, Y. Dadon, M. Viard, N. Manukovsky, R. Blumenthal and Y. Shai, *Biochem*, 2012, **51**, 2867–2878.
415 M. Dube, F. A. Rey and M. Kielian, *PLoS Pathog.*, 2014, **10**, e1004530.
416 L. Nathan, A. L. Lai, J. K. Millet, M. R. Straus, J. H. Freed, G. R. Whittaker and S. Daniel, *ACS Infect. Dis.*, 2020, **6**, 250–260.
417 D. K. Das, U. Bulow, W. E. Diehl, N. D. Durham, F. Senjobe, K. Chandran, J. Luban and J. B. Munro, *PLoS Biol.*, 2020, **18**, e3000626.
418 M. R. Straus, T. Tang, A. L. Lai, A. Flegel, M. Bidon, J. H. Freed, S. Daniel and G. R. Whittaker, *J. Virol.*, 2020, **94**, e00426.
419 G. Khelashvili, A. Plante, M. Doktorova and H. Weinstein, *Biophys. J.*, 2021, **120**, 1105–1119.
420 B. Korber, W. M. Fischer, S. Gnanakaran, H. Yoon, J. Theiler, W. Abfalterer, N. Hengartner, E. E. Giorgi, T. Bhattacharya, B. Foley, K. M. Hastie, M. D. Parker, D. G. Partridge, C. M. Evans, T. M. Freeman, T. I. de Silva, C.-G. G. Sheffield, C. McDanal, L. G. Perez, H. Tang, A. Moon-Walker, S. P. Whelan, C. C. LaBranche, E. O. Saphire and D. C. Montefiori, *Cell*, 2020, **182**, 812–827 e819.
421 Y. J. Hou, S. Chiba, P. Halfmann, C. Ehre, M. Kuroda, K. H. Dinnon, 3rd, S. R. Leist, A. Schafer, N. Nakajima, K. Takahashi, R. E. Lee, T. M. Mascenik, R. Graham, C. E. Edwards, L. V. Tse, K. Okuda, A. J. Markmann, L. Bartelt, A. de Silva, D. M. Margolis, R. C. Boucher, S. H. Randell, T. Suzuki, L. E. Gralinski, Y. Kawaoka and R. S. Baric, *Science*, 2020, **370**, 1464–1468.
422 C. B. Jackson, L. Zhang, M. Farzan and H. Choe, *Biochem. Biophys. Res. Commun.*, 2021, **538**, 108–115.
423 R. A. Mansbach, S. Chakraborty, K. Nguyen, D. C. Montefiori, B. Korber and S. Gnanakaran, *Sci. Adv.*, 2021, **7**, eabf3671.
424 L. Yurkovetskiy, X. Wang, K. E. Pascal, C. Tomkins-Tinch, T. P. Nyalile, Y. Wang, A. Baum, W. E. Diehl, A. Dauphin, C. Carbone, K. Veinotte, S. B. Egri, S. F. Schaffner, J. E. Lemieux, J. B. Munro, A. Rafique, A. Barve, P. C. Sabeti, C. A. Kyratsous, N. V. Dudkina, K. Shen and J. Luban, *Cell*, 2020, **183**, 739–751.e738.
425 D. Weissman, M. G. Alameh, T. de Silva, P. Collini, H. Hornsby, R. Brown, C. C. LaBranche, R. J. Edwards, L. Sutherland, S. Santra, K. Mansouri, S. Gobeil, C. McDanal, N. Pardi, N. Hengartner, P. J. C. Lin, Y. Tam, P. A. Shaw, M. G. Lewis, C. Boesler, U. Sahin, P. Acharya, B. F. Haynes, B. Korber and D. C. Montefiori, *Cell Host Microbe*, 2021, **29**, 23–31 e24.
426 L. Zhang, C. B. Jackson, H. Mou, A. Ojha, H. Peng, B. D. Quinlan, E. S. Rangarajan, A. Pan, A. Vanderheiden, M. S. Suthar, W. Li, T. Izard, C. Rader, M. Farzan and H. Choe, *Nat. Commun.*, 2020, **11**, 6013.
427 X. Jiang, Z. Zhang, C. Wang, H. Ren, L. Gao, H. Peng, Z. Niu, H. Ren, H. Huang and Q. Sun, *Signal Transduction Targeted Ther.*, 2020, **5**, 268.
428 J. K. Millet and G. R. Whittaker, *Proc. Natl. Acad. Sci. U. S. A.*, 2014, **111**, 15214–15219.
429 S. Gellenoncourt, N. Saunders, R. Robinot, L. Auguste, M. M. Rajah, J. Kervevan, R. Jeger-Madiot, I. Staropoli, C. Planchais, H. Mouquet, J. Buchrieser, O. Schwartz and L. A. Chakrabarti, *J. Virol.*, 2022, **96**, e0130122.
430 A. Saito, T. Irie, R. Suzuki, T. Maemura, H. Nasser, K. Uriu, Y. Kosugi, K. Shirakawa, K. Sadamasu, I. Kimura, J. Ito, J. Wu, K. Iwatsuki-Horimoto, M. Ito, S. Yamayoshi, S. Loeber, M. Tsuda, L. Wang, S. Ozono, E. P. Butlertanaka, Y. L. Tanaka, R. Shimizu, K. Shimizu, K. Yoshimatsu, R. Kawabata, T. Sakaguchi, K. Tokunaga, I. Yoshida, H. Asakura, M. Nagashima, Y. Kazuma, R. Nomura, Y. Horisawa, K. Yoshimura, A. Takaori-Kondo, M. Imai, M. Chiba, H. Furihata, H. Hasebe, K. Kitazato, H. Kubo, N. Misawa, N. Morizako, K. Noda, A. Oide, M. Suganami, M. Takahashi, K. Tsushima, M. Yokoyama, Y. Yuan, S. Tanaka, S. Nakagawa, T. Ikeda, T. Fukuhara, Y. Kawaoka, K. Sato and C. The Genotype to Phenotype Japan, *Nature*, 2022, **602**, 300–306.
431 C. A. Beaudoin, A. P. Pandurangan, S. Y. Kim, S. W. Hamaia, C. L. Huang, T. L. Blundell, S. C. Vedithi and A. P. Jackson, *J. Med. Virol.*, 2022, **94**, 4181–4192.
432 K. Yang, C. Wang, K. I. White, R. A. Pfuetzner, L. Esquivies and A. T. Brunger, *Proc. Natl. Acad. Sci. U. S. A.*, 2022, **119**, e2119467119.
433 S. Kumar, K. Karuppanan and G. Subramaniam, *J. Med. Virol.*, 2022, **94**, 4780–4791.
434 F. W. Putnam, Y. S. Liu and T. L. Low, *J. Biol. Chem.*, 1979, **254**, 2865–2874.
435 J. V. Ravetch and S. Bolland, *Annu. Rev. Immunol.*, 2001, **19**, 275–290.
436 B. Heyman, *Immunol. Lett.*, 1996, **54**, 195–199.
437 F. C. Breedveld, *Lancet*, 2000, **355**, 735–740.
438 G. Kohler and C. Milstein, *Nature*, 1975, **256**, 495–497.
439 D. Corti, J. Misasi, S. Mulangu, D. A. Stanley, M. Kanekiyo, S. Wollen, A. Ploquin, N. A. Doria-Rose, R. P. Staupe, M. Bailey, W. Shi, M. Choe, H. Marcus, E. A. Thompson, A. Cagigi, C. Silacci, B. Fernandez-Rodriguez, L. Perez, F. Sallusto, F. Vanzetta, G. Agatic, E. Cameroni, N. Kisalu,

 

I. Gordon, J. E. Ledgerwood, J. R. Mascola, B. S. Graham, J. J. Muyembe-Tamfun, J. C. Trefry, A. Lanzavecchia and N. J. Sullivan, *Science*, 2016, **351**, 1339–1342.

440 J. F. Scheid, H. Mouquet, N. Feldhahn, M. S. Seaman, K. Velinzon, J. Pietzsch, R. G. Ott, R. M. Anthony, H. Zebroski, A. Hurley, A. Phogat, B. Chakrabarti, Y. Li, M. Connors, F. Pereyra, B. D. Walker, H. Wardemann, D. Ho, R. T. Wyatt, J. R. Mascola, J. V. Ravetch and M. C. Nussenzweig, *Nature*, 2009, **458**, 636–640.

441 L. Wang, W. Shi, J. D. Chappell, M. G. Joyce, Y. Zhang, M. Kanekiyo, M. M. Becker, N. van Doremalen, R. Fischer, N. Wang, K. S. Corbett, M. Choe, R. D. Mason, J. G. Van Galen, T. Zhou, K. O. Saunders, K. M. Tatti, L. M. Haynes, P. D. Kwong, K. Modjarrad, W. P. Kong, J. S. McLellan, M. R. Denison, V. J. Munster, J. R. Mascola and B. S. Graham, *J. Virol.*, 2018, **92**, e02002.

442 P. C. Taylor, A. C. Adams, M. M. Hufford, I. de la Torre, K. Winthrop and R. L. Gottlieb, *Nat. Rev. Immunol.*, 2021, **21**, 382–393.

443 T. T. Hansel, H. Kropshofer, T. Singer, J. A. Mitchell and A. J. George, *Nat. Rev. Drug Discovery*, 2010, **9**, 325–338.

444 S. M. Tirado and K. J. Yoon, *Viral Immunol.*, 2003, **16**, 69–86.

445 I. A. Clark, *Immunol. Cell Biol.*, 2007, **85**, 271–273.

446 H. Zare, M. Rajabibazl, I. Rasooli, W. Ebrahimizadeh, H. Bakherad, L. S. Ardakani and S. L. Gargari, *Int. J. Biol. Markers*, 2014, **29**, e169–179.

447 C. Hamers-Casterman, T. Atarhouch, S. Muyldermans, G. Robinson, C. Hamers, E. B. Songa, N. Bendahman and R. Hamers, *Nature*, 1993, **363**, 446–448.

448 E. Y. Yang and K. Shah, *Front. Oncol.*, 2020, **10**, 1182.

449 Y. Hu, C. Liu and S. Muyldermans, *Front. Immunol.*, 2017, **8**, 1442.

450 H. Zare, H. Aghamollaei, M. Hosseindokht, M. Heiat, A. Razei and H. Bakherad, *Mol. Cell. Probes*, 2021, **55**, 101692.

451 S. Yu, G. Xiong, S. Zhao, Y. Tang, H. Tang, K. Wang, H. Liu, K. Lan, X. Bi and S. Duan, *Int. J. Mol. Med.*, 2021, **47**, 444–454.

452 S. Ezzikouri, J. Nourlil, K. Tsukiyama-Kohara, M. Kohara, H. El Ossmani, M. P. Windisch and S. Benjelloun, *J. Biomol. Struct. Dyn.*, 2022, **40**, 3129–3131.

453 A. C. Walls, M. A. Tortorici, B. J. Bosch, B. Frenz, P. J. M. Rottier, F. DiMaio, F. A. Rey and D. Veesler, *Nature*, 2016, **531**, 114–117.

454 L. Min and Q. Sun, *Front. Mol. Biosci.*, 2021, **8**, 671633.

455 J. Cohen, *Science*, 2020, **369**, 752–753.

456 D. Li, G. D. Sempowski, K. O. Saunders, P. Acharya and B. F. Haynes, *Annu. Rev. Med.*, 2022, **73**, 1–16.

457 D. Focosi, S. McConnell, A. Casadevall, E. Cappello, G. Valdiserra and M. Tuccori, *Lancet Infect. Dis.*, 2022, **22**, e311–e326.

458 J. Deng, K. Heybati, H. B. Ramaraju, F. Zhou, D. Rayner and S. Heybati, *Infection*, 2023, **51**, 21–35.

459 H. Qi, B. Liu, X. Wang and L. Zhang, *Nat. Immunol.*, 2022, **23**, 1008–1020.

460 C. Iannizzi, K. L. Chai, V. Piechotta, S. J. Valk, C. Kimber, I. Monsef, E. M. Wood, A. A. Lamikanra, D. J. Roberts, Z. McQuilten, C. So-Osman, A. Jindal, N. Cryns, L. J. Estcourt, N. Kreuzberger and N. Skoetz, *Cochrane Database Syst. Rev.*, 2023, **5**, CD013600.

461 D. Focosi, M. Franchini, L.-A. Pirofski, T. Burnouf, N. Paneth, M. J. Joyner and A. Casadevall, *Clin. Microbiol. Rev.*, 2022, **35**, e00200–e00221.

462 B. L. Sievers, S. Chakraborty, Y. Xue, T. Gelbart, J. C. Gonzalez, A. G. Cassidy, Y. Golan, M. Prahl, S. L. Gaw, P. S. Arunachalam, C. A. Blish, S. D. Boyd, M. M. Davis, P. Jagannathan, K. C. Nadeau, B. Pulendran, U. Singh, R. H. Scheuermann, M. B. Frieman, S. Vashee, T. T. Wang and G. S. Tan, *Sci. Transl. Med.*, 2022, **14**, eabn7842.

463 D. Wrapp, D. De Vlieger, K. S. Corbett, G. M. Torres, N. Wang, W. Van Breedam, K. Roose, L. van Schie, V.-C. C.-R. Team, M. Hoffmann, S. Pohlmann, B. S. Graham, N. Callewaert, B. Schepens, X. Saelens and J. S. McLellan, *Cell*, 2020, **181**, 1436–1441.

464 D. J. Benton, A. G. Wrobel, P. Xu, C. Roustan, S. R. Martin, P. B. Rosenthal, J. J. Skehel and S. J. Gamblin, *Nature*, 2020, **588**, 327–330.

465 A. Baum, B. O. Fulton, E. Wloga, R. Copin, K. E. Pascal, V. Russo, S. Giordano, K. Lanza, N. Negron, M. Ni, Y. Wei, G. S. Atwal, A. J. Murphy, N. Stahl, G. D. Yancopoulos and C. A. Kyratsous, *Science*, 2020, **369**, 1014–1018.

466 H. Nguyen, P. D. Lan, D. A. Nissley, E. P. O'Brien and M. S. Li, *J. Phys. Chem. B*, 2022, **126**, 2812–2823.

467 R. E. Chen, E. S. Winkler, J. B. Case, I. D. Aziati, T. L. Bricker, A. Joshi, T. L. Darling, B. Ying, J. M. Errico, S. Shrihari, L. A. VanBlargan, X. Xie, P. Gilchuk, S. J. Zost, L. Droit, Z. Liu, S. Stumpf, D. Wang, S. A. Handley, W. B. Stine, Jr, P. Y. Shi, M. E. Davis-Gardner, M. S. Suthar, M. G. Knight, R. Andino, C. Y. Chiu, A. H. Ellebedy, D. H. Fremont, S. P. J. Whelan, J. E. Crowe Jr, L. Purcell, D. Corti, A. C. M. Boon and M. S. Diamond, *Nature*, 2021, **596**, 103–108.

468 L. A. VanBlargan, J. M. Errico, P. J. Halfmann, S. J. Zost, J. E. Crowe, Jr., L. A. Purcell, Y. Kawaoka, D. Corti, D. H. Fremont and M. S. Diamond, *Nat. Med.*, 2022, **28**, 490–495.

469 M. Hoffmann, H. Hofmann-Winkler, N. Kruger, A. Kempf, I. Nehlmeier, L. Graichen, P. Arora, A. Sidarovich, A. S. Moldenhauer, M. S. Winkler, S. Schulz, H. M. Jack, M. V. Stankov, G. M. N. Behrens and S. Pohlmann, *Cell Rep.*, 2021, **36**, 109415.

470 G. M. Verkhivker, S. Agajanian, D. Y. Oztas and G. Gupta, *Biochem*, 2021, **60**, 1459–1484.

471 T. N. Starr, N. Czudnochowski, Z. Liu, F. Zatta, Y. J. Park, A. Addetia, D. Pinto, M. Beltramello, P. Hernandez, A. J. Greaney, R. Marzi, W. G. Glass, I. Zhang, A. S. Dingens, J. E. Bowen, M. A. Tortorici, A. C. Walls, J. A. Wojcechowskyj, A. De Marco, L. E. Rosen, J. Zhou, M. Montiel-Ruiz, H. Kaiser, J. R. Dillen, H. Tucker, J. Bassi, C. Silacci-Fregni, M. P. Housley, J. di Iulio, G. Lombardo, M. Agostini, N. Sprugasci, K. Culap, S. Jaconi, M. Meury,

E. Dellota, Jr., R. Abdelnabi, S. C. Foo, E. Cameroni, S. Stumpf, T. I. Croll, J. C. Nix, C. Havenar-Daughton, L. Piccoli, F. Benigni, J. Neyts, A. Telenti, F. A. Lempp, M. S. Pizzuto, J. D. Chodera, C. M. Hebner, H. W. Virgin, S. P. J. Whelan, D. Veesler, D. Corti, J. D. Bloom and G. Snell, *Nature*, 2021, **597**, 97–102.

472 D. Pinto, Y. J. Park, M. Beltramello, A. C. Walls, M. A. Tortorici, S. Bianchi, S. Jaconi, K. Culap, F. Zatta, A. De Marco, A. Peter, B. Guarino, R. Spreafico, E. Cameroni, J. B. Case, R. E. Chen, C. Havenar-Daughton, G. Snell, A. Telenti, H. W. Virgin, A. Lanzavecchia, M. S. Diamond, K. Fink, D. Veesler and D. Corti, *Nature*, 2020, **583**, 290–295.

473 P. J. Klasse and Q. J. Sattentau, *J. Gen. Virol.*, 2002, **83**, 2091–2108.

474 E. Takashita, N. Kinoshita, S. Yamayoshi, Y. Sakai-Tagawa, S. Fujisaki, M. Ito, K. Iwatsuki-Horimoto, S. Chiba, P. Halfmann, H. Nagai, M. Saito, E. Adachi, D. Sullivan, A. Pekosz, S. Watanabe, K. Maeda, M. Imai, H. Yotsuyanagi, H. Mitsuya, N. Ohmagari, M. Takeda, H. Hasegawa and Y. Kawaoka, *N. Engl. J. Med.*, 2022, **386**, 995–998.

475 G. Zhao, L. He, S. Sun, H. Qiu, W. Tai, J. Chen, J. Li, Y. Chen, Y. Guo, Y. Wang, J. Shang, K. Ji, R. Fan, E. Du, S. Jiang, F. Li, L. Du and Y. Zhou, *J. Virol.*, 2018, **92**, jvi.00837-18.

476 E. Takashita, N. Kinoshita, S. Yamayoshi, Y. Sakai-Tagawa, S. Fujisaki, M. Ito, K. Iwatsuki-Horimoto, P. Halfmann, S. Watanabe, K. Maeda, M. Imai, H. Mitsuya, N. Ohmagari, M. Takeda, H. Hasegawa and Y. Kawaoka, *N. Engl. J. Med.*, 2022, **386**, 1475–1477.

477 D. Marti, M. Alsina, C. Aleman, O. Bertran, P. Turon and J. Torras, *Biochimie*, 2022, **193**, 90–102.

478 B. E. Jones, P. L. Brown-Augsburger, K. S. Corbett, K. Westendorf, J. Davies, T. P. Cujec, C. M. Wiethoff, J. L. Blackbourne, B. A. Heinz, D. Foster, R. E. Higgs, D. Balasubramaniam, L. Wang, Y. Zhang, E. S. Yang, R. Bidshahri, L. Kraft, Y. Hwang, S. Zentelis, K. R. Jepson, R. Goya, M. A. Smith, D. W. Collins, S. J. Hinshaw, S. A. Tycho, D. Pellacani, P. Xiang, K. Muthuraman, S. Sobhanifar, M. H. Piper, F. J. Triana, J. Hendle, A. Pustilnik, A. C. Adams, S. J. Berens, R. S. Baric, D. R. Martinez, R. W. Cross, T. W. Geisbert, V. Borisevich, O. Abiona, H. M. Belli, M. de Vries, A. Mohamed, M. Dittmann, M. I. Samanovic, M. J. Mulligan, J. A. Goldsmith, C. L. Hsieh, N. V. Johnson, D. Wrapp, J. S. McLellan, B. C. Barnhart, B. S. Graham, J. R. Mascola, C. L. Hansen and E. Falconer, *Sci. Transl. Med.*, 2021, **13**, eabf1906.

479 R. Shi, C. Shan, X. Duan, Z. Chen, P. Liu, J. Song, T. Song, X. Bi, C. Han, L. Wu, G. Gao, X. Hu, Y. Zhang, Z. Tong, W. Huang, W. J. Liu, G. Wu, B. Zhang, L. Wang, J. Qi, H. Feng, F. S. Wang, Q. Wang, G. F. Gao, Z. Yuan and J. Yan, *Nature*, 2020, **584**, 120–124.

480 R. L. Gottlieb, A. Nirula, P. Chen, J. Boscia, B. Heller, J. Morris, G. Huhn, J. Cardona, B. Mocherla, V. Stosor, I. Shawa, P. Kumar, A. C. Adams, J. Van Naarden, K. L. Custer, M. Durante, G. Oakley, A. E. Schade, T. R. Holzer, P. J. Ebert, R. E. Higgs, N. L. Kallewaard, J. Sabo, D. R. Patel, P. Klekotka, L. Shen and D. M. Skovronsky, *JAMA*, 2021, **325**, 632–644.

481 S. Liu, T. Huynh, C. B. Stauft, T. T. Wang and B. Luan, *J. Chem. Inf. Model.*, 2021, **61**, 5133–5140.

482 E. Laurini, D. Marson, S. Aulic, A. Fermeglia and S. Pricl, *Sci. Rep.*, 2021, **11**, 20274.

483 Y. M. Loo, P. M. McTamney, R. H. Arends, M. E. Abram, A. A. Aksyuk, S. Diallo, D. J. Flores, E. J. Kelly, K. Ren, R. Roque, K. Rosenthal, K. Streicher, K. M. Tuffy, N. J. Bond, O. Cornwell, J. Bouquet, L. I. Cheng, J. Dunyak, Y. Huang, A. I. Rosenbaum, V. Pilla Reddy, H. Andersen, R. H. Carnahan, J. E. Crowe, Jr., A. I. Kuehne, A. S. Herbert, J. M. Dye, H. Bright, N. L. Kallewaard, M. N. Pangalos and M. T. Esser, *Sci. Transl. Med.*, 2022, **14**, eabl8124.

484 C. Kim, D. K. Ryu, J. Lee, Y. I. Kim, J. M. Seo, Y. G. Kim, J. H. Jeong, M. Kim, J. I. Kim, P. Kim, J. S. Bae, E. Y. Shim, M. S. Lee, M. S. Kim, H. Noh, G. S. Park, J. S. Park, D. Son, Y. An, J. N. Lee, K. S. Kwon, J. Y. Lee, H. Lee, J. S. Yang, K. C. Kim, S. S. Kim, H. M. Woo, J. W. Kim, M. S. Park, K. M. Yu, S. M. Kim, E. H. Kim, S. J. Park, S. T. Jeong, C. H. Yu, Y. Song, S. H. Gu, H. Oh, B. S. Koo, J. J. Hong, C. M. Ryu, W. B. Park, M. D. Oh, Y. K. Choi and S. Y. Lee, *Nat. Commun.*, 2021, **12**, 288.

485 D. K. Ryu, B. Kang, H. Noh, S. J. Woo, M. H. Lee, P. M. Nuijten, J. I. Kim, J. M. Seo, C. Kim, M. Kim, E. Yang, G. Lim, S. G. Kim, S. K. Eo, J. A. Choi, M. Song, S. S. Oh, H. Y. Chung, A. S. Tijsma, C. A. van Baalen, K. S. Kwon and S. Y. Lee, *Biochem. Biophys. Res. Commun.*, 2021, **578**, 91–96.

486 D. K. Ryu, R. Song, M. Kim, Y. I. Kim, C. Kim, J. I. Kim, K. S. Kwon, A. S. Tijsma, P. M. Nuijten, C. A. van Baalen, T. Hermanus, P. Kgagudi, T. Moyo-Gwete, P. L. Moore, Y. K. Choi and S. Y. Lee, *Biochem. Biophys. Res. Commun.*, 2021, **566**, 135–140.

487 K. M. Fung, S. J. Lai, T. L. Lin and T. S. Tseng, *Front. Mol. Biosci.*, 2022, **9**, 797132.

488 B. Ju, Q. Zhang, J. Ge, R. Wang, J. Sun, X. Ge, J. Yu, S. Shan, B. Zhou, S. Song, X. Tang, J. Yu, J. Lan, J. Yuan, H. Wang, J. Zhao, S. Zhang, Y. Wang, X. Shi, L. Liu, J. Zhao, X. Wang, Z. Zhang and L. Zhang, *Nature*, 2020, **584**, 115–119.

489 R. Wang, Q. Zhang, J. Ge, W. Ren, R. Zhang, J. Lan, B. Ju, B. Su, F. Yu, P. Chen, H. Liao, Y. Feng, X. Li, X. Shi, Z. Zhang, F. Zhang, Q. Ding, T. Zhang, X. Wang and L. Zhang, *Immunity*, 2021, **54**, 1611–1621 e1615.

490 X. Duan, R. Shi, P. Liu, Q. Huang, F. Wang, X. Chen, H. Feng, W. Huang, J. Xiao and J. Yan, *Signal Transduction Targeted Ther.*, 2022, **7**, 23.

491 L. Cheng, S. Song, Q. Fan, S. Shen, H. Wang, B. Zhou, X. Ge, B. Ju and Z. Zhang, *Cell Discov*, 2021, **7**, 112.

492 K. Westendorf, S. Zentelis, L. Wang, D. Foster, P. Vaillancourt, M. Wiggin, E. Lovett, R. van der Lee, J. Hendle, A. Pustilnik, J. M. Sauder, L. Kraft, Y. Hwang, R. W. Siegel, J. Chen, B. A. Heinz, R. E. Higgs, N. L. Kallewaard, K. Jepson, R. Goya, M. A. Smith,

 

D. W. Collins, D. Pellacani, P. Xiang, V. de Puyraimond, M. Ricicova, L. Devorkin, C. Pritchard, A. O'Neill, K. Dalal, P. Panwar, H. Dhupar, F. A. Garces, C. A. Cohen, J. M. Dye, K. E. Huie, C. V. Badger, D. Kobasa, J. Audet, J. J. Freitas, S. Hassanali, I. Hughes, L. Munoz, H. C. Palma, B. Ramamurthy, R. W. Cross, T. W. Geisbert, V. Menachery, K. Lokugamage, V. Borisevich, I. Lanz, L. Anderson, P. Sipahimalani, K. S. Corbett, E. S. Yang, Y. Zhang, W. Shi, T. Zhou, M. Choe, J. Misasi, P. D. Kwong, N. J. Sullivan, B. S. Graham, T. L. Fernandez, C. L. Hansen, E. Falconer, J. R. Mascola, B. E. Jones and B. C. Barnhart, *Cell Rep.*, 2022, **39**, 110812.

493 Y. Cao, A. Yisimayi, F. Jian, W. Song, T. Xiao, L. Wang, S. Du, J. Wang, Q. Li, X. Chen, Y. Yu, P. Wang, Z. Zhang, P. Liu, R. An, X. Hao, Y. Wang, J. Wang, R. Feng, H. Sun, L. Zhao, W. Zhang, D. Zhao, J. Zheng, L. Yu, C. Li, N. Zhang, R. Wang, X. Niu, S. Yang, X. Song, Y. Chai, Y. Hu, Y. Shi, L. Zheng, Z. Li, Q. Gu, F. Shao, W. Huang, R. Jin, Z. Shen, Y. Wang, X. Wang, J. Xiao and X. S. Xie, *Nature*, 2022, **608**, 593–602.

494 Y. Liu, W. T. Soh, J. I. Kishikawa, M. Hirose, E. E. Nakayama, S. Li, M. Sasai, T. Suzuki, A. Tada, A. Arakawa, S. Matsuoka, K. Akamatsu, M. Matsuda, C. Ono, S. Torii, K. Kishida, H. Jin, W. Nakai, N. Arase, A. Nakagawa, M. Matsumoto, Y. Nakazaki, Y. Shindo, M. Kohyama, K. Tomii, K. Ohmura, S. Ohshima, T. Okamoto, M. Yamamoto, H. Nakagami, Y. Matsuura, A. Nakagawa, T. Kato, M. Okada, D. M. Standley, T. Shioda and H. Arase, *Cell*, 2021, **184**, 3452–3466 e3418.

495 H. Tang, L. Gao, Z. Wu, F. Meng, X. Zhao, Y. Shao, G. Hou, X. Du and F. X. Qin, *Front. Immunol.*, 2022, **13**, 836232.

496 D. Li, R. J. Edwards, K. Manne, D. R. Martinez, A. Schafer, S. M. Alam, K. Wiehe, X. Lu, R. Parks, L. L. Sutherland, T. H. Oguin, 3rd, C. McDanal, L. G. Perez, K. Mansouri, S. M. C. Gobeil, K. Janowska, V. Stalls, M. Kopp, F. Cai, E. Lee, A. Foulger, G. E. Hernandez, A. Sanzone, K. Tilahun, C. Jiang, L. V. Tse, K. W. Bock, M. Minai, B. M. Nagata, K. Cronin, V. Gee-Lai, M. Deyton, M. Barr, T. V. Holle, A. N. Macintyre, E. Stover, J. Feldman, B. M. Hauser, T. M. Caradonna, T. D. Scobey, W. Rountree, Y. Wang, M. A. Moody, D. W. Cain, C. T. DeMarco, T. Denny, C. W. Woods, E. W. Petzold, A. G. Schmidt, I. T. Teng, T. Zhou, P. D. Kwong, J. R. Mascola, B. S. Graham, I. N. Moore, R. Seder, H. Andersen, M. G. Lewis, D. C. Montefiori, G. D. Sempowski, R. S. Baric, P. Acharya, B. F. Haynes and K. O. Saunders, *Cell*, 2021, **184**, 4203–4219.e4232.

497 W. N. Voss, Y. J. Hou, N. V. Johnson, G. Delidakis, J. E. Kim, K. Javanmardi, A. P. Horton, F. Bartzoka, C. J. Paresi, Y. Tanno, C. W. Chou, S. A. Abbasi, W. Pickens, K. George, D. R. Boutz, D. M. Towers, J. R. McDaniel, D. Billick, J. Goike, L. Rowe, D. Batra, J. Pohl, J. Lee, S. Gangappa, S. Sambhara, M. Gadush, N. Wang, M. D. Person, B. L. Iverson, J. D. Gollihar, J. M. Dye, A. S. Herbert, I. J. Finkelstein, R. S. Baric, J. S. McLellan, G. Georgiou, J. J. Lavinder and G. C. Ippolito, *Science*, 2021, **372**, 1108–1112.

498 N. Wang, Y. Sun, R. Feng, Y. Wang, Y. Guo, L. Zhang, Y. Q. Deng, L. Wang, Z. Cui, L. Cao, Y. J. Zhang, W. Li, F. C. Zhu, C. F. Qin and X. Wang, *Cell Res.*, 2021, **31**, 101–103.

499 D. Li, R. J. Edwards, K. Manne, D. R. Martinez, A. Schafer, S. M. Alam, K. Wiehe, X. Lu, R. Parks, L. L. Sutherland, T. H. Oguin, 3rd, C. McDanal, L. G. Perez, K. Mansouri, S. M. C. Gobeil, K. Janowska, V. Stalls, M. Kopp, F. Cai, E. Lee, A. Foulger, G. E. Hernandez, A. Sanzone, K. Tilahun, C. Jiang, L. V. Tse, K. W. Bock, M. Minai, B. M. Nagata, K. Cronin, V. Gee-Lai, M. Deyton, M. Barr, T. Von Holle, A. N. Macintyre, E. Stover, J. Feldman, B. M. Hauser, T. M. Caradonna, T. D. Scobey, W. Rountree, Y. Wang, M. A. Moody, D. W. Cain, C. T. DeMarco, T. N. Denny, C. W. Woods, E. W. Petzold, A. G. Schmidt, I. T. Teng, T. Zhou, P. D. Kwong, J. R. Mascola, B. S. Graham, I. N. Moore, R. Seder, H. Andersen, M. G. Lewis, D. C. Montefiori, G. D. Sempowski, R. S. Baric, P. Acharya, B. F. Haynes and K. O. Saunders, *Cell*, 2021, **184**, 4203–4219 e4232.

500 J. T. Ladner, S. N. Henson, A. S. Boyle, A. L. Engelbrektson, Z. W. Fink, F. Rahee, J. D'Ambrozio, K. E. Schaecher, M. Stone, W. Dong, S. Dadwal, J. Yu, M. A. Caligiuri, P. Cieplak, M. Bjoras, M. H. Fenstad, S. A. Nordbo, D. E. Kainov, N. Muranaka, M. S. Chee, S. A. Shiryaev and J. A. Altin, *Cell Rep. Med.*, 2021, **2**, 100189.

501 C. Dacon, C. Tucker, L. Peng, C. D. Lee, T. H. Lin, M. Yuan, Y. Cong, L. Wang, L. Purser, J. K. Williams, C. W. Pyo, I. Kosik, Z. Hu, M. Zhao, D. Mohan, A. J. R. Cooper, M. Peterson, J. Skinner, S. Dixit, E. Kollins, L. Huzella, D. Perry, R. Byrum, S. Lembirik, D. Drawbaugh, B. Eaton, Y. Zhang, E. S. Yang, M. Chen, K. Leung, R. S. Weinberg, A. Pegu, D. E. Geraghty, E. Davidson, I. Douagi, S. Moir, J. W. Yewdell, C. Schmaljohn, P. D. Crompton, M. R. Holbrook, D. Nemazee, J. R. Mascola, I. A. Wilson and J. Tan, *Science*, 2022, **377**, 728–735.

502 J. S. Low, J. Jerak, M. A. Tortorici, M. McCallum, D. Pinto, A. Cassotta, M. Foglierini, F. Mele, R. Abdelnabi, B. Weynand, J. Noack, M. Montiel-Ruiz, S. Bianchi, F. Benigni, N. Sprugasci, A. Joshi, J. E. Bowen, C. Stewart, M. Rexhepaj, A. C. Walls, D. Jarrossay, D. Morone, P. Paparoditis, C. Garzoni, P. Ferrari, A. Ceschi, J. Neyts, L. A. Purcell, G. Snell, D. Corti, A. Lanzavecchia, D. Veesler and F. Sallusto, *Science*, 2022, **377**, 735–742.

503 Q. Lu, Z. Zhang, H. Li, K. Zhong, Q. Zhao, Z. Wang, Z. Wu, D. Yang, S. Sun, N. Yang, M. Zheng, Q. Chen, C. Long, W. Guo, H. Yang, C. Nie and A. Tong, *J Nanobiotechnology*, 2021, **19**, 33.

504 H. Ma, W. Zeng, X. Meng, X. Huang, Y. Yang, D. Zhao, P. Zhou, X. Wang, C. Zhao, Y. Sun, P. Wang, H. Ou, X. Hu, Y. Xiang and T. Jin, *J. Virol.*, 2021, **95**, e02438-20.

505 M. Arbabi-Ghahroudi, *Front. Immunol.*, 2017, **8**, 1589.

506 E. Moreno, M. S. Valdes-Tresanco, A. Molina-Zapata and O. Sanchez-Ramos, *BMC Res. Notes*, 2022, **15**, 124.

507 X. Chi, X. Liu, C. Wang, X. Zhang, X. Li, J. Hou, L. Ren, Q. Jin, J. Wang and W. Yang, *Nat. Commun.*, 2020, **11**, 4528.

508 J. Huo, A. Le Bas, R. R. Ruza, H. M. E. Duyvesteyn, H. Mikolajek, T. Malinauskas, T. K. Tan, P. Rijal, M. Dumoux, P. N. Ward, J. Ren, D. Zhou, P. J. Harrison,

M. Weckener, D. K. Clare, V. K. Vogirala, J. Radecke, L. Moynie, Y. Zhao, J. Gilbert-Jaramillo, M. L. Knight, J. A. Tree, K. R. Buttigieg, N. Coombes, M. J. Elmore, M. W. Carroll, L. Carrique, P. N. M. Shah, W. James, A. R. Townsend, D. I. Stuart, R. J. Owens and J. H. Naismith, *Nat. Struct. Mol. Biol.*, 2020, **27**, 846–854.

509 T. F. Custodio, H. Das, D. J. Sheward, L. Hanke, S. Pazicky, J. Pieprzyk, M. Sorgenfrei, M. A. Schroer, A. Y. Gruzinov, C. M. Jeffries, M. A. Graewert, D. I. Svergun, N. Dobrev, K. Remans, M. A. Seeger, G. M. McInerney, B. Murrell, B. M. Hallberg and C. Low, *Nat. Commun.*, 2020, **11**, 5588.

510 C. Palomo, V. Mas, L. Detalle, E. Depla, O. Cano, M. Vazquez, C. Stortelers and J. A. Melero, *Antimicrob. Agents Chemother.*, 2016, **60**, 6498–6509.

511 C. J. Bracken, S. A. Lim, P. Solomon, N. J. Rettko, D. P. Nguyen, B. S. Zha, K. Schaefer, J. R. Byrnes, J. Zhou, I. Lui, J. Liu, K. Pance, Q. S. B. Consortium, X. X. Zhou, K. K. Leung and J. A. Wells, *Nat. Chem. Biol.*, 2021, **17**, 113–121.

512 J. Huo, H. Mikolajek, A. Le Bas, J. J. Clark, P. Sharma, A. Kipar, J. Dormon, C. Norman, M. Weckener, D. K. Clare, P. J. Harrison, J. A. Tree, K. R. Buttigieg, F. J. Salguero, R. Watson, D. Knott, O. Carnell, D. Ngabo, M. J. Elmore, S. Fotheringham, A. Harding, L. Moynie, P. N. Ward, M. Dumoux, T. Prince, Y. Hall, J. A. Hiscox, A. Owen, W. James, M. W. Carroll, J. P. Stewart, J. H. Naismith and R. J. Owens, *Nat. Commun.*, 2021, **12**, 5469.

513 T. Guttler, M. Aksu, A. Dickmanns, K. M. Stegmann, K. Gregor, R. Rees, W. Taxer, O. Rymarenko, J. Schunemann, C. Dienemann, P. Gunkel, B. Mussil, J. Krull, U. Teichmann, U. Gross, V. C. Cordes, M. Dobbelstein and D. Gorlich, *Embo J*, 2021, **40**, e107985.

514 J. M. Casasnovas, Y. Margolles, M. A. Noriega, M. Guzman, R. Arranz, R. Melero, M. Casanova, J. A. Corbera, N. Jimenez-de-Oya, P. Gastaminza, U. Garaigorta, J. C. Saiz, M. A. Martin-Acebes and L. A. Fernandez, *Front. Immunol.*, 2022, **13**, 863831.

515 L. Hanke, L. Vidakovics Perez, D. J. Sheward, H. Das, T. Schulte, A. Moliner-Morro, M. Corcoran, A. Achour, G. B. Karlsson Hedestam, B. M. Hallberg, B. Murrell and G. M. McInerney, *Nat. Commun.*, 2020, **11**, 4420.

516 B. Rissiek, F. Koch-Nolte and T. Magnus, *Front. Cell. Neurosci.*, 2014, **8**, 344.

517 M. Sanaei, N. Setayesh, Z. Sepehrizadeh, M. Mahdavi and M. H. Yazdi, *Immunol. Invest.*, 2020, **49**, 875–896.

518 M. Golcuk, A. Hacisuleyman, B. Erman, A. Yildiz and M. Gur, *J. Chem. Inf. Model.*, 2021, **61**, 5152–5160.

519 X. Tian, C. Li, A. Huang, S. Xia, S. Lu, Z. Shi, L. Lu, S. Jiang, Z. Yang, Y. Wu and T. Ying, *Emerging Microbes Infect.*, 2020, **9**, 382–385.

520 P. A. Koenig, H. Das, H. Liu, B. M. Kummerer, F. N. Gohr, L. M. Jenster, L. D. J. Schiffelers, Y. M. Tesfamariam, M. Uchima, J. D. Wuerth, K. Gatterdam, N. Ruetalo, M. H. Christensen, C. I. Fandrey, S. Normann, J. M. P. Todtmann, S. Pritzl, L. Hanke, J. Boos, M. Yuan, X. Zhu, J. L. Schmid-Burgk, H. Kato, M. Schindler, I. A. Wilson, M. Geyer, K. U. Ludwig, B. M. Hallberg, N. C. Wu and F. I. Schmidt, *Science*, 2021, **371**, abe6230.

521 G. M. Verkhivker, S. Agajanian, D. Y. Oztas and G. Gupta, *ACS Omega*, 2021, **6**, 26354–26371.

522 J. D. Walter, M. Scherer, C. A. J. Hutter, A. A. Garaeva, I. Zimmermann, M. Wyss, J. Rheinberger, Y. Ruedin, J. C. Earp, P. Egloff, M. Sorgenfrei, L. M. Hurlimann, I. Gonda, G. Meier, S. Remm, S. Thavarasah, G. van Geest, R. Bruggmann, G. Zimmer, D. J. Slotboom, C. Paulino, P. Plattet and M. A. Seeger, *EMBO Rep.*, 2022, **23**, e54199.

523 J. Ahmad, J. Jiang, L. F. Boyd, A. Zeher, R. Huang, D. Xia, K. Natarajan and D. H. Margulies, *J. Biol. Chem.*, 2021, **297**, 101202.

524 E. Boehm, I. Kronig, R. A. Neher, I. Eckerle, P. Vetter and L. Kaiser, *Clin. Microbiol. Infect.*, 2021, **27**, 1109–1117.

525 G. Valenzuela-Nieto, Z. Miranda-Chacon, C. Salinas-Rebolledo, R. Jara, A. Cuevas, A. Berking and A. Rojas-Fernandez, *Front. Drug Des. Discovery*, 2022, **2**, 927164.

526 Y. X. Lim, Y. L. Ng, J. P. Tam and D. X. Liu, *Diseases*, 2016, **4**, 26.

527 M. Thoms, R. Buschauer, M. Ameismeier, L. Koepke, T. Denk, M. Hirschenberger, H. Kratzat, M. Hayn, T. Mackens-Kiani, J. Cheng, J. H. Straub, C. M. Sturzel, T. Frohlich, O. Berninghausen, T. Becker, F. Kirchhoff, K. M. J. Sparrer and R. Beckmann, *Science*, 2020, **369**, 1249–1255.

528 K. Nakagawa, K. Narayanan, M. Wada, V. L. Popov, M. Cajimat, R. S. Baric and S. Makino, *J. Virol.*, 2018, **92**, e01157.

529 P. S. Masters, *Adv. Virus Res.*, 2006, **66**, 193–292.

530 Q. Peng, R. Peng, B. Yuan, J. Zhao, M. Wang, X. Wang, Q. Wang, Y. Sun, Z. Fan, J. Qi, G. F. Gao and Y. Shi, *Cell Rep.*, 2020, **31**, 107774.

531 Y. Chen and D. Guo, *Virol. Sin.*, 2016, **31**, 3–11.

532 B. Seraphin and M. Rosbash, *Cell*, 1989, **59**, 349–358.

533 Q. Wang, L. Zhang, B. Lynn and B. C. Rymond, *Nucleic Acids Res.*, 2008, **36**, 2787–2798.

534 B. Rutz and B. Seraphin, *RNA*, 1999, **5**, 819–831.

535 W. Y. Tarn, C. H. Hsu, K. T. Huang, H. R. Chen, H. Y. Kao, K. R. Lee and S. C. Cheng, *Embo J*, 1994, **13**, 2421–2431.

536 S. P. Chan, D. I. Kao, W. Y. Tsai and S. C. Cheng, *Science*, 2003, **302**, 279–282.

537 W. Y. Tarn, K. R. Lee and S. C. Cheng, *Proc. Natl. Acad. Sci. U. S. A.*, 1993, **90**, 10821–10825.

538 T. Kurosaki, M. W. Popp and L. E. Maquat, *Nat. Rev. Mol. Cell Biol.*, 2019, **20**, 406–420.

539 S. Daffis, K. J. Szretter, J. Schriewer, J. Li, S. Youn, J. Errett, T. Y. Lin, S. Schneller, R. Zust, H. Dong, V. Thiel, G. C. Sen, V. Fensterl, W. B. Klimstra, T. C. Pierson, R. M. Buller, M. Gale, Jr., P. Y. Shi and M. S. Diamond, *Nature*, 2010, **468**, 452–456.

540 E. Decroly, I. Imbert, B. Coutard, M. Bouvet, B. Selisko, K. Alvarez, A. E. Gorbalenya, E. J. Snijder and B. Canard, *J. Virol.*, 2008, **82**, 8071–8084.

541 Y. Chen, C. Su, M. Ke, X. Jin, L. Xu, Z. Zhang, A. Wu, Y. Sun, Z. Yang, P. Tien, T. Ahola, Y. Liang, X. Liu and D. Guo, *PLoS Pathog.*, 2011, **7**, e1002294.

542 E. Decroly, C. Debarnot, F. Ferron, M. Bouvet, B. Coutard, I. Imbert, L. Gluais, N. Papageorgiou, A. Sharff, G. Bricogne,

 

M. Ortiz-Lombardia, J. Lescar and B. Canard, *PLoS Pathog.*, 2011, **7**, e1002059.
543 V. D. Menachery, K. Debbink and R. S. Baric, *Virus Res.*, 2014, **194**, 191–199.
544 S. A. Shabalina, A. Y. Ogurtsov and N. A. Spiridonov, *Nucleic Acids Res.*, 2006, **34**, 2428–2437.
545 T. A. Steitz, *Nat. Rev. Mol. Cell Biol.*, 2008, **9**, 242–253.
546 K. Schubert, E. D. Karousis, A. Jomaa, A. Scaiola, B. Echeverria, L. A. Gurzeler, M. Leibundgut, V. Thiel, O. Muhlemann and N. Ban, *Nat. Struct. Mol. Biol.*, 2020, **27**, 959–966.
547 C. P. Lapointe, R. Grosely, A. G. Johnson, J. Wang, I. S. Fernandez and J. D. Puglisi, *Proc. Natl. Acad. Sci. U. S. A.*, 2021, **118**, e2017715118.
548 L. K. Clark, T. J. Green and C. M. Petit, *J. Virol.*, 2021, **95**, e02019.
549 A. S. Mendez, M. Ly, A. M. Gonzalez-Sanchez, E. Hartenian, N. T. Ingolia, J. H. Cate and B. A. Glaunsinger, *Cell Rep.*, 2021, **37**, 109841.
550 M. Afsar, R. Narayan, M. N. Akhtar, D. Das, H. Rahil, S. K. Nagaraj, S. M. Eswarappa, S. Tripathi and T. Hussain, *Elife*, 2022, **11**, e74877.
551 S. Ma, S. Damfo, J. Lou, N. Pinotsis, M. W. Bowler, S. Haider and F. Kozielski, *Int. J. Mol. Sci.*, 2022, **23**, 12448.
552 W. Kamitani, C. Huang, K. Narayanan, K. G. Lokugamage and S. Makino, *Nat. Struct. Mol. Biol.*, 2009, **16**, 1134–1140.
553 F. Benedetti, G. A. Snyder, M. Giovanetti, S. Angeletti, R. C. Gallo, M. Ciccozzi and D. Zella, *J. Transl. Med.*, 2020, **18**, 329.
554 J. W. Lin, C. Tang, H. C. Wei, B. Du, C. Chen, M. Wang, Y. Zhou, M. X. Yu, L. Cheng, S. Kuivanen, N. S. Ogando, L. Levanov, Y. Zhao, C. L. Li, R. Zhou, Z. Li, Y. Zhang, K. Sun, C. Wang, L. Chen, X. Xiao, X. Zheng, S. S. Chen, Z. Zhou, R. Yang, D. Zhang, M. Xu, J. Song, D. Wang, Y. Li, S. Lei, W. Zeng, Q. Yang, P. He, Y. Zhang, L. Zhou, L. Cao, F. Luo, H. Liu, L. Wang, F. Ye, M. Zhang, M. Li, W. Fan, X. Li, K. Li, B. Ke, J. Xu, H. Yang, S. He, M. Pan, Y. Yan, Y. Zha, L. Jiang, C. Yu, Y. Liu, Z. Xu, Q. Li, Y. Jiang, J. Sun, W. Hong, H. Wei, G. Lu, O. Vapalahti, Y. Luo, Y. Wei, T. Connor, W. Tan, E. J. Snijder, T. Smura, W. Li, J. Geng, B. Ying and L. Chen, *Cell Host Microbe*, 2021, **29**, 489–502 e488.
555 J. Borisek, A. Spinello and A. Magistrato, *J. Phys. Chem. Lett.*, 2021, **12**, 11745–11750.
556 H. Nguyen, H. L. and M. S. Li, *bioRxiv*, 2023, preprint, DOI: 10.1101/2023.02.24.529933.
557 M. K. Kellogg, E. B. Tikhonova and A. L. Karamyshev, *Front Genet*, 2022, **13**, 898083.
558 D. Akopian, K. Shen, X. Zhang and S. O. Shan, *Annu. Rev. Biochem.*, 2013, **82**, 693–721.
559 T. Powers and P. Walter, *Curr. Biol.*, 1996, **6**, 331–338.
560 M. Wilamowski, M. Hammel, W. Leite, Q. Zhang, Y. Kim, K. L. Weiss, R. Jedrzejczak, D. J. Rosenberg, Y. Fan, J. Wower, J. C. Bierma, A. H. Sarker, S. E. Tsutakawa, S. V. Pingali, H. M. O'Neill, A. Joachimiak and G. L. Hura, *Biophys. J.*, 2021, **120**, 3152–3165.
561 R. N. Kirchdoerfer and A. B. Ward, *Nat. Commun.*, 2019, **10**, 2342.
562 G. Sutton, E. Fry, L. Carter, S. Sainsbury, T. Walter, J. Nettleship, N. Berrow, R. Owens, R. Gilbert, A. Davidson, S. Siddell, L. L. Poon, J. Diprose, D. Alderton, M. Walsh, J. M. Grimes and D. I. Stuart, *Structure*, 2004, **12**, 341–353.
563 M. P. Egloff, F. Ferron, V. Campanacci, S. Longhi, C. Rancurel, H. Dutartre, E. J. Snijder, A. E. Gorbalenya, C. Cambillau and B. Canard, *Proc. Natl. Acad. Sci. U. S. A.*, 2004, **101**, 3792–3796.
564 C. Roman, A. Lewicka, D. Koirala, N. S. Li and J. A. Piccirilli, *ACS Chem. Biol.*, 2021, **16**, 1469–1481.
565 T. Brevini, M. Maes, G. J. Webb, B. V. John, C. D. Fuchs, G. Buescher, L. Wang, C. Griffiths, M. L. Brown, W. E. Scott, 3rd, P. Pereyra-Gerber, W. T. H. Gelson, S. Brown, S. Dillon, D. Muraro, J. Sharp, M. Neary, H. Box, L. Tatham, J. Stewart, P. Curley, H. Pertinez, S. Forrest, P. Mlcochova, S. S. Varankar, M. Darvish-Damavandi, V. L. Mulcahy, R. E. Kuc, T. L. Williams, J. A. Heslop, D. Rossetti, O. C. Tysoe, V. Galanakis, M. Vila-Gonzalez, T. W. M. Crozier, J. Bargehr, S. Sinha, S. S. Upponi, C. Fear, L. Swift, K. Saeb-Parsy, S. E. Davies, A. Wester, H. Hagstrom, E. Melum, D. Clements, P. Humphreys, J. Herriott, E. Kijak, H. Cox, C. Bramwell, A. Valentijn, C. J. R. Illingworth, U.-P. Consortium, B. Dahman, D. R. Bastaich, R. D. Ferreira, T. Marjot, E. Barnes, A. M. Moon, A. S. T. Barritt, R. K. Gupta, S. Baker, A. P. Davenport, G. Corbett, V. G. Gorgoulis, S. J. A. Buczacki, J. H. Lee, N. J. Matheson, M. Trauner, A. J. Fisher, P. Gibbs, A. J. Butler, C. J. E. Watson, G. F. Mells, G. Dougan, A. Owen, A. W. Lohse, L. Vallier and F. Sampaziotis, *Nature*, 2023, **615**, 134–142.
566 D. Y. Chen, C. V. Chin, D. Kenney, A. H. Tavares, N. Khan, H. L. Conway, G. Liu, M. C. Choudhary, H. P. Gertje, A. K. O'Connell, S. Adams, D. N. Kotton, A. Herrmann, A. Ensser, J. H. Connor, M. Bosmann, J. Z. Li, M. U. Gack, S. C. Baker, R. N. Kirchdoerfer, Y. Kataria, N. A. Crossland, F. Douam and M. Saeed, *Nature*, 2023, **615**, 143–150.
567 T. C. Marcink, T. Kicmal, E. Armbruster, Z. Zhang, G. Zipursky, K. L. Golub, M. Idris, J. Khao, J. Drew-Bear, G. McGill, T. Gallagher, M. Porotto, A. des Georges and A. Moscona, *Sci. Adv.*, 2022, **8**, eabo3153.
568 R. Saha, P. Ghosh and V. Burra, *3 Biotech*, 2021, **11**, 47.
569 A. Singh, M. Thakur, L. K. Sharma and K. Chandra, *Sci. Rep.*, 2020, **10**, 16219.
570 S. Sanami, M. Alizadeh, M. Nosrati, K. A. Dehkordi, F. Azadegan-Dehkordi, S. Tahmasebian, H. Nosrati, M. H. Arjmand, M. Ghasemi-Dehnoo, A. Rafiei and N. Bagheri, *Comput Biol Med*, 2021, **133**, 104390.
571 Z. Yang, P. Bogdan and S. Nazarian, *Sci. Rep.*, 2021, **11**, 3238.
572 C. Zhou, Z. Chen, L. Zhang, D. Yan, T. Mao, K. Tang, T. Qiu and Z. Cao, *Nucleic Acids Res.*, 2019, **47**, W388–W394.
573 R. Wintjens, A. M. Bifani and P. Bifani, *npj Vaccines*, 2020, **5**, 81.
574 A. Triveri, S. A. Serapian, F. Marchetti, F. Doria, S. Pavoni, F. Cinquini, E. Moroni, A. Rasola, F. Frigerio and G. Colombo, *J. Chem. Inf. Model.*, 2021, **61**, 4687–4700.